N° d'ordre : 4420

THÈSE

PRÉSENTÉE A

L'UNIVERSITÉ BORDEAUX 1

ÉCOLE DOCTORALE DES SCIENCES CHIMIQUES

Par Iban Vicario Gomez

POUR OBTENIR LE GRADE DE

DOCTEUR

SPÉCIALITÉ : Physico-Chimie de la Matière Condensée

Influence des nano-particules d'alumine (Al_2O_3) et de di-borure de titane (TiB_2) sur la microstructure et les propriétés de l'alliage Al-Si9-Cu3-Fe1 pour des applications de fonderie à haute pression

Directeurs de recherche : M. J.-F. Silvain, Mme A. Poulon

Soutenue le : 19 décembre 2011

Après avis de :

M. Felix Peñalba	Docteur – TECNALIA, Espagne	Rapporteur
M. Joël Douin	Directeur de Recherche – CEMES, Toulouse	Rapporteur

Devant la commission d'examen formée de :

Mme Angeline Poulon	Maître de Conférence – ICMCB, Bordeaux	Examinateur
M. Claude Delmas	Directeur de Recherche – ICMCB, Bordeaux	Président
M. Jean-François Silvain	Directeur de Recherche – ICMCB, Bordeaux	Examinateur
M. Pedro Egizabal	Docteur – TECNALIA, Espagne	Examinateur

Université Bordeaux 1
Les Sciences et les Technologies au service de l'Homme et de l'environnement

Influence of Alumina (Al_2O_3) and Titanium Diboride (TiB_2) nanoparticulates on the microstructure and properties of Al Si9 Cu3 Fe1 alloys for high pressure die casting applications.

OCTOBER 2011

[illegible] $_2$O [illegible] T [illegible] T B_2 [illegible] C [illegible] 1 [illegible]

AC[illegible]O[illegible]D[illegible]TS

T[illegible] T[illegible] C[illegible] C[illegible] B[illegible] C CB [illegible] C[illegible] C T [illegible] C [illegible] 0 00 200 [illegible] B [illegible] T 200 00001 2 [illegible] C T [illegible] T C [illegible] 0 00 200 [illegible] B [illegible] T 200 0000 [illegible]

[illegible] C CB [illegible] TE [illegible]

T [illegible] T [illegible] C [illegible] E [illegible] C [illegible] E [illegible] TEC [illegible]

[illegible] B [illegible] B [illegible] B [illegible] C T [illegible] T C [illegible]

[illegible]

[illegible] $_2$O [illegible] T [illegible] T B$_2$ [illegible] C [illegible] 1 [illegible]

LIST OF ACRONYMS

[illegible]

B B [illegible]

CTE C [illegible] T [illegible] E [illegible]

C [illegible]

T [illegible] T [illegible]

C [illegible]

E E [illegible]

E E [illegible] R [illegible]

C [illegible] C [illegible]

C [illegible] C [illegible]

B [illegible] T [illegible]

$_2$T [illegible] [illegible]

C [illegible] C [illegible]

[illegible]

C [illegible] C [illegible]

O O [illegible]

C [illegible] C [illegible]

R R [illegible]

[illegible]

E E [illegible]

[illegible]

[illegible]

T B$_2$ T [illegible]

T 1 [illegible] R [illegible]

T [illegible] T [illegible]

[illegible]

R R [illegible]

[illegible]

[illegible] $_2O$ [illegible] T [illegible] T B_2 [illegible] C [illegible] 1 [illegible]

I D **PA**

C O E E E T [illegible]

T O CRO [illegible]

E [illegible]

CHAPTER 1: INTRODUCTION. OBJECTIVES OF THE THESIS [illegible] 1

CHAPTER 2: LITERATURE REVIEW [illegible]

CHAPTER 3: EXPERIMENTAL PROCEDURE [illegible]

[illegible] $_2O$ [illegible] T [illegible] TiB_2 [illegible] C [illegible] 1 [illegible]

CHAPTER 4: SOLIDIFICATION & MICROSTRUCTURE [illegible]

CHAPTER 5: MECHANICAL PROPERTIES. [illegible] 12

CHAPTER 6: CONCLUSIONS. [illegible] 11

CHAPTER 1: INTRODUCTION. OBJECTIVES OF THE THESIS

[illegible] $_2O_3$ [illegible] TiB_2 [illegible] C [illegible]

CHAPTER 1: INTRODUCTION. OBJECTIVES OF THE THESIS.

1.1 Introduction

The [illegible] C [illegible] The [illegible] 0 [illegible]

[illegible] C [illegible] 1 [illegible] C [illegible]

The [illegible] C [illegible] 1 [illegible] $_2O_3$ [illegible] TiB_2 [illegible] C [illegible] 1 [illegible] C [illegible] 1 [illegible] E 0 [illegible] TiB_2 [illegible] 2 μ [illegible] 0.02 [illegible] 1 [illegible] T [illegible] E [illegible] 02 [illegible]

The [illegible] 200°C [illegible] 00 [illegible] The [illegible] 1 [illegible] 1 [illegible] 0 [illegible] 200 [illegible] TiB_2 [illegible] 2 [illegible] The [illegible] TiB_2 [illegible]

[illegible] $_2O_3$ [illegible] TiB_2 [illegible] C [illegible]

CHAPTER 1: INTRODUCTION. OBJECTIVES OF THE THESIS.

[illegible] C [illegible] C [illegible] 0.00200 [illegible] B [illegible] T200 00001 2 [illegible] C T [illegible] T C [illegible] 0.00200 [illegible] B [illegible] T200 0000 [illegible]

1.2 Objectives

[illegible] TiB_2 [illegible] $_2O_3$ [illegible] 1 [illegible]

O [illegible] C [illegible] 1 [illegible] C [illegible] 0 [illegible] C [illegible] T [illegible] TiB_2 [illegible] 2 [illegible] C [illegible] C [illegible]

1.2.1 Analysis of the influence of the TiB_2 and Al_2O_3 nano-particles on the solidification and microstructure of the Al Si9 Cu3 Fe1 alloy

TiB_2 [illegible] T [illegible] 1 [illegible] T [illegible] 0 [illegible] 0 [illegible] C [illegible] 1 [illegible] TiB_2 [illegible]

TiB_2 [illegible] TiB_2 [illegible] E [illegible] T [illegible] E 0 [illegible]

CHAPTER 1: INTRODUCTION. OBJECTIVES OF THE THESIS.

[illegible]

[illegible]

[illegible]

[illegible]

[illegible] $_2O_3$ [illegible] TiB_2 [illegible] C [illegible]

CHAPTER 1. INTRODUCTION. OBJECTIVES OF THE THESIS.

The [illegible] α [illegible] T1 [illegible] T [illegible] B1 [illegible] T [illegible] O [illegible] E [illegible] E [illegible] T [illegible] E [illegible] TE [illegible] TiB_2 [illegible] $_2O_3$ [illegible] T [illegible] TiB_2 [illegible] $_2O_3$ [illegible] C [illegible]

B [illegible]

1.2.2 Analysis of the influence of the Al_2O_3 and TiB_2 nano-particles on the mechanical and thermal properties of the Al-Si9 Cu3 Fe 1 alloy.

T [illegible] C [illegible] C [illegible] T [illegible] TiB_2 [illegible] $_2O_3$ [illegible] T [illegible] 200 °C [illegible] T [illegible] °C [illegible] T [illegible]

T [illegible]

CHAPTER 2: LITERATURE REVIEW

[illegible] $_2O$ [illegible] T[illegible] [illegible] TB_2 [illegible] C[illegible]

C[illegible]APT[illegible] 2[illegible] [illegible]IT[illegible]ATU[illegible] [illegible]I[illegible]

2.1 Introduction

[illegible] E[illegible] T[illegible] C[illegible]

[illegible] C[illegible] T[illegible] 11 [illegible] 0 [illegible] 00 [illegible] T[illegible]

T[illegible] 1[illegible] 2[illegible] T[illegible] T[illegible] C[illegible] β[illegible] T[illegible] T[illegible] TB_2[illegible]T[illegible] C[illegible] 1[illegible] T[illegible] T[illegible] B1[illegible]

[illegible] $_2$O [illegible] T [illegible] B_2 [illegible] C [illegible]

C APT 2 IT ATU I

[illegible] C T [illegible] T [illegible] $_2$O C B C T B_2 [illegible] T [illegible] T [illegible]

- [illegible]
- [illegible]
- [illegible] T [illegible] T [illegible]
- C [illegible] R [illegible] T [illegible]
- [illegible]

T [illegible] T [illegible]

[illegible]

[illegible]

[illegible]

2.2 High pressure die casting process

[illegible]

[illegible] $_2O_3$ [illegible] T[illegible] [illegible] T[illegible]B_2 [illegible] C[illegible] [illegible]

C[illegible]APT[illegible] 2[illegible] [illegible]IT[illegible]ATU[illegible] [illegible]I[illegible]

T[illegible] [illegible] [illegible] T[illegible] [illegible]

[illegible] C[illegible] [illegible] C [illegible] C [illegible] 2[illegible] [illegible] B[illegible] [illegible] C [illegible]

T[illegible] [illegible] T[illegible] [illegible] T[illegible] [illegible] T[illegible] [illegible] 2[illegible] T[illegible] [illegible] 200[illegible]00[illegible]C[illegible]

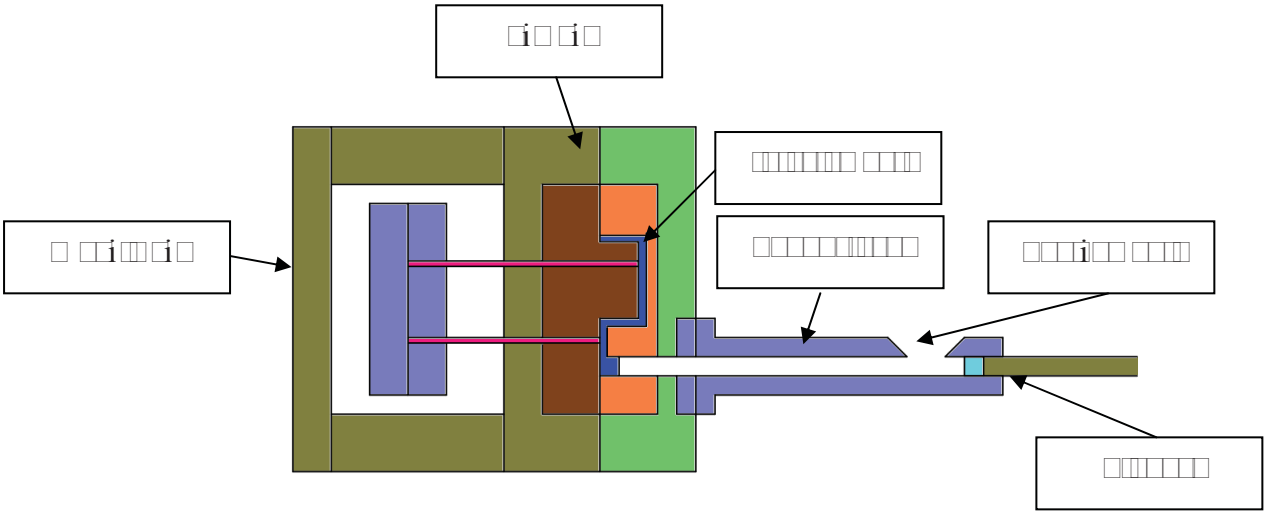

Fig.2.1 [illegible]Illustration of cold chamber high pressure die casting.

[illegible] $_2$O [illegible] T [illegible] B_2 [illegible] C [illegible]

C APT 2 IT ATU I

[illegible] C [illegible]

1 [illegible]

2 [illegible]

R [illegible]

[illegible]

T [illegible]

T [illegible]

T [illegible] 100 [illegible] 1000 C [illegible][1] T [illegible]

T [illegible] C [illegible][2] [illegible] T [illegible] [illegible][2] [illegible] C [illegible] 0 [illegible] 100 [illegible] 000 [illegible] 100000 [illegible]

[illegible]

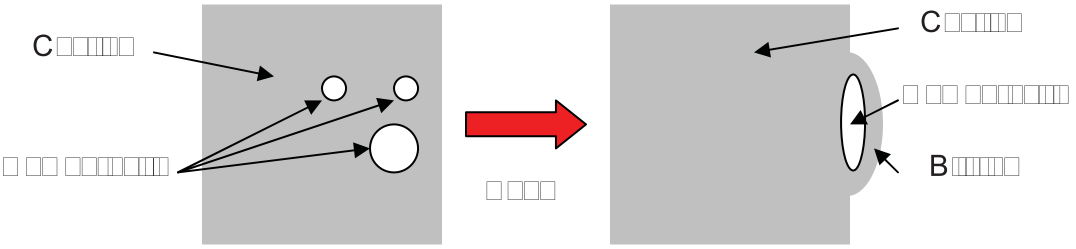

Fig.2.2 Blistering process with entrapped gas porosity.

[illegible]

[illegible]

[illegible]

[illegible] $_2O$ [illegible] T[illegible] [illegible] TB_2 [illegible] C[illegible] [illegible]

C[illegible]APT[illegible] 2[illegible] [illegible]IT[illegible]ATU[illegible] [illegible]I[illegible]

2.2.1 Aluminium alloys.

[illegible] T[illegible] O[illegible] [illegible]

T[illegible] 2[illegible]1[illegible]

Alloying elements	Designation
[illegible]00 [illegible]	1[illegible]

[illegible]

C[illegible]	2[illegible]
[illegible]	[illegible]
[illegible]	[illegible]
[illegible]	[illegible]
[illegible]	[illegible]
[illegible]	[illegible]
O[illegible]	[illegible]
[illegible]	[illegible]

Table 2.1[illegible]Aluminium [illegible] rought Alloys Classification.

2.2.2 Aluminium based die casting alloys

B[illegible] C[illegible] [illegible]0[illegible] [illegible]12[illegible] [illegible]0[illegible]2[illegible] [illegible]0[illegible] C[illegible] [illegible]

2.2.2.1 Aluminium Silicon Copper alloys

[illegible]

[illegible]

[illegible]

[illegible]

2.3 Aluminium grain refining

[illegible]

[illegible] $_2O$ [illegible] T [illegible] TiB_2 [illegible] C [illegible]

C APT 2 IT ATU I

T [illegible] 1B [illegible] T [illegible] B [illegible] T [illegible] C [illegible] B [illegible] T [illegible] T [illegible] C [illegible] B [illegible] T [illegible] C [illegible] T [illegible] C [illegible] T [illegible] C [illegible] B [illegible] R [illegible] 0 [illegible] T [illegible] T [illegible] B [illegible] T [illegible] TiB_2 [illegible] T [illegible]

T [illegible] 0 [illegible]

T [illegible] 1 [illegible] 1 [illegible] T [illegible] α [illegible] T [illegible] α [illegible] T [illegible] TiB_2 [illegible] T [illegible] C [illegible] T [illegible] 0 [illegible]

T [illegible] T [illegible] 0 [illegible]

[illegible] $_2O_3$ [illegible] T[illegible] [illegible] T[illegible]B_2 [illegible] C [illegible]

C[illegible]APT[illegible] 2[illegible] [illegible]IT[illegible]ATU[illegible] [illegible]I[illegible]

[illegible] R[illegible] 2[illegible]

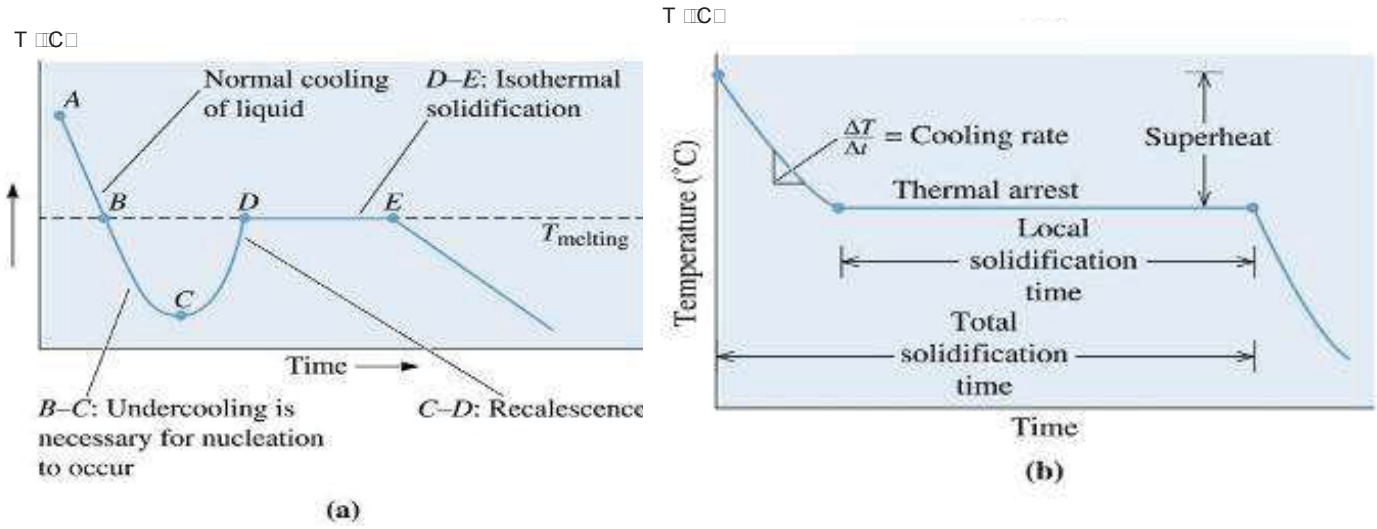

Fig.2.3. (a) and Fig.2.3. (b)[illegible]Solidification diagrams of Temperature [illegible]Time [illegible]As[illegible]03[illegible]

[illegible] $_2O_3$ [illegible] T[illegible]B_2 [illegible]

Solidification of aluminium alloys

O[illegible] T[illegible] T[illegible]

Homogeneous nucleation models of α-Al grains

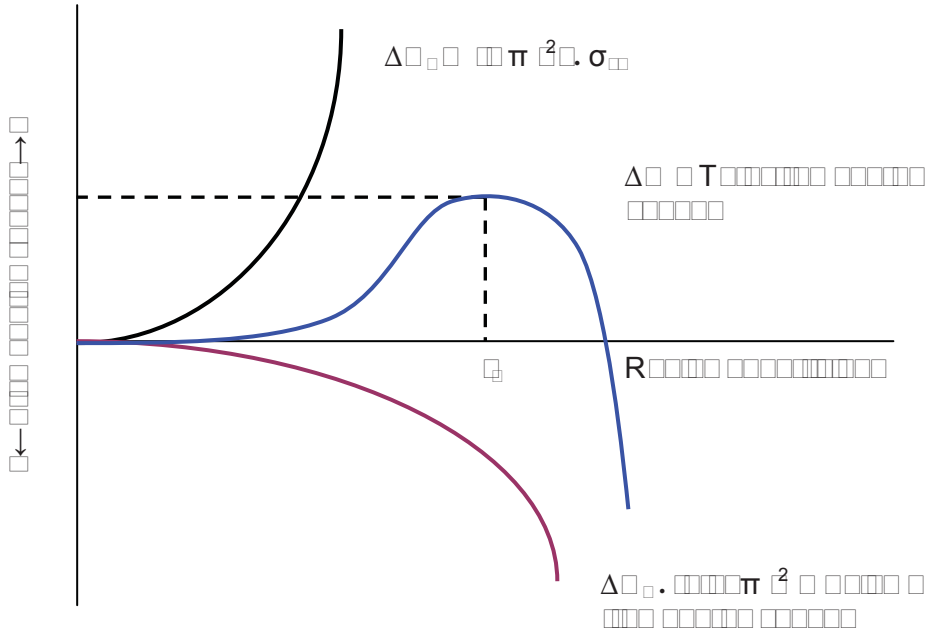

Fig.2.□□Determination of critical radius □As□03□.

[illegible] $_2O$ [illegible] T [illegible] B_2 [illegible]

[illegible] C [illegible]

C APT 2 IT ATU I

T [illegible] ΔT [illegible] Δ [illegible] $_\alpha$ [illegible] $_\gamma$ [illegible] γ [illegible] R [illegible]

$$\Delta \; \pi R^2 \; 1 \; R \; _\alpha - _\gamma \; \gamma \; \pi R \; _\alpha - _\gamma \; \pi R^2 \; \gamma$$

[illegible]

$$R \; 2\gamma \; _\alpha - _\gamma$$

[illegible] $_\alpha - _\gamma$ [illegible] $\Delta - T \Delta$ [illegible] T [illegible] T [illegible] C [illegible] Δ [illegible] T [illegible] Δ [illegible]

$$R \; 2\gamma \; _\alpha - _\gamma \; 2\gamma T \; \Delta \; \Delta T$$

T [illegible] Δ [illegible] C [illegible] 01 [illegible] 2 [illegible] C [illegible]

Δ

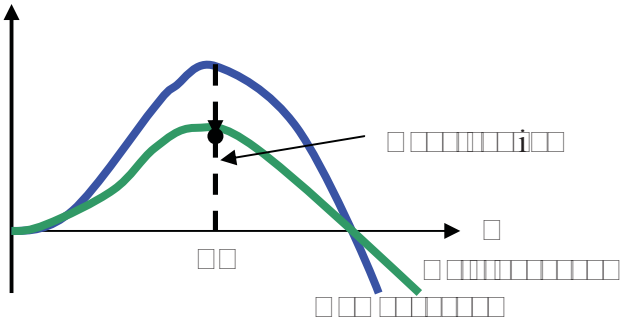

Fig.2. Undercooling variation between homogeneous and heterogeneous nucleation.

[illegible] $_2O$ [illegible] T[illegible] [illegible] TiB_2 [illegible] C[illegible] [illegible]

C[illegible]APT[illegible] 2[illegible] [illegible]IT[illegible]ATU[illegible] [illegible]I[illegible]

Heterogeneous nucleation models of α-Al grains

[illegible]

[illegible]

[illegible]T[illegible]

[illegible]

T[illegible] [illegible]T[illegible] [illegible]TiB_2[illegible]T[illegible]C[illegible]B_2[illegible]T[illegible] [illegible]B_2[illegible] [illegible] TiB_2 [illegible] $_2O$[illegible] [illegible]

A[illegible]Ti[illegible]B systems as grain refiners

T[illegible]T[illegible] [illegible]α[illegible] [illegible]C[illegible]T[illegible] [illegible] 00[illegible] [illegible]α[illegible] [illegible]0[illegible]01[illegible]

T[illegible] α[illegible]T[illegible] TiB_2 [illegible]T[illegible]B [illegible]0 0 0 1[illegible] [illegible]α[illegible]T[illegible] [illegible]α[illegible] [illegible]0 0 0 1[illegible] [illegible] α[illegible] [illegible] α[illegible] [illegible] α[illegible] [illegible]

The undercooling for which the hemispheric α-Al/liquid interface is in equilibrium marks the onset of the free growth and the effective initiation of the grain [Que 04-02]. The critical undercooling, ΔT_{fg} is calculated by:

$$\Delta T_{fg} = 4\gamma/\Delta S_{v.}d$$

Where γ is the interface energy value per surface unit between the two surfaces (solid / liquid interfacial energy), ΔS_v is the entropy of fusion per unit of volume and "d" is the particle diameter. Large particles become active nuclei at smaller undercoolings, and smaller inoculate particles remain inactive if the maximum undercooling reached in the melt does not exceed their critical ΔT_{fg}. For the aluminium alloys containing more than a 1% of silicon, the ratio Ti:B is increased to 1, with an Al Ti3 B3 composition.

In order to determinate the grain refinement of various aluminium-based alloys, we can use the grain growth index (GGI), represented as [Bac 00]:

$$GGI = \sum m_i C_i (k_i - 1) = m_1 C_1 (k_1 - 1) + m_2 C_2 (k_2 - 1) + ...$$

Where m_i is the slope of the liquidus in the binary (Al-i) system, C_i is the concentration of its dissolved solute in the alloy and k_i is the distribution coefficient of solute i between solid and liquid. m_1, C_1, K_1, etc. represents the corresponding values for each alloy constituent.

The amount of Ti results in a GGI value in refined alloy which corresponds to grain size less than equal to desired grain size (GGI_d), it can be calculated with the formula [Bac 00]:

$$Amount_{Ti} = \frac{GGI_d - GGI_b}{(K_{Ti} - 1) m_{Ti}}$$

Where "$amount_{Ti}$" is the percentage by weight of Ti to be added to the melt, "GGI_d" is the grain growth index resulting in aluminium castings having a minimal grain size, "GGI_b" is the grain growth index of the original aluminium base material, "m_{Ti}" is the slope of the liquidus in the binary (Al-Ti) system, "K_{Ti}" is the distribution coefficient of Ti between solid and liquid. Calculations can be made also with multinary systems. It exists a relationship between grain size and the dendrite coherency point (f_s*) which can be used to optimise nucleation. The dendrite coherency point is the moment when a solid phase network is established throughout the entire volume of a casting, and from the moment phenomenas like macro segregation, shrinkage, porosities and hot tearing start to develop. To establish the coherency point, the fraction solid is determined as function of the solidification rate (df_s/dt), by thermal analytical technique or by measuring the viscosity [Bac 00]. The grain size decreases (as the number of grain boundaries increases) when we increase the % of Ti [Que 04-02].

We can also see the relationship between the particle diameter and the undercooling needed for grain initiation. We can observe at Fig.2.6., that as the particle measure increases, the undercooling decreases, so the potential of been active as a nucleation site is increased. We can determinate that TiB_2 particles of about 1 micron can be active with only a 1°C of undercooling. However, very fine particles need a very high undercooling in order to be activated.

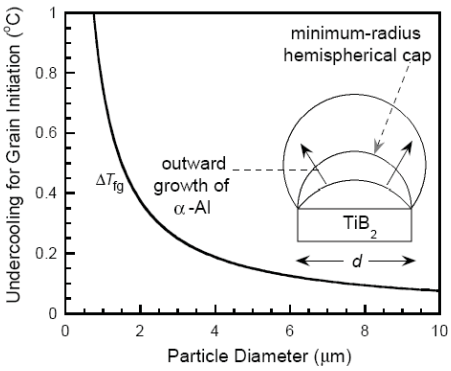

Fig.2.6.: Necessary undercooling in function of particle diameter [Que 04-02]

Maxwell-Mellawell theory (Heterogeneous nucleation) don't match the reality, being much more adequate then the isothermal-melt model. The grain refinement of aluminium silicon alloys is more difficult than with other alloys: the quantity of Si in the alloy has a great influence on it. As the silicon percentage is increased over 3 wt%, the grain refining loose their action, leading to an increase of the grain size [Que 04-02]. In the case of commercial grain refiners, there is a poisoning effect (Lost of the refiner characteristics with time), due to the interaction of silicon with refiners. This is also related with the time of effect of refiners. Refiners loose their properties in time (fading effect). As we increase the undercooling temperature, the minimum particle diameter working as a nucleus decrease, and as we increase the particle diameter, the required undercooling for nucleation decreases.

In our case the use of nano-particles should demand a higher undercooling, due to the small size, but in the other hand the fading effect should be eliminated, remaining the nucleation effect during the time. Also as they have a very high specific area and a tendency to agglomerate, clustering of particles acting as nucleation sizes could be detected.

2.4 Aluminium reinforcement

Aluminium metal matrix composites has been developed from the 1□□0□s. A composite is a heterogeneous mixture of two or more materials, which have been bonded together at a fine scale that can be considered a material with properties of its own. An aluminium metal matrix composite (A□C) contains the aluminium as the continuous matrix and a reinforcement which represents at least a few percent of the material. The two materials are originated from separate original components and which remain distinct in processing the material. The reinforcement is mostly added as particulates, but they are also for example continuous fibres, whiskers, short fibres and 3□ performs. They are several materials that are used as reinforcements as C, SiC, Si□$_2$, B_4C, Al_2□$_3$, TiB_2 [T□o 03].

The creep performance, toughness, wear resistance and the thermal stress are increased in those materials. Thermal and electrical conductivities can be high and tailorable. The biggest disadvantage of those materials is the high price, but also the galvanic corrosion, low ductility and anisotropy [□or 01]. They are many ways to obtain A□C, but they are 3 main routes, the liquid, the solid and the deposition process as we can observe in Fig.2.□ [□or1] :

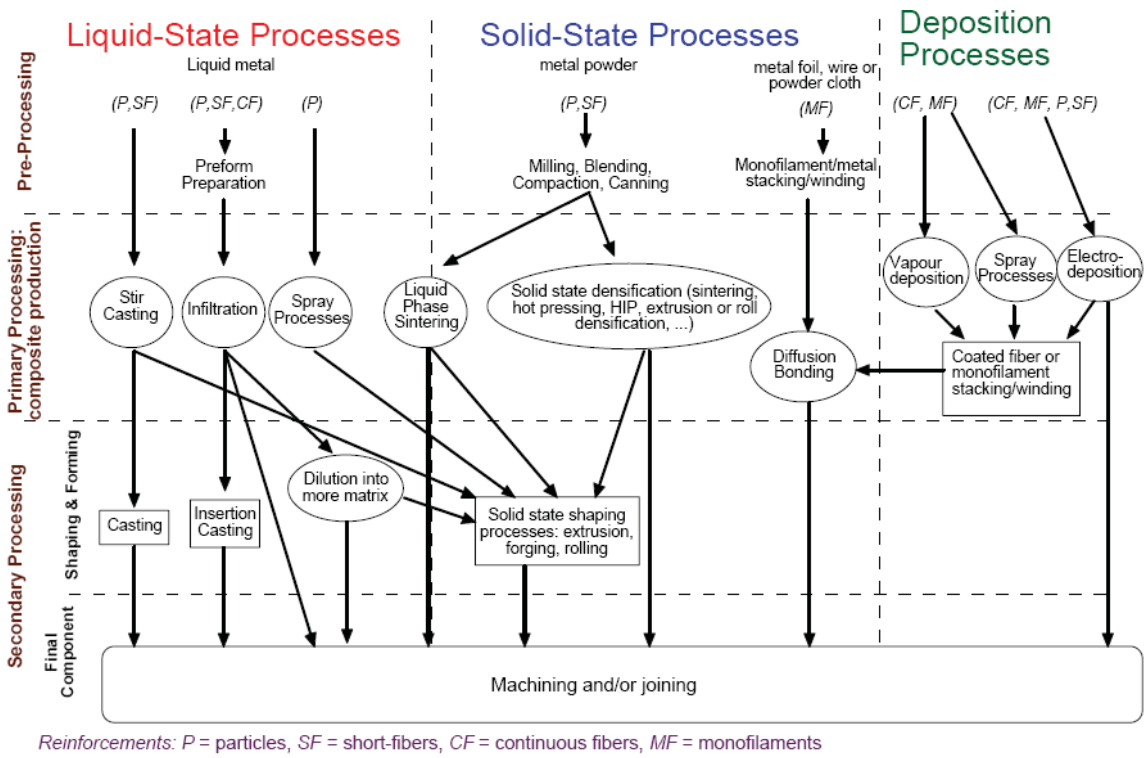

Fig.2.□: A□C processing routes [□or 0□]

CHAPTER 2: LITERATURE REVIEW

A□Cs are mostly fabricated by liquid ingot casting and powder metallurgy (□□) routes. Ingot casting process offers substantial cost reduction advantages in terms of mass production over □□ route. □owever, many structural defects such as gas porosity, oxide inclusions, agglomeration of the reinforcements and an interfacial product are often produced in cast A□Cs. Such defects affect the mechanical performances of A□Cs. From this aspect, squeeze casting can be used to eliminate gas porosity and shrinkage.

A□Cs generally are difficult to machine due to the high hardness and abrasive nature of the ceramic reinforcing phase. Accordingly, □□ route with near net shape capability is more attractive than the casting technique. Furthermore, □□ processing of A□Cs results in better mechanical properties with homogeneous microstructure, i.e. more uniform distribution of ceramic particles. Thus, the microstructures of A□Cs are sensitively determined by process conditions. Another promising method is infiltration. The ceramic reinforcement is formed previously, and placed in the die. Then aluminium is introduced in the die, covering the ceramic. Ceramic parts can be denses or have open or close porosity.

The incorporation of ceramic reinforcements to A□Cs generates the residual stresses during cooling from the material processing temperature. This is due to a large difference between the coefficient of thermal expansion (CT□) of the reinforcement and matrix. The thermal properties can be tailored through proper control of the reinforcement and matrix. TiB_2 particles increases in general the □TS and □S, and depending on the studies the elongation can increase or decrease [Tee 01] [□is 04]. Among the reinforcing particulates, titanium diboride (TiB_2) is particularly attractive because it exhibits high elastic modulus and hardness, high melting point, superior wear resistance and good thermal stability. □oreover, TiB_2 particles do not react with aluminium, thereby avoiding the formation of brittle reaction products at the reinforcement □matrix interface.

In A□Cs reducing grain size (□) has also an impact on strengthening precipitates or disperser size (δ), and increasing volume fraction (d) on strengthening in metallic alloys. The nanoscale structures can have a significant impact on the strength of metals, increasing mechanical properties [□av 0□]. □echanical properties are optimal for reinforcement size ranging from 10 to 40 nm. □owever, the particles must been desagglomerated. In our case, the nano-particles can produce a decrease of grain size and a strengthening of precipitates. Also, an increase in volume fraction by the high specific area can produce an increase of the mechanical properties.

Types of AMC materials

As metallic matrix, near all the most employed aluminium alloys have been reinforced with particles, but the most commonly used are the aluminium, magnesium and titanium, in spite of others like copper and iron. The AMC are classified according to the reinforcement shape and the name of the matrix, as we observe in Fig.2.□:

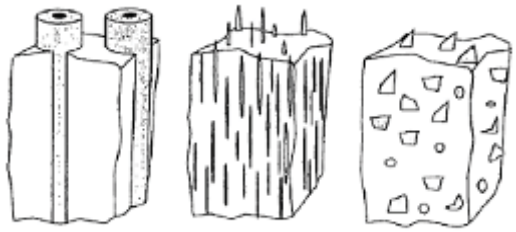

Fig.2.□: Reinforcement shape classification of AMC [□or 0□].

* ***Continuously reinforced AMCs:*** The metal is reinforced with a continuous reinforcement (monofilaments or fibre tows). The main problem is the chemical attack, because it can produce sometimes a galvanic corrosion, so if there is an interaction between the two materials, fibres are coated to avoid the galvanic par. The properties are anisotropic.

* ***Discontinuously reinforced AMCs:*** The metal is reinforced with a discontinuous reinforcement, and the reinforcement has not a chemical reaction with the matrix. The properties in this case are generally isotropic and can be tailored.

* ***Interpenetrating phase composites:*** The metal is reinforced with a three-dimensionally percolating phase, for example ceramic foam.

* ***Liquid phase sintered metallic materials:*** Include the cemented carbides, in which carbide particles are bonded together by a metal such as cobalt, or the tungsten heavy alloys.

Applications of aluminium metal matri□composites

The metal matrix composites have had a small penetration in general in fields like automotive, due to the high price of those products. The combination of good mechanical properties at high temperatures with a light weight has been employed in a wide range of products of different sectors. They are currently being used in applications such as components for aeronautics, sports, racings, etc.

Light weight automotive components: □ngine components (Connecting rods, Cylinder liners, bearing stiffeners, blocks and heads), Transmission parts (Synchronizer rings, valves, covers), Suspension components (Struts, hubs, C□□), Brake parts (Calliper bodies, brake disk, calliper pistons).

Light weight aerospace components: Aerofoils, leading edges, blades, landing gear parts, brake parts, spacecraft structural parts, mirror parts, satellite parts.

Sports: Golf puts, tennis racquets□

The most employed materials for reinforced metals by number are listed in fig.2.□. [□or 01], where we can observe how the Al_2□$_3$ and TiB_2 are one of the most commons:

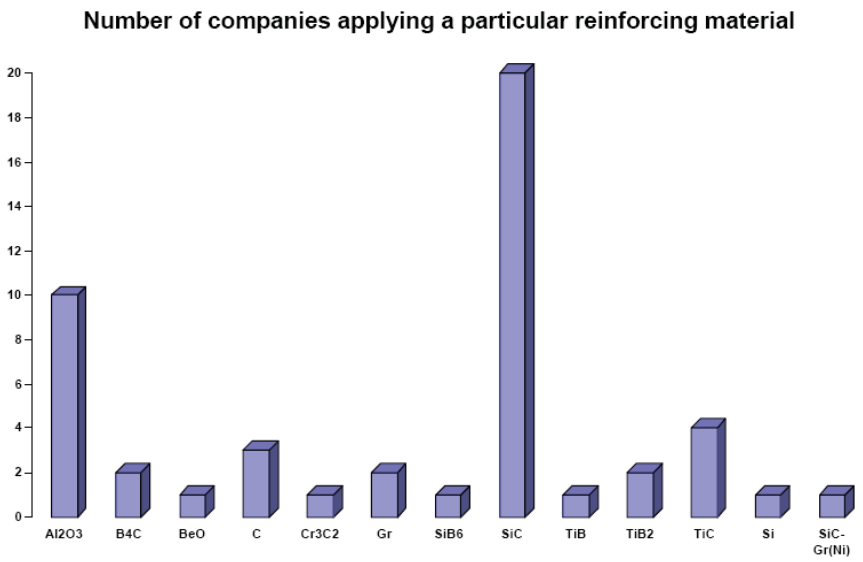

Fig.2.□: □aterials employed in □□Cs □y num□er of companies [□or 0□]

There are commercial aluminium alloys as □uralcan$^{T□}$ of Alcan, which can be employed by the □□□C casting process. □owever, there is no mass application for those materials and the developments have being employed in aeronautics, automotive and sports.

They are same problems in order to introduce A□Cs in a mass production process. □ormally those problems are related with the product price, the necessity of stirring the melt at the holding furnace, the recyclability, the cleanness of the melt, the employment of an inert gas and finally the machinability.

The porosity problems decrease, because ceramic particles tend to get around the porosity, and they decrease their volume. □owever, the higher viscosity promotes more incomplete filling, cold laps and inclusions. It□s expected to employ the developed alloys in new automotive applications, with higher requirements than nowadays products, especially at high service temperatures.

In situ produced Al/TiB_2-Al_2O_3 composites

The TiB_2 particles are reported to form from reactive hot pressing of either Al□Ti□B, Al□Ti□$_2$□B or Al□Ti□$_2$□B_2□$_3$ systems. □owever, Al_2□$_3$ particles are also in situ formed simultaneously in such systems. It is difficult to assess independently the reinforcing effect of in situ TiB_2 particles. □oreover, intermetallic compound (Al_3Ti) with plate-like structure is also induced in the above-mentioned systems. The formation of brittle Al_3Ti phase could lead to premature failure of in situ TiB_2 □Al_2□$_3$/Al composites. To eliminate intermetallic compound, the Al□TiB_2 composite can be fabricated via □□ process followed by hipping, in which the TiB_2 particulates are blended with Al powders. □ure Al is selected as the matrix material instead of the Al-alloy in order to exclude the precipitation hardening effect.

The interfaces of *in-situ* particle/matrix are clean and free of impurities or contaminants. The size of *in-situ* formed ceramic particles is in the order of 0.3 μm. They are thermodynamically stable and compatible with the matrix. *In-situ* particles formed in the aluminium alloys are typically of TiC and TiB_2 or combination of both TiC and TiB_2 phases. TiB_2 particulate is particularly attractive because it exhibits high hardness, superior wear resistance, high melting point, good thermal stability, high stiffness and high strength at elevated temperatures. In contrast to SiC, TiB_2 particles do not react with aluminium, thereby avoiding the formation of brittle reaction products at the reaction□matrix interface. Al_3Ti block particles with several tens of micrometers in size are formed in the Ti□Al□B system. The yield strength of (TiB_2□Al_2□$_3$)/Al composites tends to increase with increasing TiB_2 content. A strong interfacial bonding exists between the TiB_2 reinforcing phase and the matrix, and this contributes to superior creep resistance [□ho 11],[□it □□],[T□o 03].

CHAPTER 2: LITERATURE REVIEW

It is generally known that the particle sizes of the matrix and reinforcing ceramic powders play an important role in the distribution of reinforcing particles in the matrices of □□□Cs. Fine reinforcing particles often tend to agglomerate into clusters during □□ processing. The degree of homogeneity of the particle dispersion is determined by the relative particle size (□□S) ratio between the matrix and reinforcing particles. □igher □□S ratios (40:1□2□:1□1□:1) favour particle clustering, thereby yielding poor tensile strength and ductility. Lower □□S ratios (e.g. □:1 and 3:1) promote a more uniform distribution of the reinforcement (SiC) in the 2124 Al matrix, leading to a higher strength in the composites. Increasing the □□S ratio results in a less-uniform reinforcement distribution [Tam 0□], which in turn leads to a decrease in the material manufacture and the mechanical properties of Al□□% Cu□0.4% □n/1□% SiCp composites. It is noted that □□S ratio can be varied by changing the particle size of either the reinforcement or the matrix, separately or simultaneously. □oung□s modulus and ultimate tensile strength of the Al□TiB_2p □□Cs tend to increase with increasing TiB_2 volume content at the expense of tensile ductility. Also reduces the coefficient of thermal expansion (CT□) of the Al□TiB_2 composites.

In situ Al/TiB_2 composites can be prepared using powder metallurgical technique and casting process. □xothermic dispersion reactions (□□ process) between the elemental powders of composites i.e. Al, Ti and B under either ingot casting or □□ route are commonly adopted to prepare in situ Al/TiB_2 composites. Gotman et al. used the S□S technique to fabricate in situ Al/TiB_2 composites. In this process, elemental powders of the composites were compacted and synthesized by utilizing the heat released during the exothermic reactions of their formation. The ignition of compacted powder mixtures by an electric current initiates a combustion wave that propagates through the blend, leaving behind the reaction products. □eactive spontaneous infiltration refers to the process in which in situ TiB_2 particles are formed by simultaneous infiltration of molten aluminium into ceramic fillers (Ti□ □ B) under a protective nitrogen or argon atmosphere.

□ther casting approach involves adding mixed Ti and B bearing salts (i.e. K_2TiF□ and KBF_4) to molten aluminium, being the most employed for the refining master alloy production. The reaction is:

$$K_2TiF_6 + 2KBF_4 + 10/3Al \rightarrow TiB_2 + 4/3(3KF.AlF_3) + 2AlF_3$$

K_2TiF□ and KBF_4 react with molten aluminium to produce $TiAl_3$ and AlB_2. After, there is a reaction between them, and Ti and B ions are released and diffused into liquid Al. When they reach saturation, they will be separated out as the intermetallic compounds TiB_2, $TiAl_3$ and AlB_2. A K_3AlF□ and KF mixture are formed due to excessive KF. Consequently, elements Ti and B from the salts tend to react with Al exothermically, giving rise to the dispersion of TiB_2 particles in the Al matrix. Among these processes, □□□ is attractive due to their simplicity and flexibility. □□□ encompasses both the exothermic conversion of reactants to in situ reinforcements and the subsequent hot compaction of the porous powder mixture. They have being synthesized in situ TiB_2 particulates from the Al□Ti□$_2$□B and Al□Ti□$_2$□B_2□$_3$ systems via reactive hot pressing of the elemental powders. For the Al□Ti□$_2$□B system, three types of in situ reinforcements, i.e. Al_2□$_3$, TiB_2 and Al_3Ti can be created during reactive hot pressing process. The synthesized reactions can be summarized as:

$$3Ti\square_2 \square 13Al \rightarrow 2Al_2\square_3 \square 3Al_3Ti \quad (1)$$

$$3Ti\square_2 \square \square B \square 4Al \rightarrow 2Al_2\square_3 \square 3TiB_2 \quad (2)$$

In the absence of boron, only Ti□$_2$ reacts with Al, leading to the formation of Al_2□$_3$ and Al_3Ti phases (□eaction (1)). Al_3Ti is an intermetallic compound having low density, high melting point, high hardness, and high □oung□s modulus. Also it□s very brittle, due to its tetragonal structure and platelet morphology.

□ffort has been expended to eliminate the Al_3Ti compound in the □□□ process via the incorporation of B into the Ti□$_2$□Al system (reaction (2)). In this case, in situ TiB_2 and Al_2□$_3$ particles are created at the expense of Al_3Ti. Thus the amounts of Al_2□$_3$, TiB_2 and Al_3Ti phases can be controlled by varying the boron content. For the synthesis of in situ Al composites using Al□Ti□$_2$□B_2□$_3$ system, excess B from B_2□$_3$ can react with Ti from Ti□$_2$ to produce Al_2□$_3$ and TiB_2 reinforcement in the Al composite. The following reactions are expected:

$$B_2\square_3 \square 2Al \rightarrow Al_2\square_3 \square 2B \quad (3)$$

$$3Ti\square_2 \square 4Al \rightarrow 2Al_2\square_3 \square 3Ti: \quad (4)$$

The Ti reduced from the reaction (4) then reacts with B to form TiB_2 or with Al to form Al_3Ti according to reaction:

$$Ti \square 2B \rightarrow TiB_2 \quad (\square)$$

$$Ti \square 3Al \rightarrow Al_3Ti \quad (\square)$$

It is suggested that Ti can also react with Al and B to form titanium aluminium borides $(Ti,Al)_xB_y$ via the following reaction:

$$xTi \square xAl \square yB \rightarrow (Ti,Al)_xB_y$$

The main disadvantage of in situ composites is that TiB_2 particles are pushed to the grain boundaries and they get agglomerated [Sch 0□], having a reduced effect in the nucleating process, to reduce the interfacial energy.

Ex situ produced Al/TiB_2 – Al_2O_3 composites

Generally, the ceramic reinforcements are prepared independently and incorporated into the matrix alloy during conventional liquid casting and □□ routes. Such composites fabricated are termed as ex situ composites. The ex situ □□Cs fabricated by those methods are still not economically favourable due to the high cost of reinforcing particles. □oreover, ex situ ceramic particulates generally have a size ranging from a few micrometers to several hundred micrometers. Large ceramic particulates often act as micro concentrators of stress and give rise to particle fracture during mechanical loading.

□ecently, novel in situ processing such as exothermic dispersion (□□), reactive hot pressing (□□□), self-propagating high temperature synthesis (S□S) and reactive infiltration have attracted considerable attention. In these processes, ceramic reinforcing particles are formed in situ in the matrix melt from the chemical reactions or from the exothermic reactions between the elemental powders of composites under hot pressing conditions. □ltrafine in situ ceramic particulates are thermodynamically stable, free of surface contamination and disperse more uniformly within the matrices of □□Cs, leading to stronger particle-matrix bonding. Such unique properties make in situ □□Cs possess excellent mechanical properties and economical viability vs. their ex situ counterparts. TiB_2 particulates with the average size of about 1 μm reinforcement phase can be synthesized via self-propagating high-temperature synthesis (S□S) reaction of □0 wt.% Al□Ti□B systems, with the molar ratio of Ti to B= 1:2. Al (□□.0 purity, 2□ μm), Ti (□□.□ purity, 1□ μm), and B (□□.0 purity, 3 μm) are mixed by ball milling for □ h and are mechanically pressed into a cylindrical perform. The cylindrical perform with about □0% theoretical density is heated in a closed electronic resistance furnace filled with high purity Ar gas. At about □□0□□20 ◦C, a S□S reaction of Al□Ti□B system takes place and TiB_2□Al master alloy is then formed. Composite specimens with □.□ wt.% TiB_2 can be prepared by adding the desired amount of TiB_2□Al master alloy to molten metal and using the semisolid slurry stirring technique. The composite melt is stirred in the semisolid temperature range for 20 min, and the composite slurry is heated to □00 □C and poured into a steel mould.

CHAPTER 2: LITERATURE REVIEW

The cyclic responses of Al-based □□Cs reinforced with ex situ ceramic particles are known to be very sensitive to the matrix microstructures or aging heat-treatment. □nder aged and naturally aged composites with very fine precipitates display cyclic hardening behaviour fatigued at various applied strain amplitudes, due the interactions among dislocations. □eak aged composites exhibit cyclic hardening cycled at higher applied strain amplitudes, but the hardening is less pronounced when compared with naturally aged □□Cs. Composites prepared from the Ti□$_2$□Al□B system exhibit higher yield and tensile strengths than composites fabricated from the Al□Ti□$_2$□B_2□$_3$ system. This is due to a complete elimination of brittle Al_3Ti phase in the composite 1 by proper ad□usting of the molecular ratios of B/Ti□$_2$ to □/3. The size of in situ TiB_2 particles formed in the matrix of Al-based composites varies from 0.□ to 1.□ µm.

For the first trials, commercial TiB_2 have been chosen, with a measure of about 3 □□ µm (-32□ □esh). This material should be reduced (by ball milling) to a measure below 0.□ µm. TiB_2 is produced by using a continuous chemical process that controls stoichiometry and particle size to create high purity powder. The shapes of the processed crystals are flat, hexagonal platelets. When solidified into shapes, the resultant ceramic is electrically conductive, a property very rare among ceramic materials. This makes it valuable in electrical applications and also enables it to be formed into complex shapes using electrical discharge machining (□□□).

Applications

□□lectrically conductive composites such as aluminium evaporation boats. As an excellent conductor of both electricity and heat, TiB_2 is valuable in electronic and special applications.

□□efractory material and antioxidant additive that is no reactive to most molten non ferrous metals and alloys. Also for thermal management materials, because TiB_2 enhances thermal conductivity when used as filler in polymeric matrices.

□□ilitary armour because it□s tough enough, and also improves fracture toughness of ceramic cutting tools and other components.

□Additives for producing special ceramic composite materials. Titanium □iboride will not react with molten non ferrous metals including Cu, □n and Al. TiB_2 is used as crucibles, vacuum metallization components and electrodes for processing these materials.

As we have observed before, the alumina is greatly employed to obtain aluminium metal matrix composites. In Table 2.2. we can see some applications of nanoalumina:

Application	□ar□et segment	E□amples
Transparent improvement of scratch resistance in various coating systems	Lacquers □ coatings. Cosmetics	Scratch-proof automotive topcoats, parquet lacquers, furniture lacquers, lacquers for electronic devices. Scratch-proof nail polish.
Controlled ad□ustment of translucence and transparency	Lacquers □ coatings. Cosmetics. □lastics	□se as matting agent for lacquers and coatings. Controlled ad□ustment of translucence in creams. □se as matting agent.
Transparent control of rheological properties in liquids and pastes	Inks □ paints. Ceramics	□eduction of structural viscosity in ink □et formulations. □roduction of ceramic slurries with high solid content.
Transparent improvement of mechanical properties	□ental materials. □lastics. Fibres □ textiles	Improvement of the mechanical properties of dental nanocomposites, of plastics in general, of fibres in general and of the converting of master batches filled with particles in fibre spinning plants.

Ta□le 2.2: Applications of nanoalumina [Nan □□]□[□u□ □□].

In automotive brake discs, drums, callipers or back-plate applications are employed. □artially reinforced piston for use in diesel engines AlSi12Cu□g□i (KS 12□□□3.4032) reinforced with Saffil (α-Al_2□$_3$) short fibre 10, 1□ and 20 vol.%. □ther suitable applications are found in engine and gearbox parts. Bike and golf components are also developing rapidly. In our case, we□ll investigate the reinforcement with nano-particles of A□Cs, expecting better isotropic properties with a good particle distribution, due to the nano-particle size of the particles.

2.4.□ Influence of reinforcements in aluminium alloys properties.

The reinforcements in aluminium promote the increase of creep performance, toughness, wear resistance and the thermal distortion, with a combination of good mechanical properties at high temperatures and a light weight. Tensile measurements [□ah 0□] show that □oung□s modulus and ultimate tensile strength tend to increase with increasing reinforcement volume, but with a decrease of tensile ductility. In order to determinate the most important mechanical properties in materials that are working at traction forces, the tensile test are employed. Test bars are tested in equipments where the relation between the stress and the deformation are registered, giving a stress-strain diagram as shows simplified in Fig. 2.10. From this diagram we can determinate the yield stress, the ultimate tensile stress, the elastic modulus and the elongation, that are employed in the design of parts. The yield stress (□S) represents the stress at which plastic deformation becomes noticeable. It□s chosen when a 0,2% plastic deformation has taken place. In the yield stress area the material deforms without an increase in applied load. In the stress hardening there is an increase in the material resistance, due to the change in the atomic and crystalline structure.

We can observe a decrease in the stress after the ultimate stress point, but is promoted by the decrease in the lateral area of the sample. From the diagram we can obtain also the elastic modulus (□) that is defined as the slope in the linear region and the elongation (ε), which corresponds with the plastic deformation in the broken test bar. □TS gives the stress before necking.

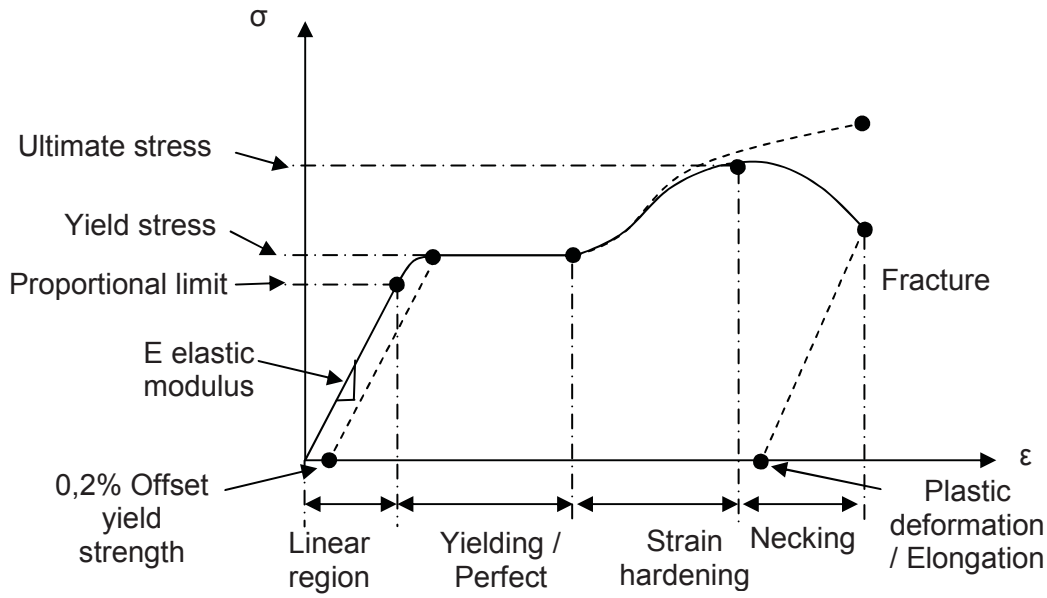

Fig.2.□0.: □tress □strain diagram

In order to design a part that must support a charge during use, we must assure that the part doesn□t plastically deform. In this case we should select a material with high □S. In the case of ductile material with an important plastic deformation, the □TS is not very important, but it can give us the hardness and the soundness of the part. In our case, both properties and the elongation are important parameters to determinate, due to the behaviour as not very plastic materials of the Al Si□Cu3 alloys.

In order to determinate the mechanical properties in function of the composition of the alloy, experimental formulas have been [□ac □□], employing an experiment design employing an L1□ and a modified L□ Taguchi orthogonal array in the limits of concentration of the allowing elements of Al Si hypoeutectic alloys. We can observe the equations for □S, □TS and □longation:

□ield □trengt□:

P1= (9.81 + 0.49 Si + 1.44 Cu + 1.48 Fe +13.07 Mg + 1.01 Mn + 1.45 Ni + 3.84 Cr + 0.34 Zn + 5.81 Ti + 12.72 Sr)x6.89512.

Ultimate Tensile Strength:

P2= (44.93 □0.46 Si + 0.67 Cu □0.18 Fe + 0.76 Mg □0.13 Mn + 0.23 Ni + 0.16 Cr + 0.32 Zn + 0.20 Ti + 0.35 Sr)x6.89512.

Elongation:

P3 = (10.62 □0.61 Si □0.50 Cu □0.46 Fe □0.57 Mg □0.21 Mn □0.07 Ni + 0.06 Cr + 0.25 Zn +0.08 Ti + 0.07 Sr)x6.89512.

□n order to increase alloys properties and specially the YS □e should study □hat are the parameters that can increase the YS. The increase in YS can □e attri□uted to the coupled effects of□

(a) Oro□an strengthening□

(□) □rain refinement□

(c) Formation of internal thermal stress due to different CTE □alues □et□een the matrix and the reinforcement particles□

(d) Effecti□e load transfer □et□een the matrix and the reinforcement□

(e) □ardening due to the strain misfit □et□een the reinforcing particulates and the matrix.

The contri□utions to the increase in the YS of the composites □y the □arious strengthening mechanisms could □e taken as a simple summation of the root of the sum of s□uares of the different mechanisms, and ha□e □een discussed in se□eral recent studies. O□ing to the presence of the dispersed nano□si□e particles in the matrix, dislocation loops form as dislocation lines □o□ and □ypass the particles.

There is a general formula (generali□ed □all Pech e□uation) to calculate the YS, taking into account more □aria□les than the medium diameter of the nucleus, as the microstructures and dislocations. □n general it has □eing assumed that a decrease of nucleus diameter promotes an increase of YS. YS can □e calculated □ith the general formula □Lem 81□, □Cly 93□, □□an 05□, □□rp 03□, □□lu 11□□

$$\sigma = \sigma_i + \sigma_s + \sigma_p + \sigma_d + \sigma_{ss} + \sigma_t + \sigma_{hp}$$

□ here□

σ_i □Stress induced resistance □ecause the friction generated □y the opposition to the dislocations mo□ement.

σ_s □ Stress induced resistance □y the solid solution elements (Function of the concentration of elements and the difference □et□een the atomic radius of solute and sol□ent).

σ_p □Stress induced resistance □y the precipitates (Function of precipitates concentration and the a□erage distance).

σ_d □Stress induced resistance □y dislocations (Function of shear modulus, □urgers □ector and the dislocation density).

σ_{ss} □Stress induced resistance □y the su□□grains or □y the su□□structure (□elation □ery similar to □all□Petch).

σ_t □ Stress induced resistance □y the texture or isotropy (Function of preferential crystallographic directions)

σ_{hp} □Stress deduced from □all□Petch relation for grain si□e. The refinement in grain si□e arises as a result of the presence of reinforcing particles □hich act as nucleation sites during recrystalli□ation, and the pinning of grain □oundaries. The contri□ution to the increase in YS due to grain si□e strengthening can □e descri□ed □y the □all□Petch e□uation □Zha 08□□

$$\sigma_{hp} = K \square d^{-1/\square}$$

□here □ is the □all□Petch coefficient, and d is the grain diameter.

□t may □e noted that, □ased on the contri□utions □y the a□o□e□mentioned strengthening mechanisms, the YS of the composites should increase □ith increasing □olume fraction of reinforcement. □o□e□er, □hen the □olume fraction of nano□particulates is increased, the strength and ductility of the composites drops □ut remains higher than compared pure metal one □□um 91□. This may □e due to the agglomeration of nanoparticulates □ith increasing □olume fraction, □hich reduces the Oro□an strengthening effect. The increment in ductility of the aluminium □y reinforcement particulates may □e attri□uted □Mah 08□ to a more uniform microstructure □here stress concentration is reduced, a uniform distri□ution of reinforcements and □ery short distances □et□een nanoparticles that pre□ent crack gro□th and their interconnection. Ultra□fine ceramic particles inhi□its stress concentration and crack gro□th. □f the S□□S decreases □□ro 09□, UTS and elongation are increased.

□n our case, □e ha□e chosen □ery lo□ percentages of reinforcement particles in order to a□oid the drop in the mechanical properties □y increasing the □olume fraction.

2□□2 Ti□$_2$ □eneralities

Titanium di□oride, Ti□$_2$, is a ceramic compound from the com□ination of titanium and □oron, □ith hexagonal crystal structure and space group P6/mmm. □t has a high melting point (around 3225□C), hardness, strength to density ratio and □ear resistance. □t can□t □e found in the nature, and can □e prepared □y many different methods as direct reaction, car□othermal reduction, S□S reaction□

□t is resistant to oxidation at high temperatures and to □F and □Cl acids, □ut not to alkalis, □$_2SO_4$ and □NO_3. □t don□t reacts □ith many melted metallic alloys, so is employed in aluminium melting as thermocouples, cathodes for aluminium smelting, chemical applications and as a reinforcement for composites. □t□s a ceramic □ith high thermal and electrical conducti□ity. □t can □e shaped to a desired shape □ith high or lo□ densification porosity, and can □e also machined □y electrical discharge. □n order to produce near dense Ti□$_2$, se□eral methods ha□e □een employed, including sintering, hot pressing, hot isostatic pressing, micro□a□e sintering, dynamic compactness, □acuum arc melting, spark plasma sintering and S□S □Mor1□.

The production of **<u>in sit□ Al□Ti□$_2$</u>** metal□matrix composites (MMC) is □ased on a process in □hich titanium (□$_2TiF_6$) and □oron (□□F_4) containing salts are reacted □ith molten aluminium to generate *in-situ* Ti□$_2$ particulates. Cryolite salts react □ith the molten □l alloy such that the titanium and □oron enter the aluminium and com□ine to form in situ Ti□$_2$ particles of a□out 1□m si□e. The remaining cryolite slag is decanted from the furnace and the □l□Ti□$_2$ master alloy is alloyed to its final composition and cast to □illet or □affle plate □Mor 01□.

They are also ne□ techni□ues to prepare *ex-situ* nanocrystalline Ti□$_2$, □y S□S, mechanical alloying, sol□othermal reaction □□u 02□and solution phase reaction. □n the next chapters □e □ill explain a ne□ method de□eloped in the pro□ect for the nano Ti□$_2$ production. The process has □een optimised to achie□e a 20 □t.% reinforcement on la□oratory scale. Superior material properties are strongly dependent on the homogeneous distri□ution of fine Ti□$_2$ particles in the □l matrix. The a□erage particle si□e is 1 to 2 □m, gi□ing additional mechanical strength due to dispersion hardening □MMC 01□. □n our case, □e ha□e employed t□o different *ex-situ* Ti□$_2$ particles, □ith the same high energy □all milling process, in order to o□tain Ti□$_2$ nano□particles □ith an a□erage si□e of 500 nm. The 2 employed Ti□$_2$ particles are□

1) **SHS Ti□$_2$ □ro□□□e□ at Te□nalia** from Ti and □ □ith a Ti□$_2$ grain si□e from 1 to 6 microns.

2) **Sol□othermal □ro□esse□ □ommer□ial Ti□$_2$** produced □y the □ith a mesh 325 grain si□e.

Structure

The Ti□$_2$ has a pre□alent co□alently □ounded and hexagonal close□packed crystal structure of the □l□$_2$ type, designated C32, □ith space group P6/mmm. The lattice parameters ha□e slight □uadratic dependence, and a = □=302.9, c = 322.9, α = β =90□, γ = 120□, as □e can o□ser□e in Fig.2.11. The pre□alent co□alent □onding determinates the lo□ ductility, high hardness and high melting point.

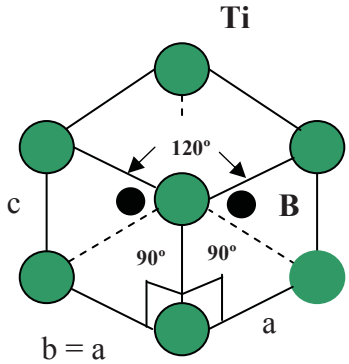

□ig□2□□□: S□heme o□the □r□stal str□□t□re o□Ti□$_2$□

Properties

Ti□$_2$ has a high hardness and stiffness, in com□ination □ith high electrical and thermal conducti□ity. The thermal and electrical conducti□ity is not a normal characteristic of most con□entional ceramics. □t offers a com□ination of attracti□e properties, □ith high hardness, high strength, high specific modulus, high melting point, excellent □earing and oxidation resistance at high temperatures (Up to 1400 □C).

In the Table 2.3. we can resume the TiB_2 properties for a material with a density of 4.5 ± 0.1 g/cm^3 and a grain size of 9±1 µm [Mun 00]. We can observe TiB_2 properties, and specially the maintenance of the elastic modulus and flexural strength at high temperatures, that can provide the increase of mechanical properties at higher temperatures for the elected alloy. We will test how TiB_2 particles modify alloy properties and if we get the expected improvements.

Property	20ºC	500ºC	1000ºC	1200ºC	1500ºC	2000ºC
Bulk modulus (GPa)	240	234	228			
Compressive strength (GPa)	1.8					
Creep rate[c] (10^{-9} s^{-1})					0,005	3,1
Density[d] (g/cm^3)	4.500	4.449	4.389	4.363	4.322	4.248
Elastic modulus (GPa)	565	550	534			
Flexural strength (MPa)	400	429	459	471	489	
Fracture toughness (MPa m$^{1/2}$)	6,2					
Friction coefficient[e]	0.9	0.9	0.6			
Hardness (GPa)[f]	25	11	4.6			
Lattice parameter[d] a /Å	3.029	3.039	3.052	3.057	3.066	3.082
Lattice parameter[d] c /Å	3.229	3.244	3.262	3.269	3.281	3.303
Poisson's ratio	0.108	0.108	0.108			
Shear modulus (GPa)	255	248	241			
Sound Velocity, longitudinal[g] (Km/s)	11.4	11.3	11.2			
Sound velocity, shear[g] (km/s)	7.53	7.47	7.40			
Specific heat (J kg^{-1} K^{-1})	617	1073	1186	1228	1291	1396
Thermal conductivity (W m^{-1} K^{-1})	96	81	78.1	77.8		
Thermal diffusivity (cm^2/s)	0.30	0.17	0.149	0.147		
Thermal expansion[d,h] αa (10^{-6} K^{-1})	6.4	7.0	7.7	7.9	8.3	8.9
Thermal expansion[d,h] αc (10^{-6} K^{-1})	9.2	9.8	10.4	10.6	11.0	11.6
Thermal expansion[h] αm (10^{-6} K^{-1})	7.4	7.9	8.6	8.8	9.2	9.8
Wear coefficient[e] (10^{-3})	1.7					
Weibull modulus	11					

Table 2.3: properties of TiB_2 [Mun 00]

[a] Density 4.32 g/cm^3, grain size 2 µm, V_{slide} /P_{load} = 0.2 ms^{-1} MPa^{-1}

[b] Vickers indentation, load = 5 N

[c] □ingle crystal, hexagonal unit cell.

[d] Single crystal.

[e] ρ = 4.32 g/cm3, g = 2 µm, vs/Pc = 0.2 m s^{-1} MPa^{-1}.

[f] Vickers hardness, load = 5 N.

[g] vshear = $(G/\rho)^{1/2}$; vlongitudinal = $[(4/3)\ G/\rho + B/\rho]^{1/2}$.

[h] Coefficient of thermal expansion $\alpha_x = (1/x_0)(x-x_0)/(T-T_0)$, x = a or c , cumulative from the reference state at 20 ºC(Corresponding to T_0 = 293 K); $\alpha_m = (2\alpha_a+\alpha_c)/3$.

Applications

TiB_2 applications have been limited to very specific applications, due to the processing cost of the material and the variability in the material properties. It has been employed in aluminium melting, impact resistant armors, cutting tools, crucibles and resistant coatings.

2.□3 Alu□ ina □Al_2□$_3$□. □eneralities.

Aluminium oxide is an amphoteric oxide of aluminium with the chemical formula Al_2O_3. It is also commonly referred to as alumina or aloxite in the mining, ceramic and materials science communities. It is produced by the Bayer process from bauxite. Its most significant use is in the production of aluminium metal, although it is also used as abrasive, due to its hardness, and as a refractory material due to its high melting point.

Corundum is the most common naturally-occurring crystalline form of aluminium oxide. Much less-common rubies and sapphires are gem-□uality forms of corundum with their characteristic colours due to trace impurities in the corundum structure. □ubies are given their characteristic deep red colour and their laser □ualities by traces of the metallic element chromium. Sapphires are in different colours given by various other impurities, such as iron and titanium.

Properties

Aluminium oxide is an electrical insulator but has a relatively high thermal conductivity (40 W/m K). In its most commonly occurring crystalline form, called corundum or α-aluminium oxide, its hardness makes it suitable for use as an abrasive and as a component in cutting tools. Aluminium oxide is responsible for metallic aluminium□s resistance to wearing. Metallic aluminium is very reactive with atmospheric oxygen, and a thin passivation layer of alumina □uickly forms on any exposed aluminium surface. This layer protects the metal from further oxidation. The thickness and properties of this oxide layer can be enhanced using a process called anodising. A number of alloys, such as aluminium bronzes, exploit this property by including a proportion of aluminium in the alloy to enhance corrosion resistance. The alumina generated by anodising is typically amorphous, but discharge assisted oxidation processes such as plasma electrolytic oxidation result in a significant proportion of crystalline alumina in the coating, enhancing its hardness. Aluminium oxide was taken off the □nited States Environmental Protection Agency□s chemicals lists in 1988. Aluminium oxide is in the Toxics □elease Inventory (T□I) list of the Environmental Protection Agency (EPA) if it is in a fibrous form.

CHAPTER 2: LITERATURE REVIEW

Aluminium oxide, also known as alumina, is the main component of bauxite, the principal ore of aluminium. The largest manufacturers in the world of alumina are Alcoa, Alcan and □usal. Companies which are specialized in the production of special aluminium oxides and aluminium hydroxides. The bauxite ore is made up of impure Al_2O_3, Fe_2O_3, and SiO_2. Bauxite is purified by the Bayer process [Hid 99]□

$$Al_2O_3 + 3\ H_2O + 2\ NaOH \rightarrow 2\ NaAl(OH)_4$$

The Fe_2O_3 does not dissolve in the base. The SiO_2 dissolves as silicate $Si(OH)_6^{2-}$. □pon filtering, Fe_2O_3 is removed. When the Bayer li□uor is cooled, $Al(OH)_3$ precipitates, leaving the silicates in solution. The mixture is then calcined (heated strongly) to give aluminium oxide□

$$2\ Al(OH)_3 + Heat \rightarrow Al_2O_3 + 3H_2O$$

The alumina formed tends to be multi-phase, i.e. constituting several of the alumina phases rather than solely corundum. The production process can therefore be optimized to produce a tailored product. The type of phases present affects, for example, the solubility and pore structure of the alumina product which, in turn, affects the cost of aluminium production and pollution control.

Structure

The crystal system of corundum (α-Alumina) is a trigonal Bravais lattice with a space group □-3c, 2 formula units per unit cell of aluminium oxide, but is most commonly referred to a slightly distorted hexagonal close-packing of oxygen ions, or a larger hexagonal cell with 6 formula units, as we can observe in the Fig.2.12. Alumina has also other phases (γ,δ,ε,η,θ,χ,□), all corresponding to the Al_2O_3 formula, but the only one that its thermo stable is the α-Alumina. The electro negativity of alumina is 2, with a 63□ of ionic character and 37□ of covalent.

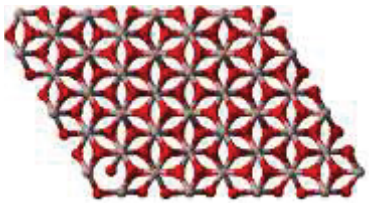

□i□.2.□2.: □□□e□ e of t□e □rystal stru□ture of Al_2□$_3$ [Wi□ □□].

Properties

Alumina has a very interesting combination of mechanical, electrical and chemical properties. Mechanically is very hard, resistant to abrasive wear and dimensional stable. Electrically it has high resistivity, good dielectric strength and low dielectric loss factor at high fre□uencies. It is inert against from chemicals, maintaining characteristics at high temperature [Jac 77]. The melting temperature is 2030 – 2050 ºC, boiling temperature□3500 ºC, thermal conductivity □k□is 30.1 W/m.K, the lineal dilatation coefficient is 8.3 - 9 x 10^{-6} ºC, thermal conductivity 10^{-10} – 10^{-12} $(\Omega.m)^{-1}$, the tensile strength is 380 GPa, Poison coefficient of 0.26, hardness of 18-23 HV (GPa), ultimate strength of 200 - 345 MPa and a density of 3.97 g/cm^3. In the table 2.4., we can resume the Alumina properties for a high purity (99.5 □ or higher) and nearly fully densified (98 □ of the theoretical density, or higher) sintered alpha-alumina materials with a nominal grain size of 5 µm. The good properties of the elastic modulus and flexural strength at high temperatures can provide the increase of mechanical properties at higher temperatures for the elected alloy. Because of that we want to explore the potential application of Al_2O_3 in the reinforced alloys.

Property	20ºC	500ºC	1000ºC	1200ºC	1400ºC	1500ºC
Bulk modulus (GPa)	257	247	237	233	229	227
Compressive strength (GPa)	3.0	1.6	0.7	0.4	0.3	0.28
Creep rate (10^{-9} s^{-1}) at 150 MPa	0	0	4	280	6600	24600
Density (g/cm^3)	3.984	3.943	3.891	3.868	3.845	3.834
Elastic modulus (GPa)	416	390	364	354	343	338
Flexural strength (MPa)	380	375	345	300	210	130
Fracture toughness (Mpa $m^{1/2}$) for crack length of 300 µm	3.5	3.0	2.7	2.6	2.5	2.5
Friction coefficient [] at 2 GPa	0.40	0.8	0.4			
Hardness (GPa) (Vickers, 1 kg) [GPa]	15	8.5	4.6	3.7	2.9	2.5
Lattice parameter a /Å	4.761	4.777	4.797	4.806	4.815	4.820
Lattice parameter c /Å	12.991	13.040	13.102	13.129	13.156	13.169
Poisson's ratio	0.231	0.237	0.244	0.247	0.250	0.252
Shear modulus (GPa)	169	158	146	142	137	135
Sound Velocity, longitudinal (Km/s)	11.00	10.77	10.54	10.44	10.35	10.30
Sound velocity, shear (km/s)	6.51	6.33	6.14	6.06	5.97	5.93
Specific heat (J kg^{-1} K^{-1})	755	1165	1255	1285	1315	1330
Tensile strength (MPa)	267	267	243	140	22	13
Thermal conductivity (W m^{-1} K^{-1})	33	11.4	7.22	6.67	6.34	6.23
Thermal diffusivity (cm^2/s)	0.111	0.0251	0.0150	0.0136	0.0127	0.0124
Thermal expansion from 0ºC αm (10^{-6} K^{-1})	4.6	7.1	8.1	8.3	8.5	8.6
Wear coefficient (10^{-3})	-4	-6				
Weibull Modulus	11	11	11	11	11	11
Weibull modulus	395	390	360	310	210	125

Table 2.□: properties of AL_2□$_3$ [MU□ □□] [MMC 0□□2].

Applications

Annual world production in 2005 of alumina is approximately 45 million tones, over 90□ of which are used in the manufacture of aluminium metal. The ma□or uses of special aluminium oxides are in refractories, ceramics, polishing and abrasive applications. Large tonnages are also used in the manufacture of zeolites, coating titania pigments, and as fire retardant /smoke suppressants.

Alumina is a medium for chemical chromatography, available in basic (pH 9.5), acidic (pH 4.5 when in water) and neutral formulations. In lighting, GE developed □Lucalox□in 1961, a transparent alumina used in sodium vapor lamps. Aluminium oxide is also used in preparation of coating suspensions in compact fluorescent lamps.

Health and medical applications include it as a material in hip replacements. It is used in water filters (derived water treatment chemicals such as aluminium sulfate, aluminium chlorohydrate and sodium aluminate, are one of the few methods available to filter water-soluble fluorides out of water). It is also used in toothpaste formulations.

Most pre-finished wood flooring now uses aluminium oxide as a hard protective coating. In 2004, 3M developed a techni□ue for making a ceramic composed of aluminium oxide and rare earth elements to produce a strong glass called transparent alumina. Alumina can be grown as a coating on aluminium by anodizing or by plasma electrolytic oxidation (see the □Properties□section, Table 2.3.). Its strength and abrasive characteristics are due to aluminium oxide□s great hardness (position 9 on the Mohs scale of mineral hardness).

It is widely used as a coarse or fine abrasive, including as a much less expensive substitute for industrial diamond. Many types of sandpaper use aluminium oxide crystals. In addition, its low heat retention and low specific heat make it widely used in grinding operations, particularly cutoff tools. As the powdery abrasive mineral aloxite, it is a ma□or component, along with silica, of the cue tip □chalk□used in billiards.

Aluminium oxide powder is used in some CD/DVD polishing and scratch-repair kits. Its polishing □ualities are also behind its use in toothpaste. Is also widely used in the fabrication of superconducting devices, particularly single electron transistors and superconducting □uantum interference devices (S□ □ID), where it is used to form highly resistive □uantum tunneling barriers.

2. Processing of aluminium matrix reinforced alloys

2.1. Introduction.

As we have seen before, there are several ways to produce aluminium reinforced alloys. In our case, we have elected the reinforcement with externally produced particles in the liquid state because is a cheap process that generates the same properties in all the directions. However, in order to get the better properties, a good process must be employed. Ceramic particles must have for our project the smallest possible size, and we have chosen SHS as the process for the production on TiB_2 particles because it produces small TiB_2 particles about 1-5 microns at a good processing cost. As we decrease particle size, particles tends to agglomerate, promoting a decrease in properties and a more inhomogeneous structure. Also the introduction of ceramic particles in liquid aluminium is very complicated, due to the tendency to get indissolved in the dross. In order to produce parts in an economic and industrial way, HPDC process has been elected. In the next points we'll review all the process aspects that have to be studied in order to get the best properties for an industrial process.

2.2 Formation and particle segregation

2.2.1 In situ formation of reinforcement particles

In the case of producing TiB_2, in order to introduce the borides particles in the melting, the most employed process is by reacting borides particles with the aluminium in the melt, by means of a salt which reacts with aluminium to produce boron, and one or more salts which reacts with aluminium to produce a boride-forming metal or metals. In situ production of the boride particles produces particles with less than 1 micron in size.

2.2.2 Ex situ formation of reinforcement particles

However, AMC have been fabricated by the dispersion of very fine (Less than 0.1 micron) oxide or carbide particles throughout the metal or alloy matrix, by mechanical mixing of metal powders of 5 micron diameter or less with the oxide or carbide powder (Preferably 0.01 micron to 0.1 micron). Presence of oxygen can result in oxide formation at the interface of the ceramic, and the metal desinhibit interfacial binding between the ceramic phase and the matrix, adversely effecting ductility, reducing strength, loss of elongation and crack propagation. It's important that the metal is capable of dissolving or sparingly dissolving the constituents of the ceramic phase, and having a lesser capability for dissolving the ceramic precipitate. Metal matrix component must act as a solvent for the reaction species, but not for ceramic precipitate. In the case of Al_2O_3 lot of commercial types of nanosized particles are available, because it's one of the most employed nano-particles.

For our pro□ect, we have elected the composition and size of commercial Al_2O_3 nano-powders to be introduced in li□uid aluminium, avoiding li□uid dissolutions that should promote an explosion, and we have developed the reduction of SHS formed TiB_2 from the micron size to the nano-size, because no commercial nano-TiB_2 was available at the beginning of the pro□ect.

2.□.3 Mi□ture an□ □ettin□ of parti□les

2.□.3.□ □oli□ state □ i□ture of parti□les

The mixture of aluminium and reinforced particles can be made in the solid or li□uid state. In the case of solid state, nanocrystalines powders made by milling process must be consolidated in a bulk form. Powder consolidation lead to significant grain growth, because traditional consolidation involves high temperatures (at least 0.8 T_m, with T_m the melting temperature). Nanometric surface modification of the nanometric powders consisting on zincating and further on, electroless plating of copper in nanoparticulate form on nanostructured makes the conventional powder metallurgy consolidation possible at much lower temperatures. This is a result of the Gibbs-Thompson effect under which nanoparticles freely coalesce into agglomerates until the energy of the agglomerates e□uals the surface energy. An increase in temperature reactive the nanoparticle coalescent mechanism, which finally results in complete compact at lower temperatures. Atomic-scale computer simulations have previously identified a deformation mechanism, which becomes important in nanocrystalline metals with grain sizes below 10–15 nm. Instead of proceeding through dislocation activity in the grains, the deformation occurs by slip events in the grain boundaries, leading to a reverse Hall–Petch effect, i.e. a decrease in hardness with decreasing grain size.

In most coarse-grained metals, severe plastic deformation leads to grain refinement. Indeed, severe plastic deformation is often used to generate nanocrystalline metals with grain sizes down to hundred nanometres. Simulations indicate that those processes are suppressed in sufficiently small grains, and instead the sliding events in the grain boundaries dramatically enhance diffusion processes, and lead to grain coarsening as the deformation proceeds [Sch 04]. Grain boundaries are found to participate directly in the deformation process of nanocrystalline metals, and at sufficiently small grain sizes they appear to be carrying the ma□ority of the deformation.

A systematic variation of the mechanical properties with grain size is seen. The metal becomes harder as the grain size is decreased, but if the grains reached a small enough size, the critical grain size which is typically less than 100 nm (3.9 □10□6 in), the yield strength would either remain constant or decrease with decreasing grains size [Con 00]. This is called the reverse Hall-Petch effect, since the opposite behaviour is usually seen in metals with larger grain sizes.

In coarse-grained metals, the plastic deformation is carried by dislocations, and the grain boundaries act as barriers to the dislocations. □educing the grain size thus reduces the mobility of the dislocations, and leads to a harder metal. In nanocrystalline metals with sufficiently small grain sizes, the ma□or part of the plastic deformation is carried by the grain boundaries at least according to the computer simulations. It is, therefore, not surprising that decreasing the grain size leads to a softening of the metal, as the volume fraction of the grain boundaries increases.

Based on the simulations, one can therefore predict that there should be an □optimal□ grain size, where the hardness of a metal is maximal [Sch 01], as we can observe in fig.2.13. We can note that grain sizes about 20 nm has the highest hardness, with a reduction in hardness in case we reduce more the grain size

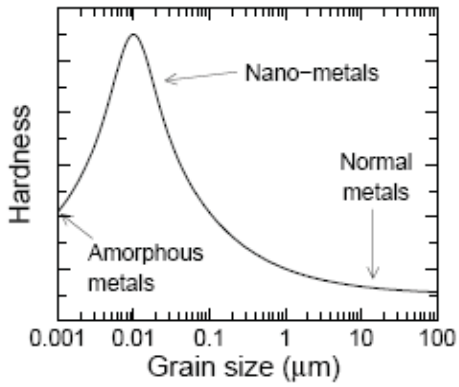

□i□.2.□3.: Relation bet□een □rain si□e an□ □ar□ness [□□□ 0□]

2.□.3.2 Li□ui□ state □i□ture of parti□les

The li□uid mixture is made as its name indicates the mixing of ceramic particles in the aluminium matrix by different methods. One of the ways of dispersing the materials in the li□uid aluminium is to wrap them into an aluminium film. After pouring the metal over the film, powders are reduced and correctly dispersed in the aluminium matrix [Miy 73]. The particles that are hard, insoluble and with pin shape are not ade□uate to be dispersed in the li□uid aluminium, due to their tendency to create defects as pin holes and tears [Sig 86]. It's beneficial to introduce the powder over an extended period of time, wrapped in a foil of aluminium [Ban 88].

The reasonably uniform distribution of reinforcement particulates can be attributed to suitable blending parameters and the high extrusion ratio used in secondary processing. In theory, homogeneous distribution of reinforcements can be obtained, irrespective of the size difference between the matrix powder and the reinforcement particulates, provided a large deformation load is applied during secondary processing.

However, a limited amount of clustering of reinforcement is unavoidable in this case, owing to the high surface energy associated with the nanoparticles. Minimal standard deviation in density measurement results also reflects the uniform distribution of reinforcement in the synthesized materials. Marginal grain refinement in composite samples as a result of the presence of particulates can be attributed to□

(a) The ability of nano-size particulates to nucleate grains during recrystallization;

(b) The restricted growth of grains due to grain boundary pinning. There is also an ideal percentage of nano-reinforce.

□esults are better for nano than micro reinforcing particles. Nanoclusters are formed in the initial stage of the phase decomposition and play very important roles in producing nanoprecipitates. Micro alloying elements are also expected to modify the nanostructures of aluminium alloys. Nanoclusters act as useful nucleation sites for precipitates inside the grain and near the grain boundaries [Sat 06].

TiB_2 and Al_2O_3 crystals are insoluble in aluminium. □apid cooling must be got for avoiding crystal to increase its size. If TiB_2 crystal have a measure □ of 1 μm, it don't increase their size, maintaining their dimensions at high temperatures in long periods of time [All 74]. If matrix grains are smaller than 30 μm, TiB_2 crystals are very well dispersed, due to the abundance of grain borders and also by the dispersion of same TIB_2 particles inside the grains.

In our case we have elected the stirring method. Aluminium and reinforcement particles are ball milled and cold pressed. In order to get a better distribution of nanoparticles in the li□uid aluminium a vigorous stirring process is employed.

Al_2O_3 crystals are excellent insulators. They have large band gap energies (Eg), i.e., Eg(Al_2O_3) =8,8 eV. Electrons in these oxides are strongly localized and the production and diffusion of ionic defects in the oxides are limited. Therefore, long-range charge transfer and ion transport do not occur in those oxides at relatively low temperature (e.g., □1.000 ºC). Metal interactions with these insulating oxides are often confined to the interfaces, which only involve oxide surface atoms and metal atoms in contact with the substrate surface. The interactions are strongly dependent on the surface properties of oxide substrates. Surface stoichiometry, surface finishing, and surface defects are the most important factors influencing the metal–oxide interactions.

CHAPTER 2: LITERATURE REVIEW

Among the various polymorphs of alumina, corundum, α-Al_2O_3, is the most stable phase and has been sub□ected to extensive studies. In particular, the crystallographically simple and energetically stable α-Al_2O_3(0001) surface offers a good playground for understanding of insulating oxide surfaces and metal–Al_2O_3 interactions. Alumina surfaces are often prepared by mechanical polishing, ion sputtering, and annealing. Naturally, different surface preparation processes result in various surface properties, which, in turn, may cause different behaviours of metal growth on these surfaces. The most stable structure of Al/Al_2O_3 interfaces is reached for metals on the oxygen terminated surface as long as the oxygen chemical potential is above a critical value. Many theoretical results show that hydroxylation of the clean α-Al_2O_3(0001) surfaces may result in a further lowering of the energy of those surfaces. The above mentioned O^- and Al terminated surfaces are expected to be reactive to water.

The theoretical results of metal interactions on alumina surfaces rely on the choice of the surface termination (Al-terminated or O-terminated), calculation models (cluster or slab) and metal coverage (isolated atom or metal film). The bonding between the metals with small Pauling electro negativity and Al_2O_3 is mainly ionic. Abs initio calculations of bonding at Al(111)/α-Al_2O_3(0001) interface also indicate that Al–O bonds constitute the primary interfacial interaction. The bonds are very similar to the cation–anion bonds found in Al_2O_3 bulk and are mainly ionic. Various surface science studies have confirmed that oxidation reactions can happen between metals and α-Al_2O_3(0001) surfaces near room temperature. In the oxidation, reactions are strictly limited to the interfaces. Subse□uently, metallic over layers will develop with metal coverage above 1 monolayer. The results clearly show that all of the interfaces are atomically sharp and no interface reaction phases thicker than a monolayer have been observed.

The results indicate that only those metal and atoms right at the interface, which are in contact with surface oxygen, became oxidized. Alumina has a high thermodynamic stability ($\Delta H^o f$ □ □600 kJ $mol^{□1}$) and oxygen diffusion in the crystal is highly limited. The oxidation of metal multilayer may be either thermodynamically impossible or/and kinetically limited [Fu 07].

Aluminium oxide nanoparticles have important applications in ceramic industry and can be used as an abrasive material, in heterogeneous catalysis, as an absorbent, a biomaterial and as reinforcements of metal–matrix composites (MMCs). In order to be used for effective discontinuous reinforcements in a continuous metal–matrix, Al_2O_3 particles have to fulfil certain structural and morphological re□uirements□small particle size and narrow size distribution, large surface area, spherical morphology and the absence of agglomerates. As far as the hot wall aerosol synthesis method (Spray Pyrolysis), as basic chemical route for obtaining advanced materials, is concerned, it offers several advantages in the preparation of well-defined oxide powders over conventional synthesis [Mar 08].

□educing the sizes of low dimensional materials leads to dramatic increase in the portion of surface/interface atoms. The properties of a solid are essentially controlled by related surface/interface energies. Although such changes are believed to dominate behaviours of nanoscale structures, little experience or intuition for the expected phenomena, especially for the size-dependence of the energies and their practical implications, are modelled analytically. The classic thermodynamics as a powerful traditional theoretical tool is used to model different bulk interface energies and the corresponding size dependences. During the modelling, an emphasis on size dependences of the interface energies is given, which is induced by size dependence of coherent energy of atoms within nanocrystals. It is found that solid–vapour interface energy, li□uid–vapour interface energy, solid–li□uid interface energy, and solid–solid interface energy of nanoparticles and thin films fall as their diameters or thickness decrease to several nanometres while the solid–vapour interface energy ratio between different facets is size-independent and e□uals to the corresponding bulk value. Predictions of the established analytic models without any free parameters, such as size and temperature, dependences of these four kinds of interface energies and related surface stress, correspond to experimental or other theoretical results. The established models are suitable for low dimensional materials with different dimensions and different chemical bond natures. Moreover, several related applications in the fields of nanophase transitions, nanocrystal growth, and self-diffusion of li□uids are known [Jia 08].

In our case, the election of Al_2O_3 has been done in order to have as we have note before a small particle size and narrow size distribution, large surface area, spherical morphology and the absence of agglomerates in order to have an effective reinforcement. All these aspects are cover with the 15 nm γ Al_2O_3 and 40 nm α Al_2O_3, because they have a spherical morphology and a very narrow size distribution. In the case of TiB_2, we have not so rounded particles, with 3 different dispersion curves, but the most important distribution if about 500 nm. However, the particle size is smaller, due to the differences in size measure due to agglomeration.

CHAPTER 3: EXPERIMENTAL PROCEDURE

CHAPTER 3: E□PERIME□TAL PR□CE□URE

3.□Intro□u□tion

High pressure die casting (HPDC) is a foundry process that belongs to the family of metallic die casting technologies, in which a metallic die (Normally H11 or H13 steel) are used to produce complex parts. The metal is feeded inside the cavity, and during the solidification, a pressure is applied in order to decrease the porosity, to feed all the part and to decrease the lineal contraction (From 1.5□ to 0.7□). Dies are submitted to thermal cycles, due to the heat transferred from in□ected metal to the die. In order to avoid the metal to get stuck in the die, lubricants and cooling lines are employed, and finally thermo-regulating the temperature of the die. The HPDC has been selected to carry out the study of the influence of TiB_2 or Al_2O_3 reinforced metals as it's a very attractive way of mass production of MMC components. On the one hand, it's possible to cast near shape components that reduce machining operations (Very important to avoid the wear of toolings when they work with ceramic reinforcements). On the other hand, it's also a very suitable foundry technology to produce high □uality automated mass productions with a very □uick and inexpensive process. The final cost may be compensated by the production of big series (Due to the very expensive dies employed in the process) and by replacing materials more expensive or with higher density.

The industrialization of MMC by HPDC has in the other hand the problem of getting a good distribution and wettability of reinforcement particles. Same intents to get MMC□s by HPDC infiltration of performs are being investigated, but some problems as the good infiltration and the fixation of performs to die must be overcome [Kau 07]. The number of publications dealing with MMCs processed through HPDC is low, in comparison with semisolid or molten metal in□ected by HPDC. The literature is based in Die casting of MMC by the li□uid metallurgy and by mechanical alloying and sintering.

3.2 □ele□tion an□ a□□uisition of □ aterials

3.2.□ Intro□u□tion. □ele□tion of □ aterials

The reinforced materials employed for this work are not all commercially available and are produced at lab scale for research related pro□ects or industrial casting trials. They are based on the Al Si9 Cu3 Fe1 aluminium alloys to which up to 1 wt. □ TiB_2 or Al_2O_3 nanoparticles were incorporated to improve their performance. The Al Si9 Cu3 Fe1 is a hypoeutectic aluminium-silicon alloy. The castability of the alloy for die casting is □uite good, but alloys with increased Si have more fluidity.

In order to have a common nomenclature in the next sections, we define the different reinforced alloys as□

1) 0.2 wt.□ SHS TiB_2 reinforced alloy. 500 nm of average size.
2) 0.2 wt.□ Commercial TiB_2 reinforced alloy. 500 nm of average size.
3) 0.17 wt.□ α alumina reinforced alloy. 40 nm of average size.
4) 0.1 wt.□ γ Alumina reinforced alloy. 15 nm of average size.

3.2.□.□ TiB_2

TiB_2 particles are commercially available and have been produced by the Momentive performance materials company, by using a continuous chemical process that controls the stoichiometry and particle size to create high purity powders. The product is named HCT-F. The shapes of the processed crystals are flat, hexagonal platelets. They have a size in the range of 3-6 μm (Mesh -325). The surface area is 1.0 (m^2/g). Also SHS produced TiB_2 has been produced at Tecnalia, with a TiB_2 grain smaller than 5 μm. As the minimum particle size is of 0.5 μm, and the desired shape is not the platelets, a dry ball milling process with stainless steel balls and a wet high energy ball milling has being made in order to decrease to a nanometric size and to round the TiB_2 particles, with SHS and commercial TiB_2 particles. There was not any nano TiB_2 commercially available at the beginning of this work.

□ele□tion of □ aterials an□ pro□essin□ □ et□o□ for □H□ TiB_2

The employed e□uipment for SHS reaction is composed by a mixer, a bri□uetting tool, an SHS reactor and generator, and a ball milling device, as we can observe in Fig. 3.1. We can see the process□ 1) Aluminium and TiB_2 particles are mixed in a mixer machine, 2) they are cold pressed, obtaining a bri□uette that is placed in reaction base, 3) Vacuum is made in the reactor, 4) the electric generator gives the necessary electrical discharge for start the SHS reaction, 5) a master alloy is obtained and 6) finally is milled to reduce its size.

Mixer	Cold Press
	
Bri□uette	**SHS Preparation**
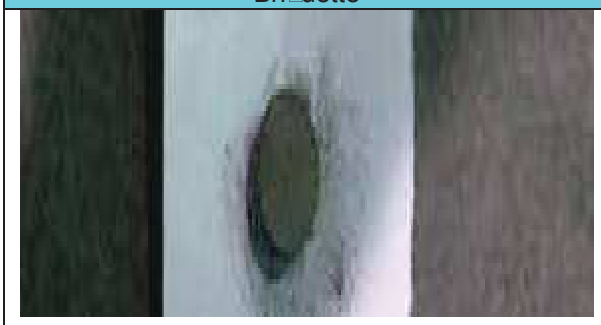	
□eactor	**Generator**
	
Master Alloy	**Ball Milling**
	

Table 3.□: □H□ pro□ess.

We can observe in Fig. 3.2. how the SHS reaction provides the formation of an Aluminium matrix with TiB_2 particles and porosity from the cold press Ti, Al and B particles. The reaction is self propagated in along the master alloy. In our case, it doesn't matters porosity inside the matrix, because we use the obtained product to produce ceramic particles by ball milling.

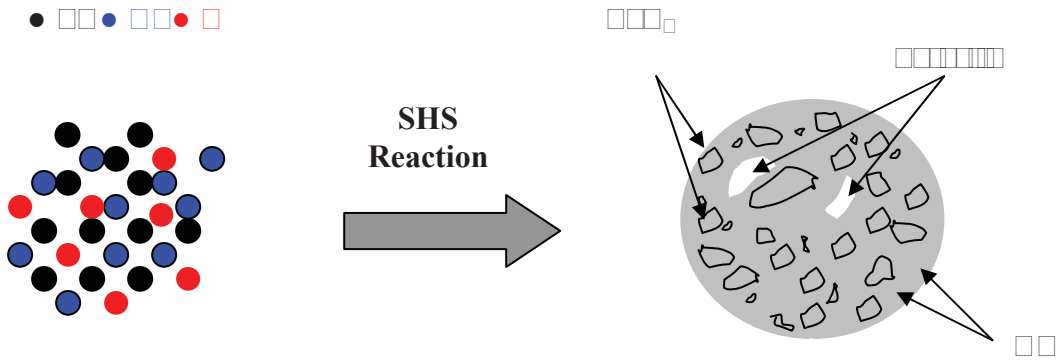

□i□ure 3.2.□□□□e□ ati□ □H□ Rea□tion □it□ initial rea□ti□e po□ □ers an□ obtaine□ p□ase pro□u□ts

Several trials have been developed in order to obtain the master alloy with good characteristics but at a better price. 1) Commercial Titanium with a size up to 1 mm and 96.06□ commercial Boron with and average particle size of 0.6 µm has been tried in order to decrease the raw material price; 2) □eaction without reactor in air or with argon supply in order to eliminate the reactor and high vacuum process; 3) The introduction of Na Cl/ K Cl to improve homogeneous dissolution and the introduction of KBF4 and Na2B4O7 as an economical boron source. The main reactions involved in the SHS process are[Nik 00],[Li 03]□

$$3\ Al + Ti \rightarrow Al_3Ti$$

$$Ti + B \rightarrow TiB_2$$

Or□

$$3\ Al + 2Ti + 2B \rightarrow Al_3Ti + TiB_2$$

In the Table 3.1. we can observe how there is a maximum limit about the 30 wt.□ of aluminium to react, how it's possible to make the reaction without reactor and in Table 3.2. what are the products obtained by the reactions. In order to characterize the raw materials and the obtained products we have employed different e□uipments. First we have study the raw particles and reactions with the EDS and SEM. In order to determinate the composition and structures we have employ the □□D, obtaining the product composition.

	Composition (□Wt)											
□eference	Ti	B	Al	Mo	NaCl/KCl	KBF_4	$Na_2B_4O_7$	d (mm)	P (ton)	Gas P (bar)	□esult	Milling
Ti B with reactor	69	31						25	10	2	□eaction	8h
Ti fine B 30□ Al without reactor	48,2	21,8	30								□eaction	
Ti gross B 30□ Al without reactor	48,2	21,8	30								□eaction	
Ti B fine without reactor	69	31									□eaction	
Ti B fine without reactor with Argon	69	31									□eaction	
Ti B gross without reactor	69	31									□eaction	
Ti B fine Al 50□ without reactor	34,5	15,5	50					25	10	2	No reaction	
TiB-1 with gross Ti	48,2	21,8	30					25	10	2	□eaction	8 h
TiB-2 with gross Ti	44,8	20,3	27,9	7				25	10	2	□eaction	8 h
TiB-3 with gross Ti	47,7	21,6	29,7		1			25	10	2	□eaction	8 h
TiB-4 Ti fine	47,7	21,6	29,7		1			25	10	2	□eaction	8 h
TiB-5 Ti fine	18,2	4,1	30			47,7		25	10	2	□eaction forming white crystals	
TiB-6 Ti fine	34,5	15,5	50					25	10	2	□eaction	
TiB-7 Ti fine	20,7	9,3	70					25	10	2	No reaction	
TiB-8 Ti fine	22,4	5	30				42,6	25	10	2	No reaction	
TiB-9 Ti fine	28,5	6,4	38,1				27	25	10	2	No reaction	

Table 3.□: □H□ pro□esse□ □ aterials an□ rea□tion results.

Material □o□ position	Results
Al 30□ wt. with fine Ti + boron without reactor	We can observe the formation of Al_2TiO_5, Gibbsite Al_2O_3. $3H_20$, Ti_5O_5 and TiB_2, but lot of the Titanium combines with the Oxygen. Aluminium is dispersed in the matrix.
Al 30□ wt. with gross Ti + boron without reactor	We can observe □utile ($Ti_{0.992O2}$, Al_2TiO_5) and TiB_2. There is not a pure aluminium matrix.
Ti fine + B without reactor	A ceramic matrix of TiB_2 and TiB is formed, with particles size of about 5 microns.
Ti fine + Boron with argon and without reactor	A TiB_2 matrix is observed, with same □utile TiO_2 and TiB. Particle size is □uite inhomogeneous, but with a media of 10 microns approximately.
Ti gross + Boron without reactor	A TiB_2 matrix can be observed, and also free boron and rutile (TiO_2). Particle size is about 10 microns.
Ti + B +KBF_4	In the □□D, $KAlF_4$ is analyzed and apart also Aluminium and TiB_2. Not TiB or KBF_4 are observed. The structure is the fused matrix. When the salt melts, it covers everything, also formed TiB_2 particles, with a particle measure less than 5 microns. The main size of particles is smaller than 1 micron, with agglomerations.
Al 30□ wt. +Ti + B +Mo 7□	We can observe by □□D TiB_2, Aluminium, metallic Mo, Al_3Ti and Al_6MoTi phases. Some aluminium particles covers with fine ceramic particles are also observed. The ceramic particles have a measure minor than 5 microns.
Al 30□ wt. +Ti + B	Particle size smaller than 2 microns. It contains TiB_2, Al and Al_3Ti. □uite big aluminium particles covered with ceramics are observed.
Al 30□ wt. +Ti fine+ B + Na Cl / K Cl 1□	We can observe that we obtain Ti B_2, Al, and Al_3Ti covered aluminium with particles size smaller than 5 microns of TiB_2, and same areas with fused salts. Not salt compounds are detected in the □□ diffraction analysis.
Al 50□ wt. +Ti+ B	Aluminium and TiB_2 are observed. No Al_3Ti is detected. Aluminium matrix with TiB_2 particles size smaller than 0,5 microns. Some plate like structures are detected, probably deformed aluminium.

Table 3.2: □H□ Results of TiB_2 reinfor□e□ ent rea□tions.

We can resume that TiB_2 and master alloys can be produced from gross industrial materials, and for some applications, no reactor is necessary. Some Ti oxides are formed when the reaction is made out of the reactor, but those particles in reaction with molten aluminium they can act also as reinforcements. The □uantity of oxides is relatively low and is concentrated in the external surface of samples. Near all the Ti and B reacts to produce TiB_2, and in the cases where there are supplementary Ti, this Ti reacts with aluminium to give $TiAl_3$, with not free boron detected.

In□ustrial □□ross□Ti □B □it□ rea□tor:

When we made the SHS reaction under vacuum with commercial Ti and B, we can observe in our experiment that only TiB_2 has formed, with a grain size smaller than 10 microns, and an average size of about 5 microns. In comparison with SHS reaction with fine Ti and B, created particles are bigger, because with fine particles TiB_2 grains produce smaller TiB_2 grains of about 1-2 microns. We can observe that particles are brittle, with sharp edges with porosity in the created structure. Also very fine particles, in the nanoscale around the formed particles are observed. In Fig. 3.3 we can observe how the broken area shows a brittle fracture in two different areas.

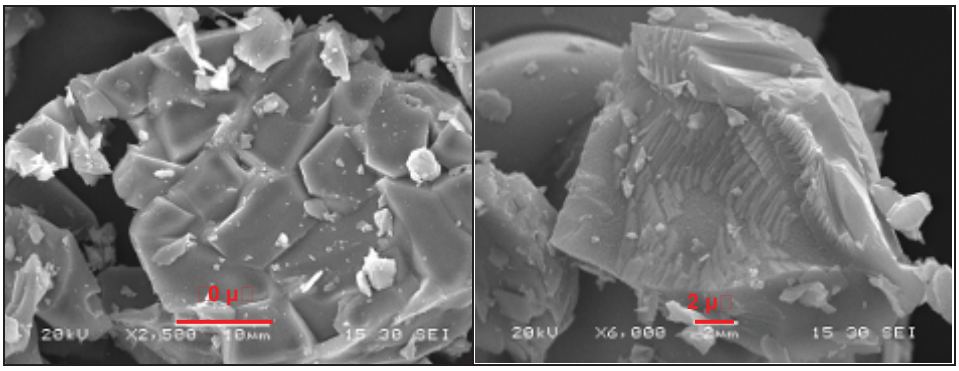

□i□ures 3.3: □EM i□ a□es of TiB_2 obtaine□ by □H□ □it□ rea□tor.

□H□ Ti B_2 □et □i□□ ener□y ball □illin□

After the SHS process, ceramic SHS performs must be broken, which will induce particle size decrease. As the ceramic particles are reduced, particles have a rounder shape, increasing the possibilities to increase wettability and properties of the reinforced alloy. After 6 hours of high energy ball milling, TiB_2 particles are smaller, with an average size about 500 microns, but with lot of particles under 400 microns (Fig. 3.4)

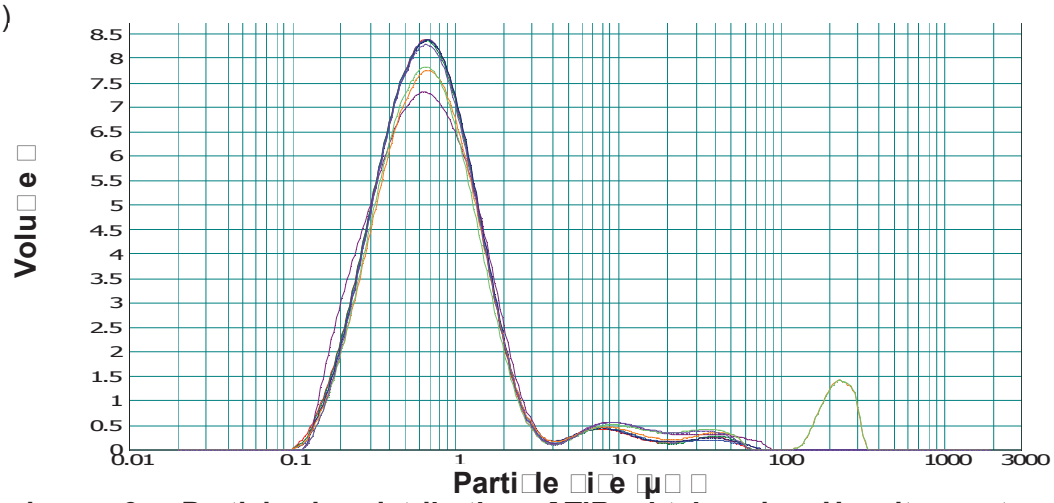

□i□ures 3.□: Parti□le si□e □istribution of TiB_2 obtaine□ by □H□ □it□ rea□tor.

Lot of particles are formed by agglomeration of lot of particles, having a structure similar to black berry structures. As we can see in the size determination there are same particles that still remains with a size of about 8 µm, but it volume percentage is very small (□0.5□), as we can see in Fig. 3.4. In Fig. 3.5. we can observe how very fine particles cover the biggest particles.

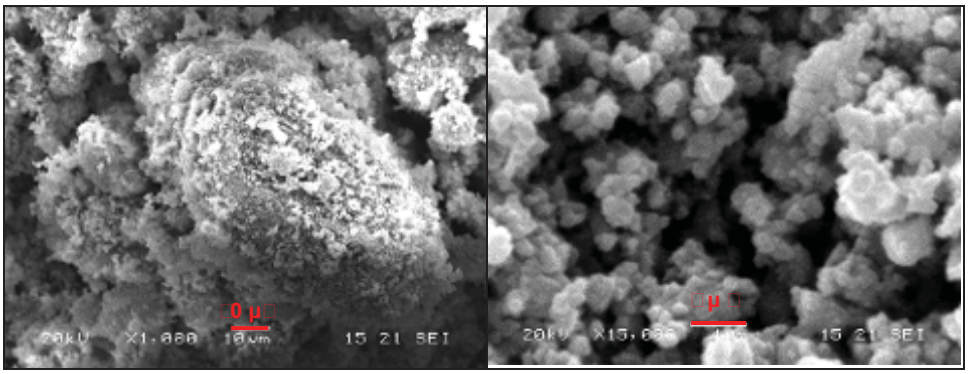

□i□ures 3.□: □EM i□ a□es of □H□ □ ille□ □ aterials.

Very similar results are got with commercial TiB_2 after 6 hours of wet high energy ball milling in comparison with the SHS produced particles, as we can observe in Figures 3.6. We can notice how again particles are much rounded, because of milling, and are also agglomerates.

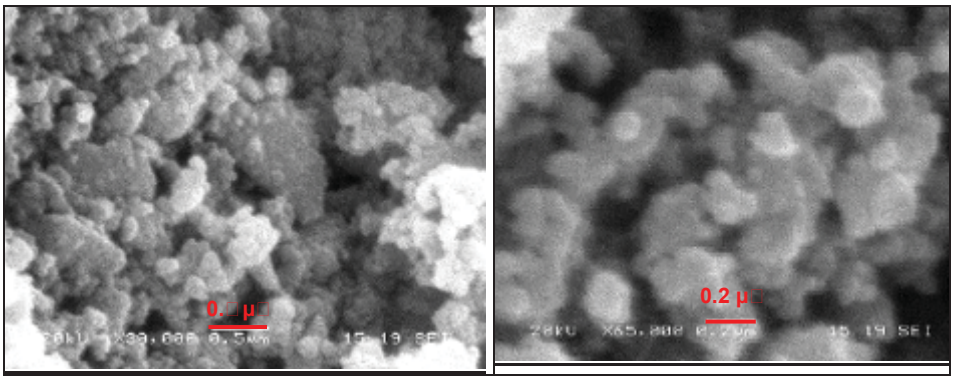

□i□ures 3.□.: □EM i□ a□es of □o□ □ er□ial □ ille□ □ aterials.

□anosi□e Ti B_2 □ ille□ □it□ alu□ iniu□ □it□ steel balls an□ □ontainer:

In order to have a better dissolution and distribution of TiB_2 particles in the molten aluminium, the ceramic particles were milled with pure aluminium with steel bars in a steel container connected to land. That process was made with the idea of breaking the agglomerates and distributing them over the aluminium surface homogeneously. We can observe in Figures 3.7. how aluminium particles get covered with TiB_2 uniformly, with incrusted TiB_2 particles in the aluminium grains. Aluminium particles got a rounded shape, due to the plastic deformations in the ball milling process.

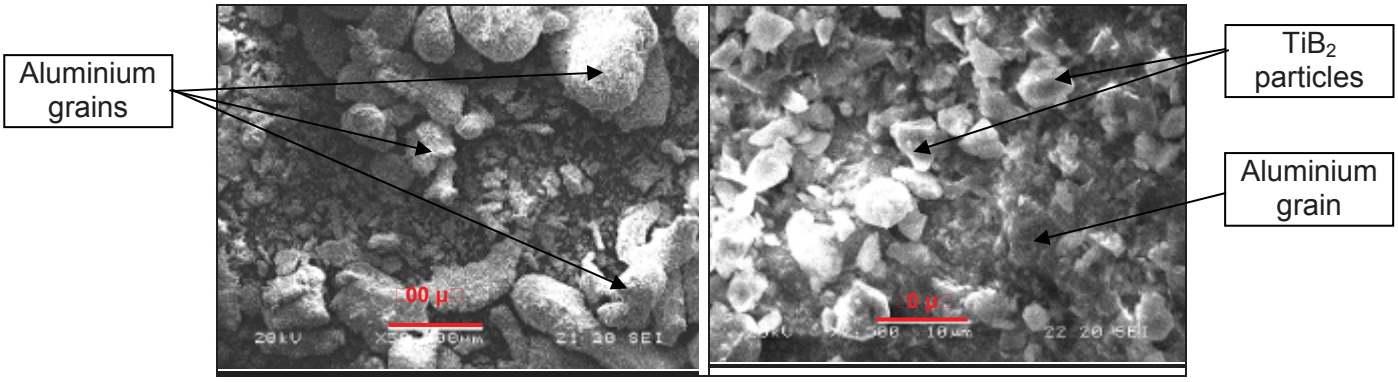

□i□ures 3.□: □EM i□ a□es of □ano □o□ □ er□ial TiB_2 □ille□ □it□ alu□ iniu□ .

3.2.□.2 Al_2□$_3$

Knano (Divn. Of K Impex – Canada) nano-Al_2O_3 are commercially available, with the reference MKN-Al2O3-AO40 for α- Al_2O_3 99.5□ pure, with and APS□40nm and MKN-AL2O-Go15 reference is γ-Al2O3 99.5□ pure, with an APS□15 nm. Pure α and γ-Alumina with a size of 40 nm and 15 nm has been chosen because they cover the most used nanoparticles and the average size is near the ideal for getting the best performance. α alumina is a stable phase and γ-Alumina is metastable, but it's the most stable between the different alumina phases. It's not expected any change of phase of γ-Alumina. Difference in behavior can be observed between α and γ nanostructures.

3.2.□.3 Al □i□ Cu3 □e□

The Al Si9 Cu3 Fe1 alloy is the most popular aluminium alloys in HPDC (70□), because of the excellent combination of properties that it presents. It is also known as A380 or EN AC-46.000. Its castability is very good thanks mainly to its silicon content and its small solidification interval. It is heat treatable, even though it □s normally used in the as cast condition. It is one of the casting aluminium alloys for which more experimental data is known and it is extensively used in the HPDC foundries. The table 3.1. shows the composition range for this alloy, and the figure 3.3. the phase diagram [□ol 07]□

Element	Si	Cu	Fe	Mn	Mg	□n	Ti	Al
wt. □	8 – 11	2 – 3.5	Max. 1.2	0.1–0.5	0.1-0.5	Max. 1.2	Max. 0.15	Balance

Table 3.3.: Typi□al □o□ position ran□es of t□e Al□□i□Cu3 alloy [□in □0].

The Al-Si phase diagram presents several specific features, as we can see in Fig. 3.8. The eutectics formed by Si and α- aluminium are one of the main distinct aspects. The eutectic composition is around 12.6□ of Si and its formation takes place at 577ºC. Furthermore the presence of silicon particles has a great influence on the properties and behaviour of the material as it controls the fluidity of the alloys as well as their mechanical properties.

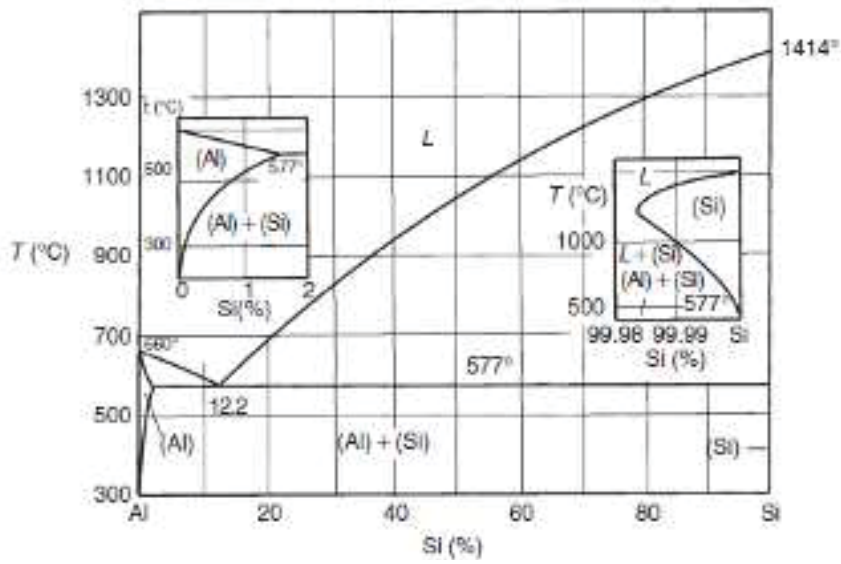

□i□. 3.□: Al-Si phase diagram [Zol 07]

The solidification and microstructure of the Al Si alloys have been deeply studied. The microstructure is characterized by α-aluminium solid solution dendrites and the needle shaped eutectic network formed by α-Al-Si. There are, depending on the alloy, also black dispersed Mg_2Si phases as well as α (AlFeMnSi) phases. Other shapes that can also appear are the β-Al_5FeSi dark needles and AlFeMnSi more light Chinese / skeleton type structures, as we can observe in Fig. 3.9.

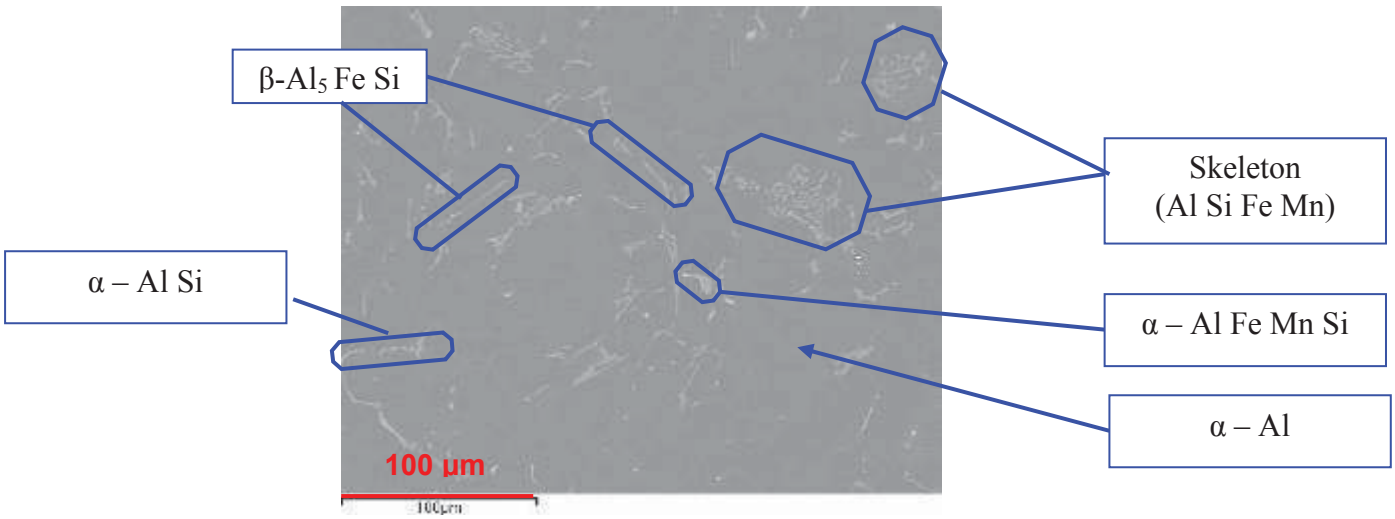

Fig. 3.9: Fe phases determination

The mechanical properties of the Al-Si9Cu3 alloy depend on multiple variables such as foundry process and parameters used, composition, use of silicon grain modifiers and α-aluminium dendrite refiners, purity of the alloy, porosity levels and thermal treatment (Normally not used). The standard properties for Al-Si9Cu3 alloy in the DIN 1706 standard are as follows (Minimum values of standards):

□s □ast □□□□: **□□S:□□0 □ □a** **□S: 1□0 □pa** **□longation: □1□**

There are different possible thermal treatments that have been applied to this alloy. The T6 treatment is the most commonly used and has not been selected in the present work because it causes to appear the porosity in the surface of the parts (Blistering). In this case, the hardening effect is attained through the solid solution and quenching treatment followed by an artificial ageing. There is not information on Al-Si9Cu3 reinforced with nano-Ti B_2. There is also no information about Al-SI9Cu3 with nano-Al_2O_3 fabricated by the liquid metallurgical process.

□□□□isition o□the allo□s

The alloys were produced by Tecnalia, with Al Si9 Cu3 commercial Befesa aluminium alloy as matrix. Their composition is based on the Al Si9 Cu3. The nanoparticles have been created *ex-situ* and pulled into the alloy. The Table 3.4. presents the composition of the alloy as supplied by Befesa Aluminio, that it's the real composition before the addition of nanoparticles.

Element	Si	Cu	Fe	Mn	Mg	Cr	Ni	Zn	Ti	Pb	Sn	Sr	Al
wt.%	8.4	1.56	0.7	0.13	0.03	0.03	0.047	0.94	0.04	0.05	0.01	0	88.063

□a□le 3.□: □omposition o□the □l-Si9□□3 allo□emplo□ed □ase allo□

3.3 □rod□□tion o□rein□or□ed allo□s and setting □p o□the □asting pro□esses

Because the price of HPDC trials is high, in order to test the behavior of materials, those are measured first in a metal die casting die and after adjusting the composition to the most suitable, parts have been made in the testing HPDC die of Tecnalia, to produce different test bars, in order to cover the necessary trials to get the characterization of materials. The DC process provides also better metallographic samples in order to study the phases and structures of the alloy.

3.3.1 □rod□□tion o□□omponents and samples

First trials were made by melting the aluminium alloy in a 3 □g induction furnace, stirring and pouring of □*Ex-Situ*□prepared nanoparticles. In order to get the TiB_2 nanoparticles in a size below 0.5 µm, 3 different systems has been probed:

1) □Momentive□bought particles □ ball milling□2) SHS TiB_2 produced at Tecnalia □ ball milling and 3) SHS TiB_2 (70%) produced at Tecnalia □ Al (30%) (As master alloy).

The particles with the nanosizes have been alloyed to the molten aluminium by gravity and stirring, in a induction furnace with a vessel of 3.5 □g and a stirring device with a regulation control up to 2.000 r.p.m. (Mixing rotation speed: 250 r.p.m.).

For the final trials, different compositions and addition routes were tested. Briquettes made at Tecnalia have a 500 MPa briquetting force, with the aluminium and the ceramic particles mixed and milled in a steel mill with steel balls connected to land. Some of them where sinterized by Spark Plasma Synthesis (SPS). Other briquettes that contain also a 10% of iron powder are briquetted with 5 ton force. Prepared powders were introduced by stirring in the molten metal, and commercial AlTi5B1 rod was used as standard refining agent. Protection fluxes were used to protect the liquid metal from oxidation, leaving up the dross before adding the briquettes. Briquette dissolution temperature was 720□C, in order to simulate the working temperatures of HPDC. The briquettes were submerged during 2 minutes in the melt before stirring. Approximately in 1 minute, the briquettes were dissolved into the melt. After stirring 10 minutes, composition, TP1 and DTA samples were obtained, to establish the composition, grain size and solidification curve. Prepared material was poured in the HPDC machine and injected, in order to obtain the test bars for the definition of the mechanical properties.

The first DC trials have consisted in the study of 18 different TiB_2 reinforced alloys with commercial and Tecnalia□s developed SHS-TiB_2 (Table 3.5). The first 8 samples were made by introducing the TiB_2 powders into the liquid aluminium by stirring, with reinforce percentages from 0.01 to 0.2 wt. %. The second trials were made with of aluminium reinforced with TiB_2 particles made from SHS process briquettes. The best results were obtained with briquettes, that were the elected format for the second DC trials.

The developed trials in die casting (DC) are:

□enomination	□aterial	Format	□t.□ o□addition
AlSi9Cu3Fe1 Sample 1			
0.01 wt.% SHS-TiB_2	SHS	Powder	0.01
0.05 wt.% SHS-TiB_2	SHS	Powder	0.05
0.1 wt.% SHS-TiB_2	SHS	Powder	0.1
0.2 wt.% SHS-TiB_2	SHS	Powder	0.2
0.01 wt.% Commercial TiB_2	Commercial	Powder	0.01
0.05 wt.% Commercial TiB_2	Commercial	Powder	0.05
0.1 wt.% Commercial TiB_2	Commercial	Powder	0.1
0.2 wt.% Commercial TiB_2	Commercial	Powder	0.2
0.01 wt.% SHS-TiB_2	SHS	Briquette	0.01
0.05 wt.% SHS-TiB_2	SHS	Briquette	0.05
0.1 wt.% SHS-TiB_2	SHS	Briquette	0.1
0.2 wt.% SHS-TiB_2	SHS	Briquette	0.2
0.1% AlTi5B1 (AlSi9Cu3Fe1)	Commercial	□od	0.1
AlSi9Cu3Fe1 Sample 2			
0.01 wt.% Commercial TiB_2	Commercial	Briquette	0.01
0.05 wt.% Commercial TiB_2	Commercial	Briquette	0.05
0.1 wt.% Commercial TiB_2	Commercial	Briquette	0.1
0.01 wt.% SHS-TiB_2	SHS	Briquette	0.01
0.05 wt.% SHS-TiB_2	SHS	Briquette	0.05
0.1 wt.% SHS-TiB_2	SHS	Briquette	0.1

□a□le 3.□.: □ie □asting □i□ rein□or□ed samples

The samples of grey and blue cells were ball milled with iron balls in an iron container conneted to ground before cold press, and rose briquettes were cold pressed after mixing without ball milling.

In the second DC trials, 6 alloys were made with briquettes reinforced with commercial and SHS processed particles, and they were also tested and compared with commercial AlTi5B1 refining rods, with a percentage from 0.01 to 0.1 wt. % (see Table 3.6.). Also in the second trials aluminium powders and TiB_2 particles were ball milled with iron balls in an iron container connected to ground before cold press.

□enomination	□aterial	Format	□t.□ o□addition
AlSi9Cu3Fe1 Sample 1			
0.01 wt.% α - Al_2O_3	Alpha alumina	Powder	0.01
0.03 wt.% α - Al_2O_3	Alpha alumina	Powder	0.03
0.05 wt.% α - Al_2O_3	Alpha alumina	Powder	0.05
0.01 wt.% γ - Al_2O_3	□amma alumina	Powder	0.01
0.03 wt.% γ - Al_2O_3	□amma alumina	Powder	0.03
0.05 wt.% γ - Al_2O_3	□amma alumina	Powder	0.05
1 wt.% γ - Al_2O_3	□amma alumina	Powder	1
AlSi9Cu3Fe1 Sample 2			
0.01 wt.% α - Al_2O_3	Alpha alumina	Briquette	0.01
0.05 wt.% α - Al_2O_3	Alpha alumina	Briquette	0.05
0.1 wt.% α - Al_2O_3	Alpha alumina	Briquette	0.1
0.01 wt.% γ - Al_2O_3	□amma alumina	Briquette	0.01
0.05 wt.% γ - Al_2O_3	□amma alumina	Briquette	0.05
0.1 wt.% γ - Al_2O_3	□amma alumina	Briquette	0.1

□a□le 3.□.: □ie □asting □l□□$_3$ rein□or□ed samples

In the case of DC trials with Al_2O_3 reinforced alloys, 7 reinforced alloys were made with the α and γ alumina by introducing by stirring the Al_2O_3 powders into the liquid aluminium, with reinforce percentages from 0.01 to 1 wt.%. 6 reinforced alloys were made with the 2 compositions with briquettes with aluminium powders and Al_2O_3 particles were ball milled with iron balls in an iron container connected to ground before cold press, with a percentage of reinforcing particles from 0.01 to 0.1 wt.%.

From those trials, at least 3 samples have being taken in order to make the mechanical characterization, and for the HPDC trials, the most suitable composition and percentages have been applied. Mechanical, thermal and microstructural analyses have been taken in order to study the properties and the causes. For the HPDC trials the table 3.6. resumes the materials, formats and percentajes of reinforcements:

Influence of Alumina (Al_2O_3) and Titanium Diboride (TiB_2) nanoparticles on the microstructure and properties of Al-Si9 Cu3 alloys for high pressure die casting applications.

□□□□□□□ **3:** □□□□□□□□ □□□□□ □□□□□□□□□□

□enomination	□aterial	Format	□t.□ o□addition
Sample alloy	Al Si9 Cu3	Ingot	0%
Al Ti5 B1 estandar rod	Al Ti5 B1	□ot	0,3%
TiB_2 commercial with 94% Al, Ti:B 2,2:1 relation	Commercial TiB_2	SPS Briquette	0,3%
TiB_2 commercial with 94% Al, Ti:B 2,2:1 relation and free Ti and B.	Commercial TiB_2	SPS Briquette	0,2%
TiB_2 commercial with 96% Al, Ti:B 2,2:1 relation	Commercial TiB_2	SPS Briquette	0,2%
TiB_2 commercial with 90% Al, Ti 69% B 31% relation	Commercial TiB_2	SPS Briquette	0,2%
TiB_2 commercial with 90% Al, Ti 69% B 31% relation	Commercial TiB_2	SPS Briquette	0,1%
TiB_2 SHS with 90% Al, Ti 69% B 31% relation	Commercial TiB_2	SPS Briquette	0,2%
TiB_2 SHS with 90% Al, Ti 69% B 31% relation	Commercial TiB_2	SPS Briquette	0,1%
TiB_2 SHS with 94% Al, Ti 69% B 31% relation	Nano TiB2	SPS Briquette	0,3%
TiB_2 SHS with 94% Al, Ti 69% B 31% relation	Nano TiB2	SPS Briquette	0,15%
80% Al□10% Fe□10% Commercial TiB_2	Commercial TiB_2	Briquette	0,2%
80% Al□10% Fe□10% Commercial TiB_2	Commercial TiB_2	Briquette	0,1%
TiB_2 commercial (AlSi9Cu3Fe1)	Commercial TiB_2	Powder	0,01%
TiB_2 commercial (AlSi9Cu3Fe1)	Commercial TiB_2	Powder	0,05%
TiB_2 commercial (AlSi9Cu3Fe1)	Commercial TiB_2	Powder	0,1%
TiB_2 commercial (AlSi9Cu3Fe1)	Commercial TiB_2	Powder	1%
TiB_2 SHS (AlSi9Cu3Fe1)	Nano TiB_2	Powder	0,01%
TiB_2 SHS (AlSi9Cu3Fe1)	Nano TiB_2	Powder	0,05%
TiB_2 SHS (AlSi9Cu3Fe1)	Nano TiB_2	Powder	0,1%
10% TiB_2 commercial□90%Al	Commercial TiB_2	Briquette	0,2%
10% TiB_2 commercial□90%Al	Commercial TiB_2	Briquette	0,1%
10% TiB_2 SHS□90%Al	Nano TiB_2	Briquette	0,2%
10% TiB_2 SHS□90%Al	Nano TiB_2	Briquette	0,1%
0.01 wt.% α Al_2O_3	Alfa	Powder	0.01
0.01 wt.% α Al_2O_3	Alfa	Powder	0.01
0.05 wt.% α Al_2O_3	Alfa	Powder	0.05
0.1 wt.% α Al_2O_3	Alfa	Powder	0.1
0.1 wt.% α Al_2O_3	Alfa	Powder	0.1
1 wt.% α Al_2O_3	Alfa	Powder	1
0.01 wt.% γ Al_2O_3	□amma	Powder	0.01
0.05 wt.% γ Al_2O_3	□amma	Powder	0.05
0.1 wt.% γ Al_2O_3	□amma	Powder	0.1
1 wt.% γ Al_2O_3	□amma	Powder	1
0.2 wt.% γ Al_2O_3	□amma	Briquette	0.2
0.1 wt.% γ Al_2O_3	□amma	Briquette	0.1
0.17 wt.% α Al_2O_3	Alfa	Briquette	0.17

□a□le 3.7.: □omposition o□the □l-Si9□□3 allo□emplo□ed □ase allo□

□ e can observe in Fig. 3.10. the process employed to make the study of reinforcing the Al Si9 Cu3 alloy, from the mixing of the particles to the final test to determinate all the properties to study.

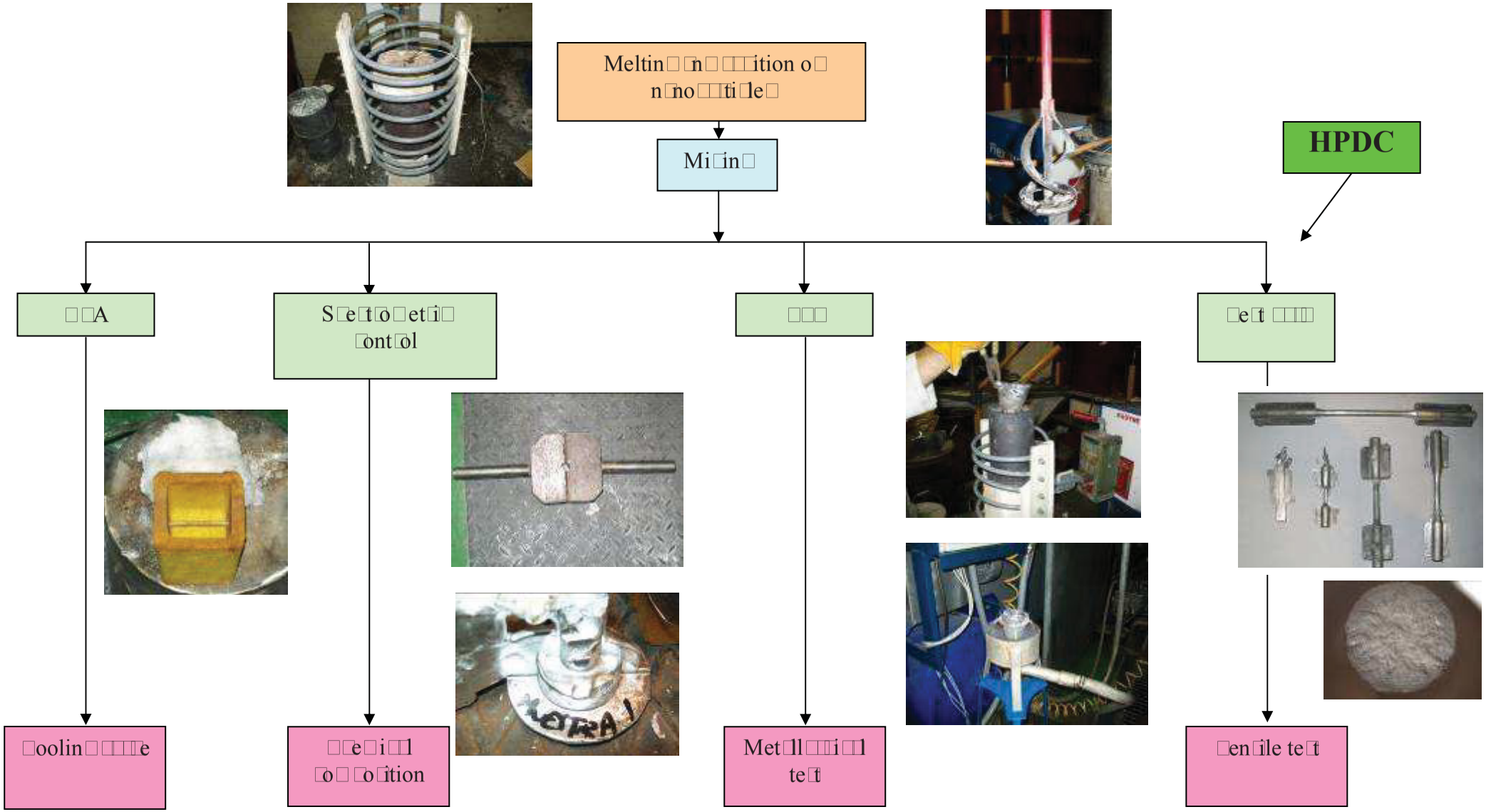

Fig. 3.10 : □est pre□ed□re

3.□ □□perimental te□hni□□es □sed □or the anal□sis o□the res□lts

The different materials (A380, A380 □%TiB_2 and A380 □% Al_2O_3) were cast following the procedure explained in the previous section, with the same working and temperatures parameters. Specimens were machined from them for tensile tests at room temperature and 200□C. The equipments and test bar employed are signalled in Fig. 3.11., including tensile test bars for room and 200□C temperatures, resilience and dynamic test bars.

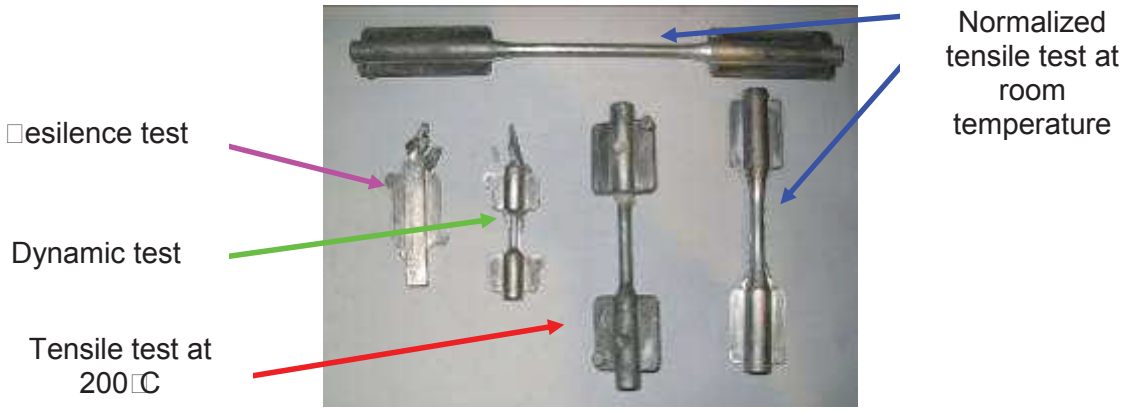

Fig□re 3.11.- □□□□ □est □ars.

□etermination o□me□hani□al properties:

In order to determinate the mechanical properties of the reinforced alloys we have employed the specimens obtained from the DC and HPDC, employing the Tensile tests at room temperature and 200□C,

□etermination o□mi□rostr□□t□re and □omposition o□the □omponents o□the allo□s

In order to determinate the microstructure and composition of the different elements, phases and products we have employ different techniques: A□ D analysis (together with line profile analysis), AFM analysis, SEM analysis, TEM analysis, OM analysis, Measurement of density and porosity (□ ater displacement and geometrical measurement, i.e. volume and weight relation), Chemical analysis, □□D, CTE measurements, TP1 grain size normalized essay.

The solidification curves of the materials were obtained through a time-temperature recording system based on the use of commercial sand cups which incorporate a thermocouple protected by a glass tube. The control system is based on a high speed signal capturing system connected to a computer, were the signals are processed by a specific programme developed at Tecnalia. In order to determinate the solidification curve, a commercial sand cup with a centerd thermocouple was connected to the control system. The pouring temperature, 710□C, was controlled by a thermocouple connected to the furnace automatic temperature control system. Signals were registered every 1 second, obtaining the T□t curve. Curves were studied in combination with their first 5th derivatives curves, with a proper escalation ad smoothening of curves. Solidification curves gives very interesting information, as the solidification rate, grain and SDAS size, kind and temperature precipitation of metallic precipitations, and of course the correct or not nucleation and modification of the alloy. In order to determinate the nucleation and modification effect, solidification and their derivative curves gives very interesting parameters, as nucleation temperature, undercooling and solidification time.

DTA has been employed normally for alloys employed in others process different from HPDC, and in the case of castings especially in the study of A356 alloy and the A356 reinforced alloys. Those studies show a reduction of the latent heat and solidification time, with a better nucleation □Egi 07□.

Solidi□i□ation o□the S□S- □□□□ and nano-□l□□$_3$ rein□or□ed allo□s

The aluminium alloy solidification curves obtained with the Al-Si9Cu3 base and reinforced alloys together with their derivative curves will be analyzed in order to determinate their differences. All the materials have been cast in the same conditions, sand mould temperature at 20□C and casting temperature 710□C. The casting step has been controlled so that there were no differences in the casting parameters and procedure. The repetitively of the test has being checked in order to validate the process. □ e can observe in Fig. 3.12. the sand cup with the thermocouple and connection wire.

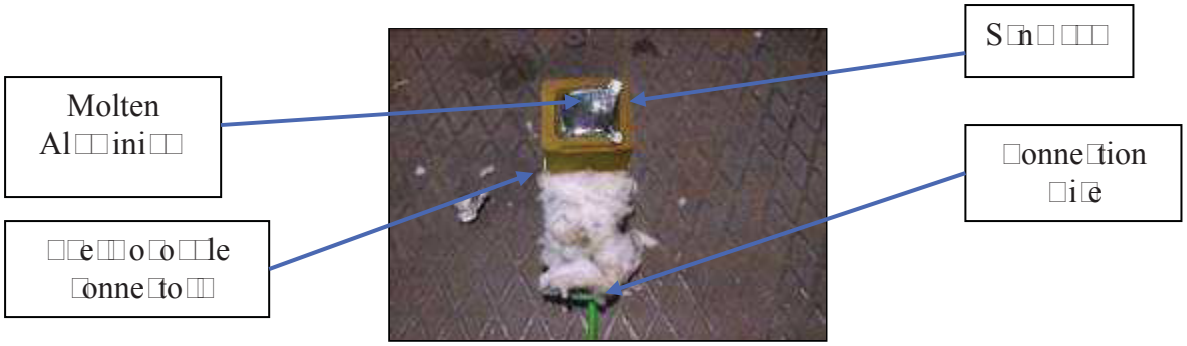

Fig□re 3.1□.- □ommer□ial sand □□p □or □□□ determination

□etermination o□mi□rostr□□t□res and □ompositions.

In order to determinate the microstructures and phases we have employed different equipments. OM gives us the microstructure, grain size and determination of main phases, SEM□EDS gives as the same information, but also the composition of the different phases and structures. TEM□EDS has been employed to the determination of the differences between the peripheral and central area. TEM samples were prepared through conventional thin film preparation: cutting, mechanical grinding and ion milling. After ion milling, the observable regions for TEM have thickness smaller than 50 nm. It has to be mentioned that the TEM observable areas are very small in compare with SEM areas. Having this in memory 2 things can be mentioned:

1. The microstructure analyzed by TEM are not easily directly correlated with global microstructure of the composite materials
2. Due to the very small volume concentration of both reinforcement (TiB_2 and Al_2O_3), to the hardness difference and therefore ion milling rate between matrix and reinforcement the analysis of area with both matrix and reinforcement is very difficult. Indeed, we have not been able to analyze any of this area for both samples. Therefore, all of the analyses are strictly associated with the microstructure of the aluminium-alloyed matrix.

Energy Dispersive Analysis (EDS) analysis has been associated with TEM analysis in order to map the distribution of the elements presents in the analysis zones (Oxygen, Aluminium, Silicon, Iron and Copper). Diameter of the EDS spot is close to 2 nm and analysis step on □ and □ close to 4 nm.

□etermination o□□i□ nanoparti□le si□e distri□□tion:

In order to determinate the particle size distribution, laser (Also MA□S and AFM) measures have been determinate. The average measure of the particle with the laser is 690 nm, but there is an agglomeration of the particles that don't let to define exactly the real size of the particles. Also a big percentage of particles (About a 30% of total particles) are below 200 nm.

□ensit□

The density of the composite materials have been measured with a Mettler AE240 precision balance, with the measure of the samples in air and in water (Archimedes determination). Samples were taken from TP1 obtained samples, similar to a die casting with a high cooling rate.

□le□tri□al □ond□□ti□it□

The electrical conductivity has been tested with an Autosigma 3000 electrical conductivity meter of □E Inspection technologies. The equipment is posed over the sample and it automatically gives a value in %IACS (International Annealed Copper Standard). The %IACS value is %100 for copper, so the higher %IACS in the sample, the more conductive the material is.

CHAPTER 4: SOLIDIFICATION & MICROSTRUCTURE

Influence of Alumina (Al_2O_3) and Titanium Diboride (TiB_2) nanoparticles on the microstructure and properties of Al-Si9 Cu3 alloys for high pressure die casting applications.

□□□□□□□ □: **S□□□□F□□□□□□□ □ □□□□S□□□□□□□□**

□.1 □ntrod□□tion

The study of the solidification and the microstructures of the alloys with and without ceramic particles as reinforcement should provide the necessary information to determinate the influence of nano TiB_2 and nano Al_2O_3 particles. Indeed, the direct relation between the microstructure and the alloys properties, give the clues to understand the differences in the mechanical, electrical and thermal properties of nano-reinforced alloys in comparison with the unreinforced alloys, which will be developed in chapter 5.

The HPDC casting process used to produce the different samples is characterized by a high solidification rate due to the high thermal conductivity of the metal that is used to build the moulds, in comparison with the thermal conductivity of sand or ceramic moulds. Ceramic particles such as TiB_2 and Al_2O_3 have a strong influence on the solidification and final microstructure of the alloys, as they creates nucleus , nucleating and modifying the solidification parameters, variating the temperatures and composition of the formed intermetallic phases. □ hen they are added externally, in the form of ceramic particles, they tend to agglomerate, in order to reduce the free energy of particles. They can be detected in the nucleus of the grains, when acting as nucleus, but normally they are pushed toward the grain boundaries, during the solidification process. □ e should expect to have the same behavior by addicting the ceramic particle, but as much as they are in the nano-scale, different properties are expected, including the decrease of grain size and SDAS. □58-60, 65□

The first study is related with the **solidi□i□ation**, and has been done employing the Differential Thermal Analysis (DTA), with the aid of a computer controlled acquisition device that provides Temperature □time registration. The equipment takes the information from the thermocouple placed in the center of a commercial sand cup employed for DTA determination. Temperature is controlled from the pouring temperature to the finish of solidification and intermetallic precipitation, having a frequency of measuring of 1 measurement per second. The T-t curves are registered, and scale and softening of curves are adjusted to permit to detect clearly the different points in the curves. The derivatives of the solidification curves are employed to determinate the parameters in relation with the nucleation, modification and intermetallic precipitation. The derivative of each point in the curve corresponds to the cooling rate of the material. An increase in the derivative is a decrease in the solidification rate, so a new phase releases latent heat.

The study of solidification curves provides the information to determinate the influence of TiB_2 and Al_2O_3 reinforcement particles on solidification, modification and precipitation. The second part is the **anal□sis o□the mi□rostr□□t□re and □hemistr□** of the reinforced alloys, and the comparison with the unreinforced materials. Optical Microscopy (OM), Scanning Electron Microscopy (SEM), □ avelength Dispersive Spectroscopy (□ DS) and Transmission Electron Microscopy (TEM) techniques have been used to analyze the microstructure and the chemistry of the composite materials. The analysis of the information collected from the obtained micrographs and the comparison with the microstructure of the corresponding unreinforced alloy provide the necessary information to explain the behaviour and properties of the reinforced materials.

□.□ □n□□en□e o□□i□ and □l□$_3$ parti□les on solidi□i□ation

□.□.1 □ntrod□□tion. Solidi□i□ation □□r□es

The study of the solidification curves shows the effect on grain refining and alloy modification. □hen there are not heterogeneous nucleation sites, the metal solidification curve shows an undercooling area ($\Delta T_{□-□}$). Instead, where impurities or homogeneous nucleation is activated, as shown in Fig.4.1. If the grain refining provides enough nucleation sites, solidifications goes with low or not undercooling □□as 01□, providing a fine grain size.

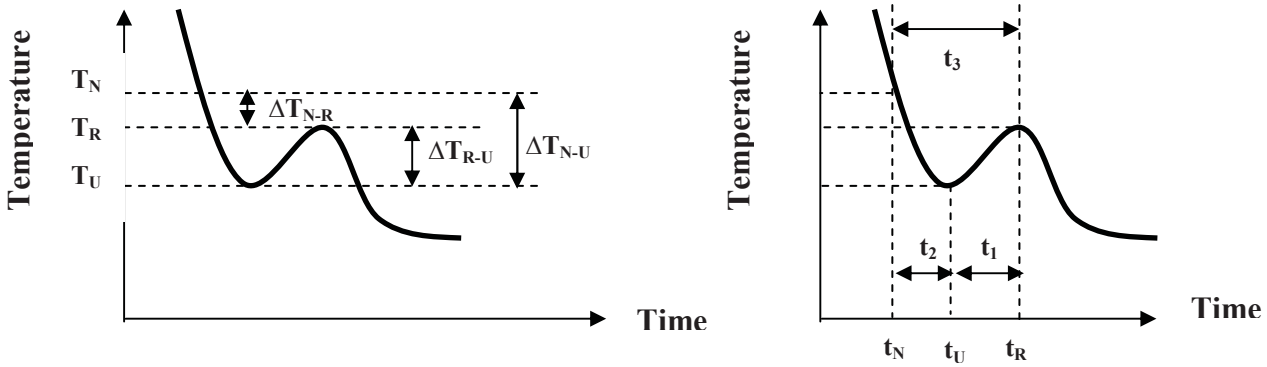

Fig□re □.1.- □□□t□□□r□e aspe□ts and □e□ parameters in n□□leating □one.

The parameters represented in Fig. 4.2 are explained in Table 4.1. and Table 4.2.:

□omen□l.	□arameter	□□e□t
T_N	Nucleation temperature (□C)	Start of primary α -Al dendrites nucleation temperature. Beginning temperature of a series of nucleation events. There is a correlation with grain size only at high cooling rates. If the value increases, the grain size decreases □lba 99□.
$T_□$	Maximum undercooling temperature (□C)	□nsteady state growth temperature. The temperature beyond which the newly nucleated crystals grow to such extent that the latent heat liberated surpasses the heat extracted from the sample. One of the best correlations with grain sizes. The maximum density of heterogeneous nucleation is reached. Increasing the value, reducing the grain size.
$T_□$	Maximum recalescence temperature (□C)	□ecalescence of steady state growth due to release primary α-Al dendrites.
$\Delta T_{□-□}$	Temperature variation $T_□$ □ $T_□$ (□C)	If this value (undercooling) tends to zero, they are sufficient favorable sites for nucleation. The grain size decrease if the undercooling value decreases.
$\Delta T_{N-□}$	Temperature variation T_N □ $T_□$ (□C)	Not as good correlation as $\Delta T_{□-□}$
$\Delta T_{N-□}$	Temperature variation T_N □ $T_□$ (□C)	Not as good correlation as $\Delta T_{□-□}$

□a□le □.1.- □emperat□re □e□ parameters signi□i□ation in n□□leating □one.

Nomencl.	Parameter	Effect
t_1	Recalescence duration (sec.)	Liquidus undercooling duration. Good correlation with grain size. The grain size decreases if the value decreases. Related to grain growth. Not affected by thermocouple calibration.
t_2	Time between nucleation and beginning of recalescence (sec.)	Indicate the beginning of several nucleation events. Correlation problems with grain size. The grain size decreases if the value decreases.
t_3	Time between nucleation and end of recalescence (sec.)	Determinates the duration of recalescence, and has only good correlation at fast cooling rates. The grain size decreases if the value decreases.
t_N, t_U, t_R	Nucleation, recalescence starting and recalescence end times (sec.)	Correspondent times of Nucleation, maximum undercooling and maximum recalescence temperatures.

Table 4.2.- Time key parameters signification in nucleating zone.

We can observe the different structures that we can get from the cooling curve in Fig. 4.2, with two different areas, the Area 1 (nucleation zone) and Area 2 (modification zone). In function of the solidification curves the grain size is fine or coarse in Area 1 and the eutectic has an acicular, laminate, modified or overmodified structure.

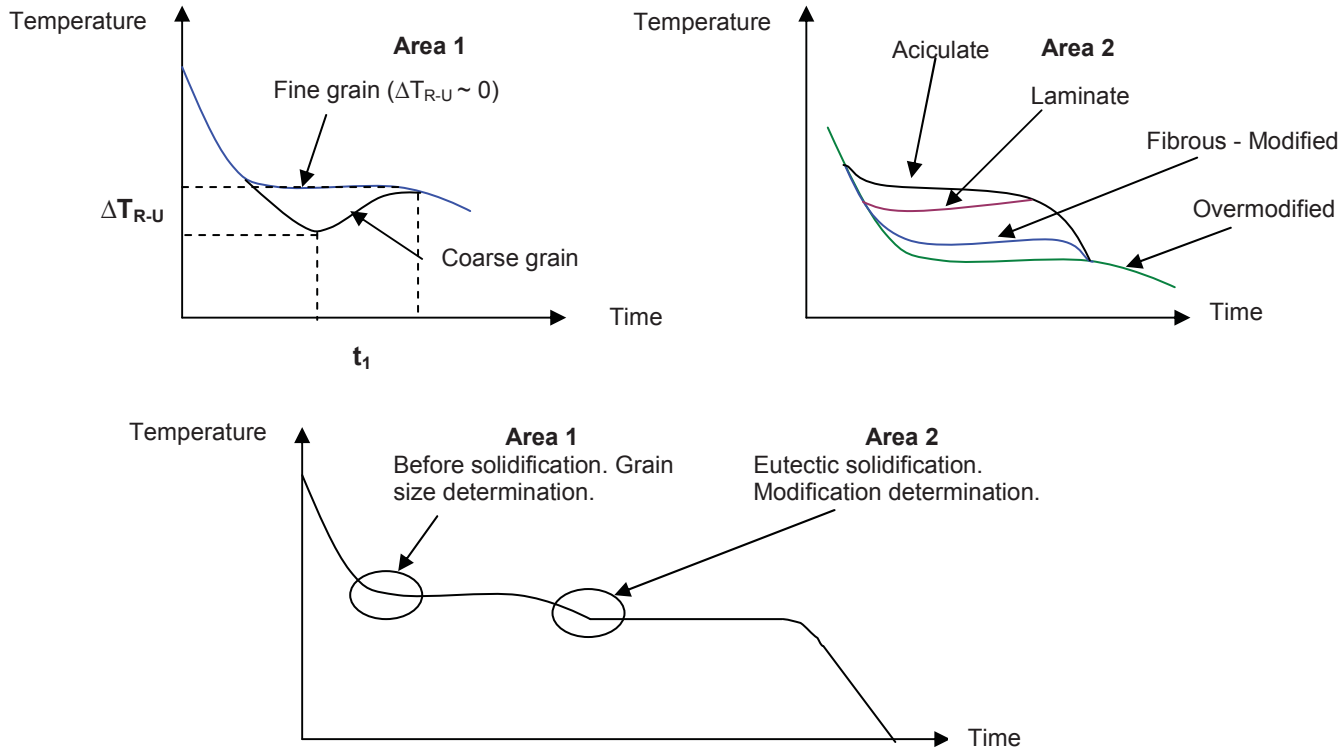

Figure 4.2.- Nucleation (Area 1) and Modification (Area 2) curves and arrests.

In order to determinate the parameters related to the nucleation temperature, first, second and fifth derivatives of temperature versus time are used (Spa 10). Indeed to the small amounts of heat involved by certain phase transformations, emphasized small heat effects. The **times of beginning and end of recalescence** are the minimum and maximum on the cooling curve, and can be detected as zeros on the first derivative curve (dT/dt=0). If we represents (-dT/dt), exothermic reactions move the curve (-dT/dt) up and endothermic down. The exothermic reactions are caused when the atoms become more ordered, increasing the entropy, giving heat on cooling. We can observe in Fig. 4.3. the main reactions with the solidification curve and its first derivative.

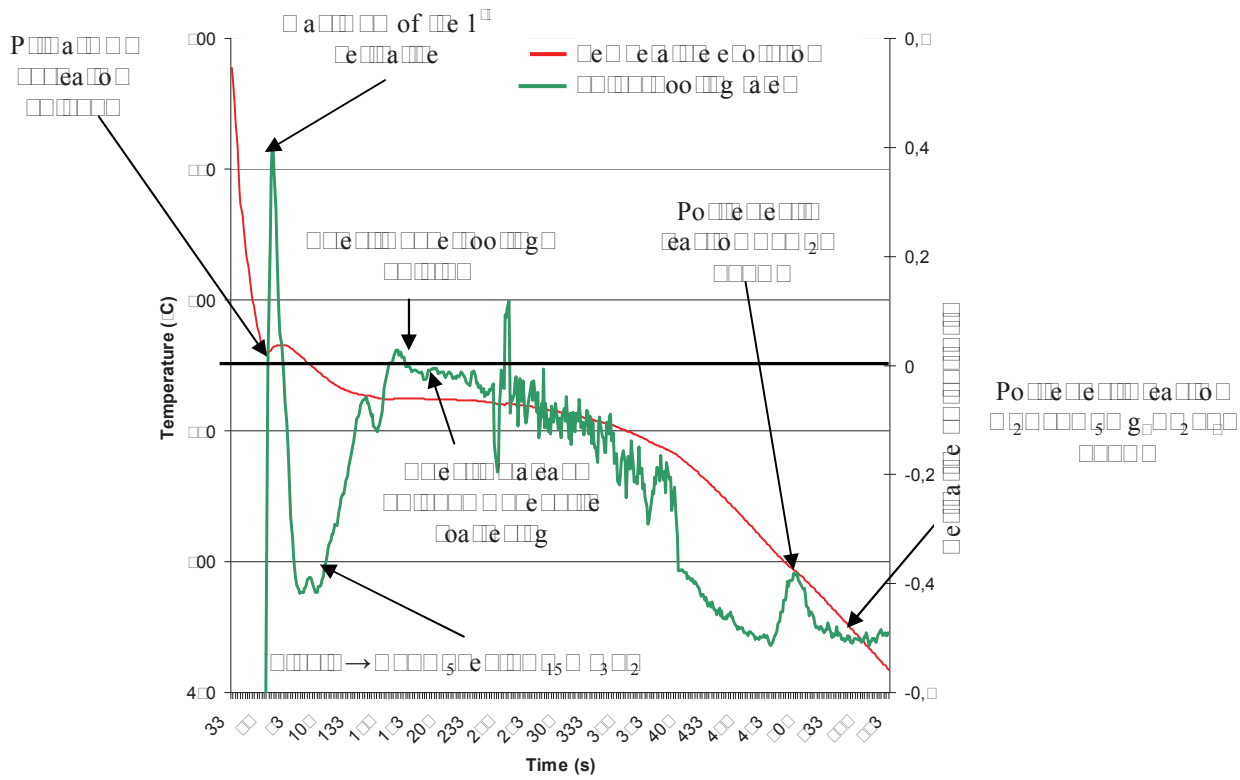

Figure 4.3.- T=f(t) and dT/dt curves with main identified reactions

The **solidification rate** (□c□s) is determinate by the first derivative (dT□dt) in the area before the first arrest, as we can observe in Fig. 4.4. First derivative and successive derivatives has been calculated as□

$$\frac{dT}{dt} = \frac{T_2 - T_1}{t_1 - t_2}$$

Where T is temperature and t is time. It depends on the material, size and form of the cup the quantity of heat that can be extracted per second. The solidification rate is expected to be increased by ceramic particle additions □Egi 0□□. In our case, the solidification rate is approximately 0.1□ □C□s.

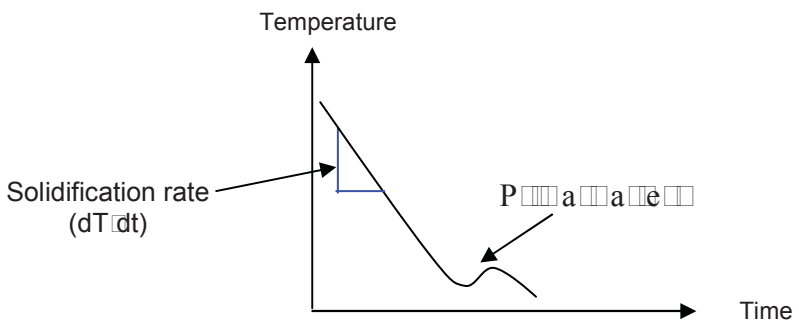

Figure 4.4.- T□f(t) and dT□dt curves □it□ main identified reactions

The second derivative is used as a precise indicator of the **Nucleation temperature** T_N, with a minimum pea□that shows the precise moment when the cooling rate (dT□dt)cc goes upwards, indicating the start of latent heat evolution, as we can see in the blue line in Fig. 4.□. The second derivative passes through zero in a positive direction (going up) at the strongest part of the exothermic (going down) arrest. The **nucleation time** is defined from the maximum pea□on the second derivative. It□s used also to determinate minor reactions, as the formation of iron-rich intermetallics, Al□FeSi, Aluminium-Silicon eutectic, Mg_2Si-Al eutectic and Al_2Cu-Al eutectics □Spa 10□. It□s expected to have an increase in T_n and a decrease of t_n, because the addition of ceramic particles □Egi 0□□.

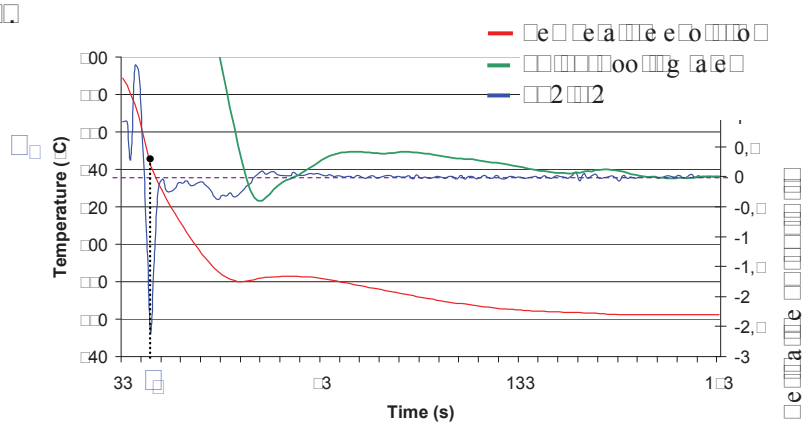

Figure 4.□.- Nucleation temperature (T_n) and time (t_n) determination.

If we want to determinate the points in the liquidus arrest, we employ 4th and □th derivatives □Spa 10□. The point of **stars of li□uidus** (N) is given by the intersection of the □th derivative with zero, as in Fig.4.□.

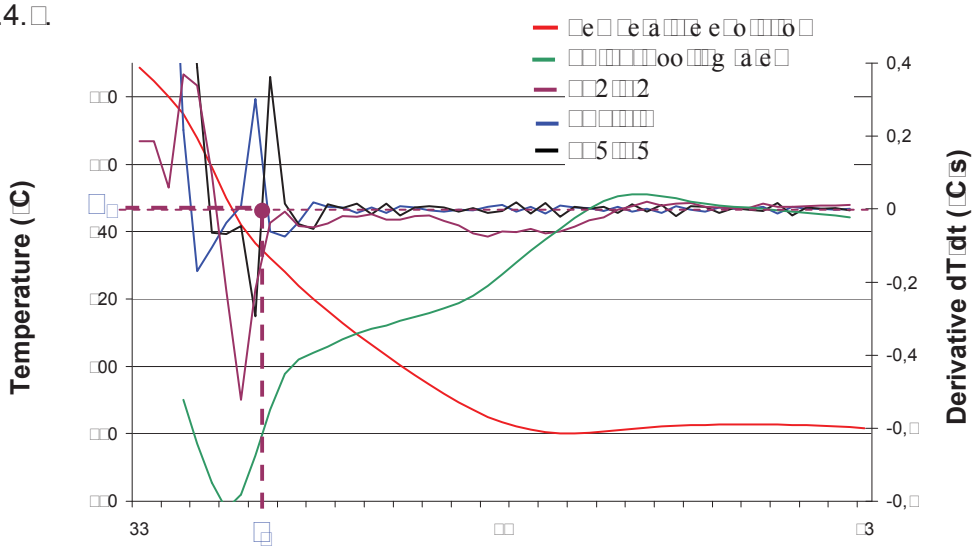

Figure 4.□.- Point of start of li□uidus (N) determination □it□ □t□ derivative

In order to determinate the eutectic reaction, we can see in Fig 4.□. what are the employed characteristic parameters□

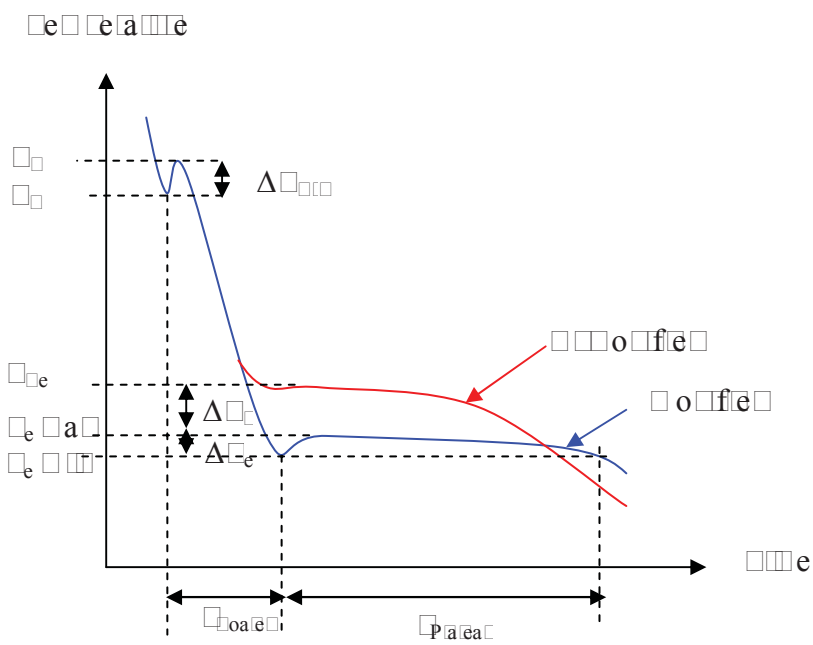

Figure 4.□.- Eutectic reaction c□aracteristic parameters

As the temperature of main eutectic reaction in the sample has a higher value, a more acicular structure is created by the aggregation of nano-particles. Lower eutectic temperature and times imply better modification □Ni□ 11□.

If we study the second derivative, we can also determinate very interesting points □Mac 9□□.

- The first maximum of the second derivative occurs before the **β-p□ase** thermal anomaly. The second maximum occurs before the eutectic growth. If we want to determinate the time and temperature of β-phase, we employ the first two maximums of second derivative.

- In order to determinate the **time and eutectic temperature**, that corresponds to the time between the start of beginning of eutectic growth and the beginning of the post-eutectic reaction, we use the second maximum and the maximum of second derivative. The end of the eutectic reaction is the minimum in the second derivative.

The main **reactions during t□e solidification** of the Al-Si9Cu3 alloys have been already previously studied by different researchers □Bac 90□,□□ol 0□□. The temperature at which the reactions ta□e place may vary according to the exact alloy composition and process conditions but the main features of the solidification of these types of alloys have been identified as follows□

1) *Preliquidus area with $Al_{15}(Fe,Mn)_3Si_2$ formation at around 605ºC.*

2) *Development of the α-aluminium dendrites at around 600ºC.*

3) *Precipitation of rich Al Mn Fe based intermetallics around 578-575ºC*

   Liquid $\longrightarrow$ *$Al + Al_{15}(Fe,Mn)_3Si_2$ and Liquid*

4) *Main eutectic reaction with rich Si and Mn-Fe phases at around 562ºC*

   Liquid $\longrightarrow$ *$Al + Si + Al_5FeSi$*

5) *Precipitation of the Mg_2Si at around 512-509ºC (Only for high Mg percentages)*

   Solid $\longrightarrow$ *$Al + Mg_2Si$*

6) *Precipitation of the Al_2Cu at around 494-476ºC*

   Solid $\longrightarrow$ *$Al + Al_2Cu$*

7) *Precipitation of complex eutectics rich in Al_2Cu and $Al_5Mg_8Si_6Cu_2$ at around 494-476ºC*

   Solid $\longrightarrow$ *$Al + Si + Al_2Cu + Al_5Mg_8Si_6Cu_2$*

As we are going to see in the solidification curves in Fig.4.10 to 4.1□, obtained values are near the calculated interval. With Thermo-calc we can determinate the **precipitations** of the alloy. In our case, we show the results for the Silicon and Copper, which are the two main allowing elements. We can observe in Fig. 4.□. A and B that for our composition, the liquidus temperature about □□0□C and the development of alpha dendrites about □00□C, the eutectic point about □□0□C and the Al Fe Si in the Beta structure at □□□□C.

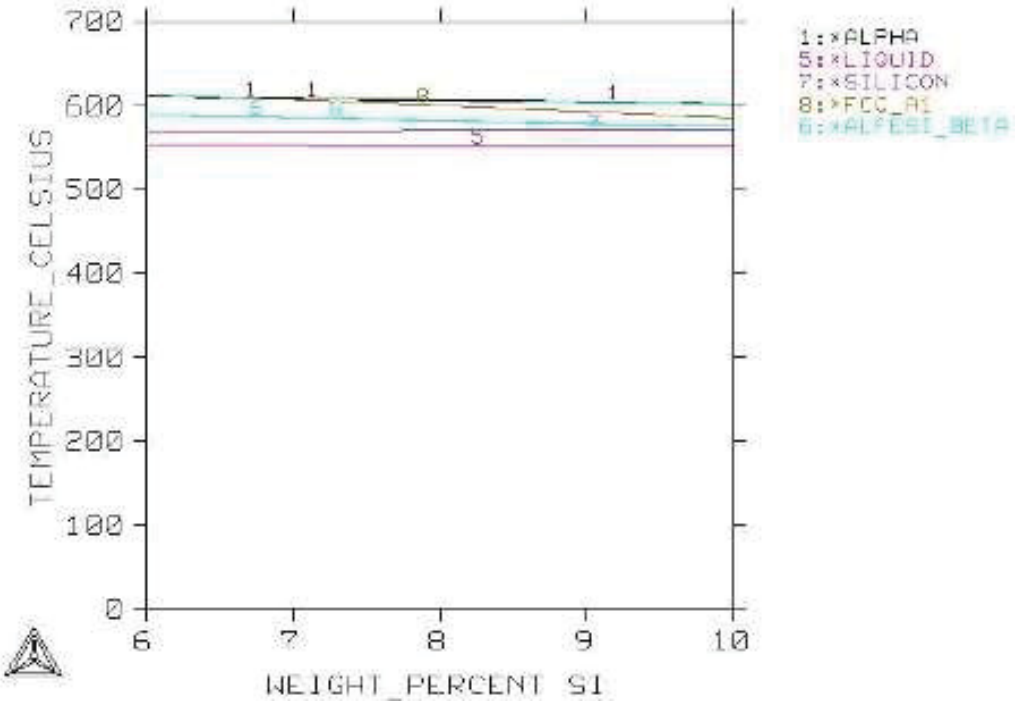

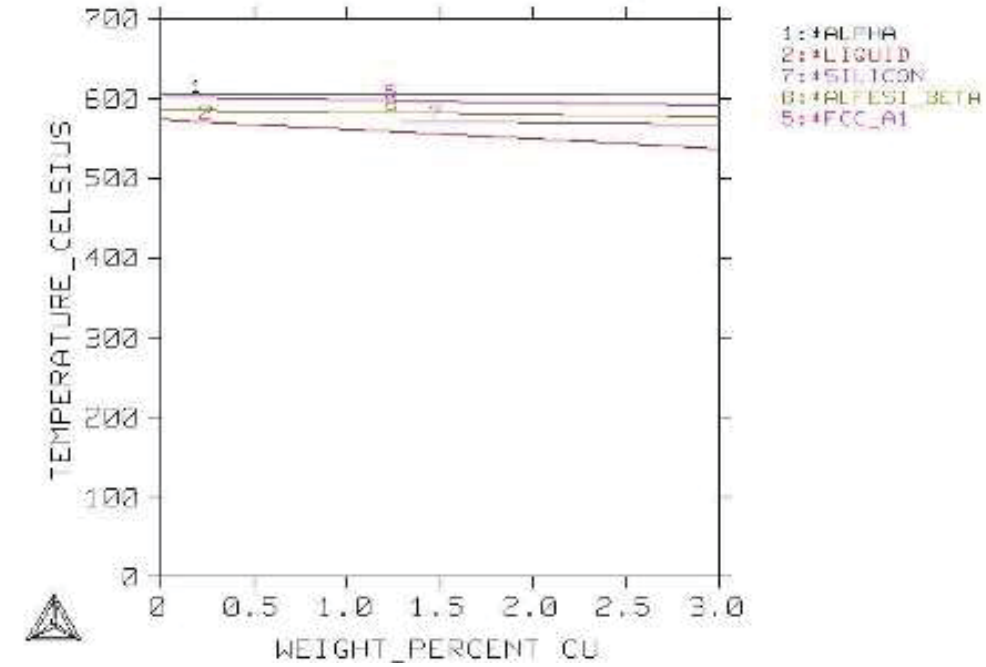

Figures 4.□. A and □- Determination of li□uidus temperature and precipitations □it□ T□ermo-calc

The point of starting of **Al_2Cu precipitation** (A) is determinate by the intersection with zero of 4th and th derivative, using the th derivative to filter out the zero crossovers due to bac ground noises. The point of starting of **Al Mg Cu_2Si precipitation** (B) is determined also as the point (A), as they are signalled in Fig. 4.9. Another way to determinate the beginning of the post-eutectic reaction is obtaining the maxima of the second derivative Mac 9 .

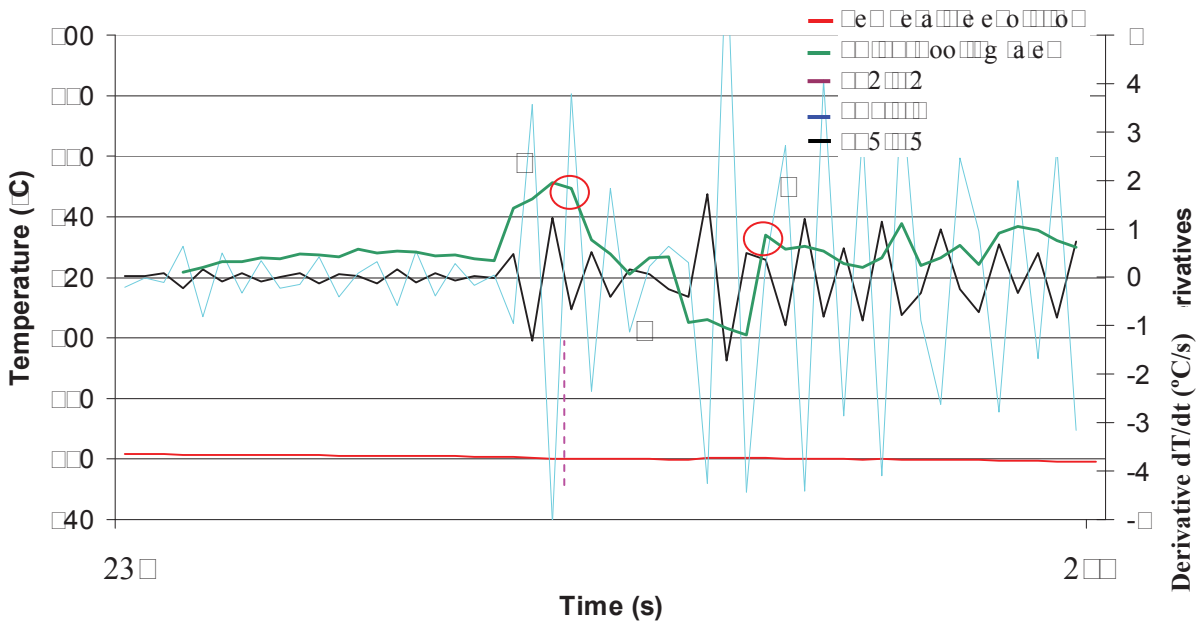

Figure 4. - Determination of Al_2Cu and Al Mg Cu_2Si start point and area

We are going to analyse the unreinforced and reinforced alloys in order to compare the solidification curves. As the percentage of reinforcement in the alloys is low (of 0.2 wt.) we want to determinate the influence over the microstructures and phases formation, what can give to us the necessary information to interpret why there are the differences in the properties of the reinforced alloys. As we have mentioned before, the changes on the curves indicates what will be the internal microstructure of alloys, and also the refining and modifying effect.

In Fig.4.10. we can determinate the **solidification reactions and t□eir temperatures** (Second derivative eliminated to simplify). We can observe differences with the predicted temperatures for reactions during solidification, due to the reinforcement. The differences between the solidification curves can be observed on Fig. 4.11 to 4.1□. The red circle numbers (From 1 to □) correlates with the explained reactions during solidification of page □4.

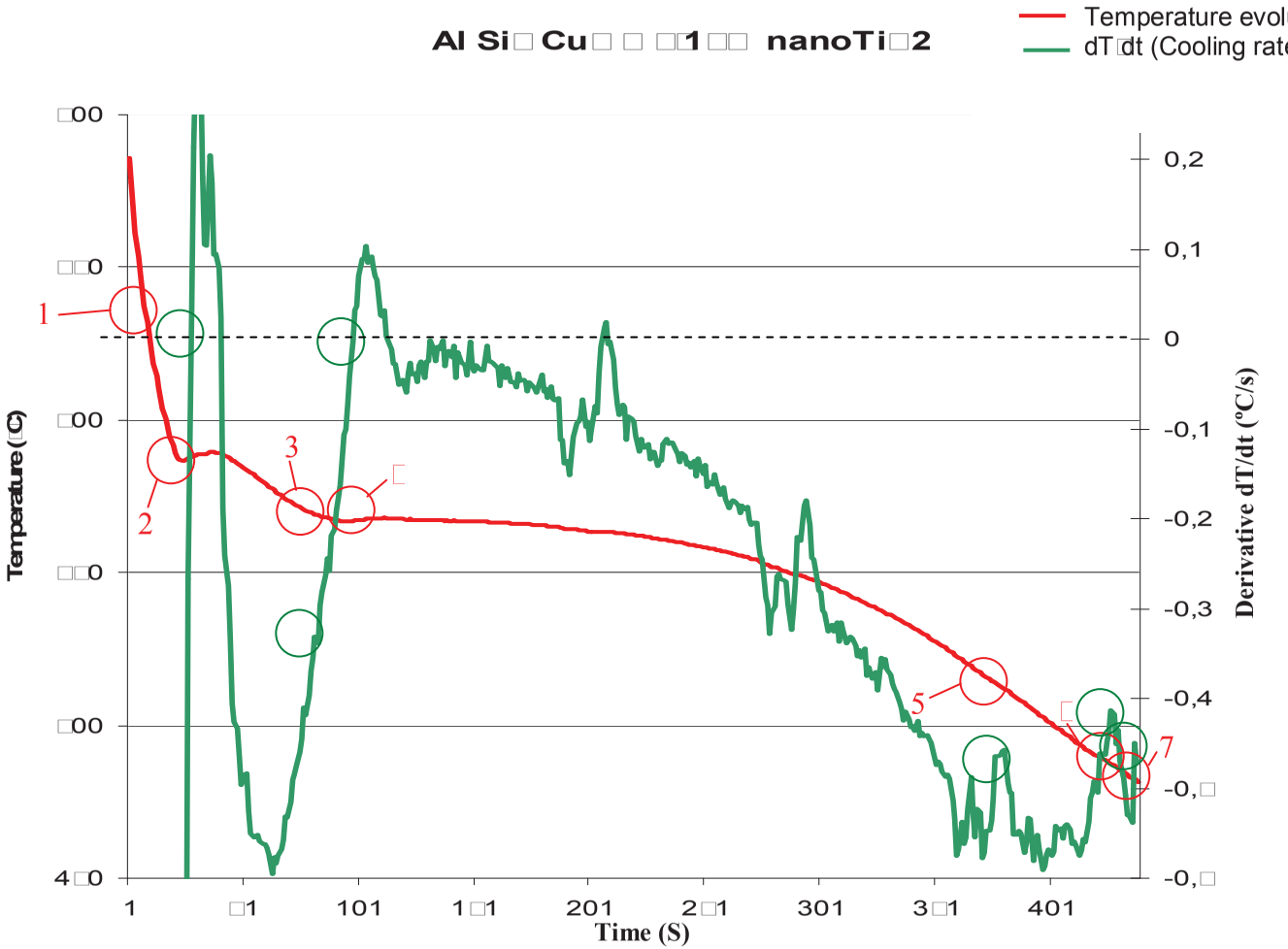

Figure 4.1□.- DTA solidification of Al Si□ Cu□ □ □.1□□ nano Ti□$_2$ sample.

In Fig. 4.11. we can observe the solidification curve with the temperature evolution y the 1st,2nd, 4th and □th derivatives for the base Al SI9 Cu3 alloy. As we have seen before, the analysis of the derivatives give us the main solidification parameters and precipitation phases. The obtained results match the results of the previous literature review for the solidification parameters and precipitation phases. The red circle numbers (From 1 to □) correlates with the explained reactions during solidification of page □4.

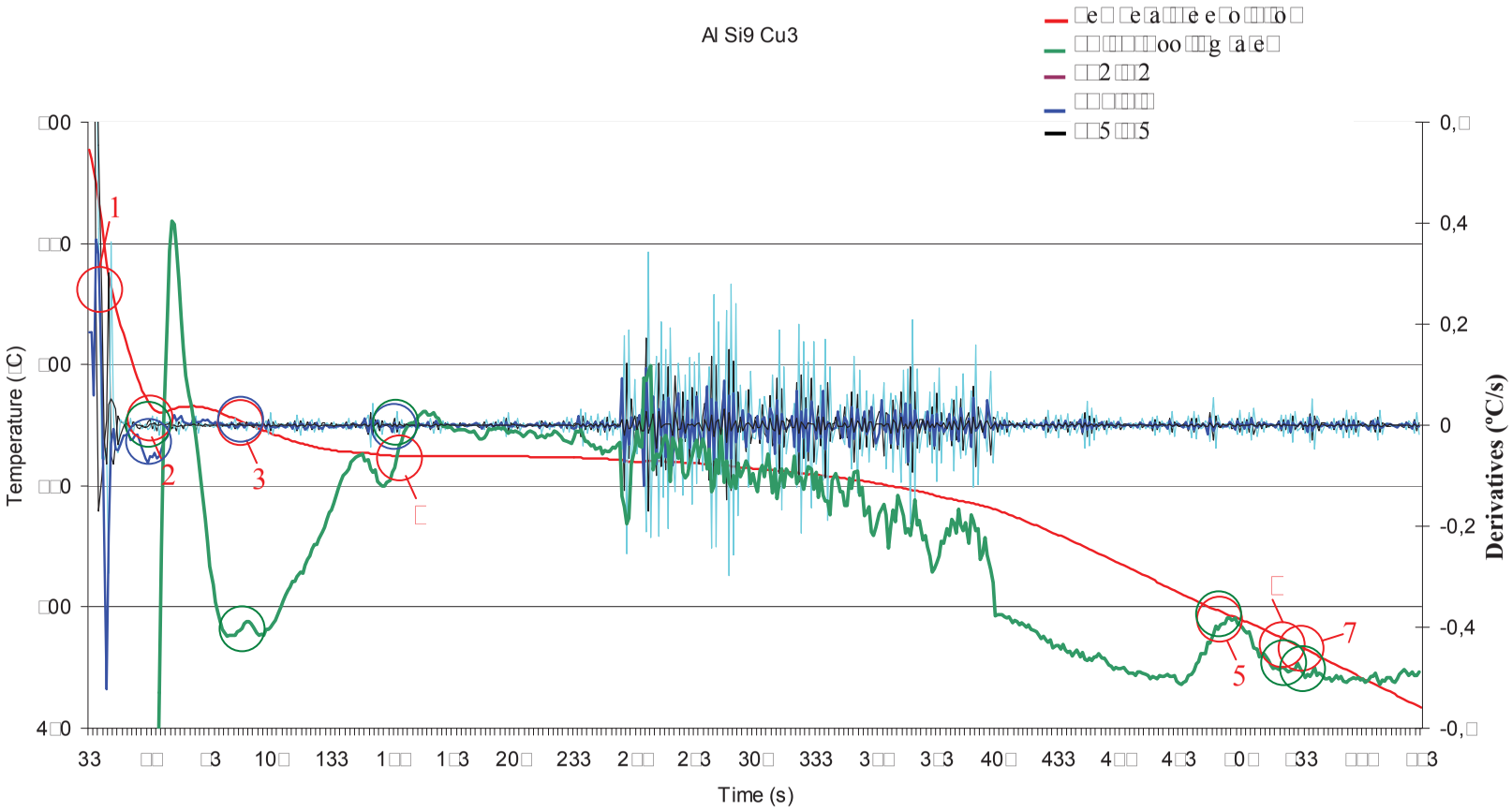

Figure 4.11.- DTA solidification of Al Si□ sample.

Ti□$_2$ reinforced alloys

In Fig. 4.12. and 4.13. we can observe the solidification curves of TiB_2 reinforced alloys, with the temperature evolution and 1st and 2nd derivatives. We are going to study the variations in the solidification parameters to determinate the refining effect of TiB_2 particles, the eutectic modification, the aluminium grain size, the microstructure and the precipitation phases with their temperatures. The red circle numbers (From 1 to 4) correlates with the explained reactions during solidification of page □4.

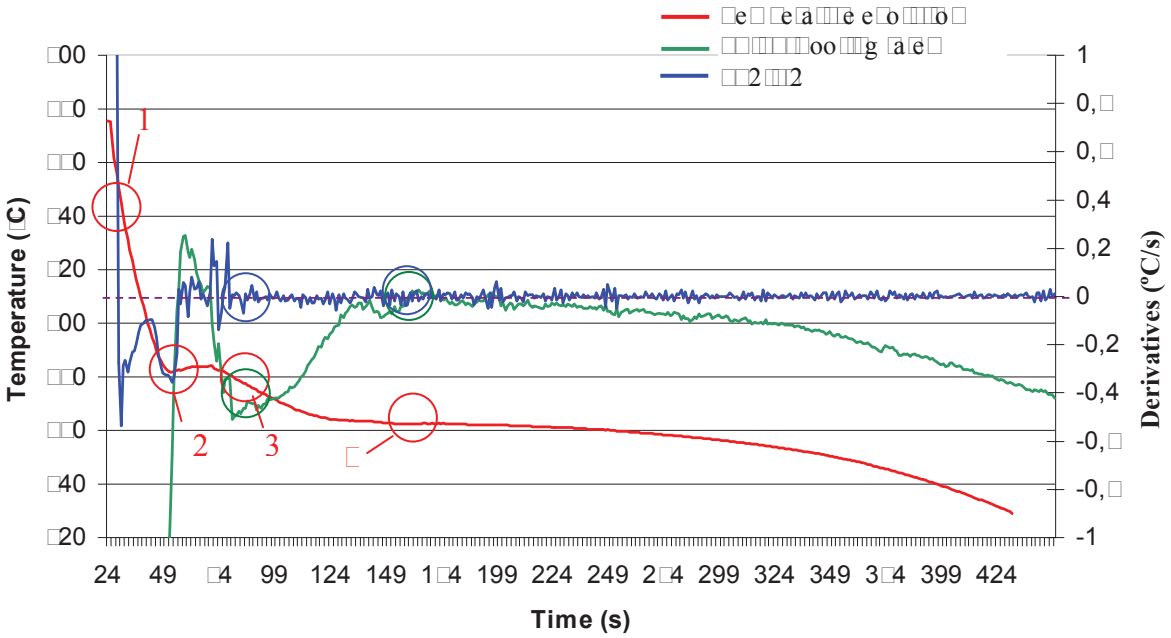

Figure 4.12.- DTA solidification of □.2□ SHS-Ti□$_2$

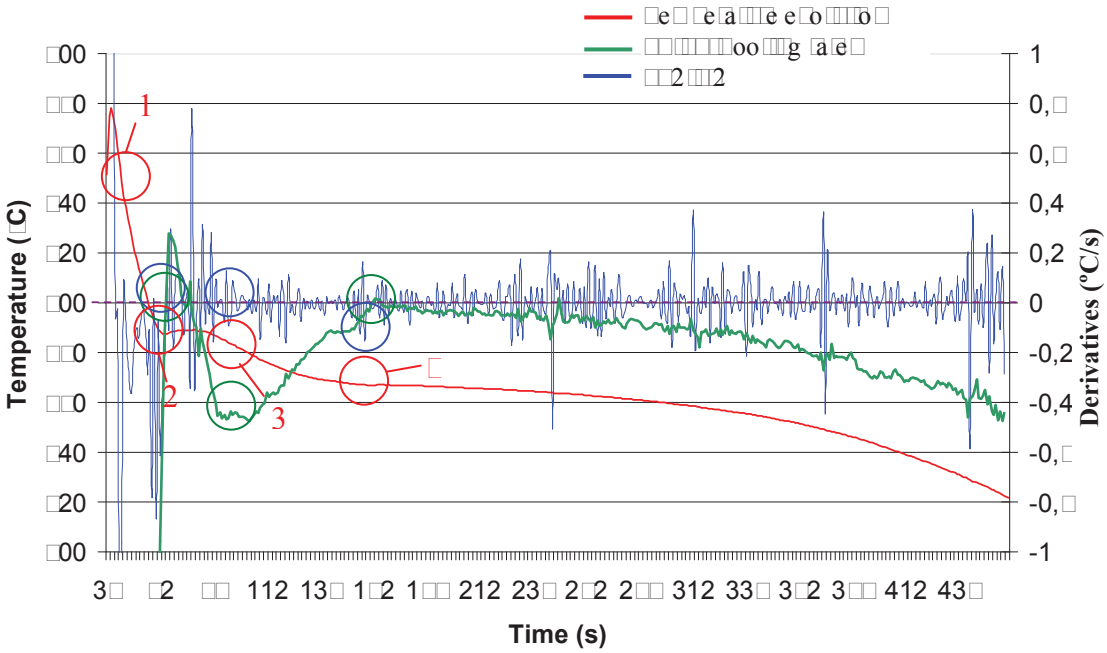

Figure 4.1□.- DTA solidification of □.2□ commercialTi□$_2$ bri□uette

The **main solidification characteristics**, analysed during this study of the TiB_2 reinforced curves are listed in Table 4.3, with an accuracy in the temperature measure of 0.1 °C. We can observe□

- An increase of temperature in the **$Al_{1□}(Fe□Mn)_{□}Si_2$** formation of about 10°C. This increase is related with the incorporation of TiB_2 to the melt, as explained in the literature review section, in page 3.
- An increase in the **α □aluminium dendrites** development temperature, due to the refining effect of TiB_2, that tends to increase the nucleation temperature an to decrease the undercooling temperature. The difference in the undercooling temperature is about 1.□ °C.
- The **temperature of precipitation of Al Mn Fe based intermetallics** is also higher in the reinforced alloys, because the effect of introducing ceramic particles as reinforcements. The difference variates from 2 to □ °C.
- The **eutectic reaction temperature** is higher also, promoting a more pronounced acicular structure for TiB_2 reinforced alloys than the Al Si9 Cu3 sample, with a variation of 4°C maximum for commercial TiB_2.

Solidification crystal structures	**Al Si□ Cu□ (°C)**	**□.2□ SHS-TiB$_2$ (°C)**	**□.2□ commercial TiB$_2$ (°C)**
Preliquidus area with $Al_{1□}(Fe,Mn)_3Si_2$ formation. Point 1 in the graphics.	□41.9	□□0.□	□4□.1
Development of the α-aluminium dendrites. Point 2 in the graphics.	□□2.□	□□4.1	□□4.1
Precipitation of rich Al Mn Fe based intermetallics (point 3 in the graphics)□ Liquid ⟶ Al □$Al_{1□}(Fe,Mn)_3Si_2$ □Liquid	□□4.9	□□□.□	□□2.□
Main eutectic reaction with rich Si and Mn-Fe phases (point 4 in the graphics). Liquid ⟶ Al □Si□ Al□FeSi	□□2.2	□□2.4	□□□.9

Table 4.□: Main solidification crystal structures of the Al Si□ Cu□ TiB$_2$ reinforced alloys obtained from the experimental castings.

Other main parameters obtained from the experimental curves and their derivatives have been summarized in the Table 4.4 with an accuracy in the temperature measure of 0.1 □C. We can observe that□

- The nucleation (Tn), maximum undercooling (Tu) and maximum recalescence temperature (Tr) are increased with the TiB_2 addition. The explanation is that introducing TiB_2 as ceramic reinforcement increases these values as seen in the literature review.
- The undercooling ΔT_{R-U} is lower after the TiB_2 addition. TiB_2 particles act as a grain refiner and the undercooling decreases with the refining of the structure,
- Comparing the two alloys containing TiB_2 , commercial TiB_2 has a better refining effect.
- The liquidus undercooling time is higher in TiB_2 reinforced alloys. That could suppose a higher grain size. As in the rest of parameters the nucleation is better, we could expect fine acicular dendrites in the microstructure of the reinforced alloys.

Reference	T_N (□C)	T_U (□C)	T_R □C)	ΔT_{R-U} (□C)	ΔT_{N-U} (□C)	ΔT_{N-R} (□C)	t_1 (s)	t_2 (s)	t_3 (s)
Al Si9 Cu3 Sample	□49.9	□□2.□	□□0.1	2.□	□□.0	□9.□	13	24	3□
0.2 wt.□ S□S-TiB_2	□□0.□	□□4.1	□□1.□	2.4	□□.□	□□.9	1□	24	41
0.2 wt.□ CommercialTiB_2	□□□.1	□□9.3	□□□.3	1.9	□□.□	□□.□	14	21	3□

Table 4.4: Main parameters obtained of Ti□$_2$ reinforced alloys.

We can see in Table 4.□. what are the controlled parameters in the zone eutectic as explained in Fig.4.9 with an accuracy in the temperature measure of 0.1 □C. The eutectic temperature is increased, also the coalescence time is increased but the plateau time is decreased.

Modification	T_{Re} (□C)	Te, max (□C)	Te, min (□C)	ΔT_e (□C)	ΔT_d (□C)	$t_{coalesc.}$ (□C)	$t_{e.plat}$ (□C)
Al Si9 Cu3 Sample	□□□.4	□□2.4	□□2.2	0,23	4,0	100	90
0.2 wt.□ S□S-TiB_2	□□□.4	□□2.□	□□2.4	0,24	3,□	10□	□□
0.2 wt.□ CommercialTiB_2	□□□.2	□□□.0	□□□.9	0,0□	-0,□	11□	□□

Table 4.5: Eutectic temperatures and times

As a conclusion, TiB_2 ceramic particles acts as grain refiners without an excess of titanium (About a 0.1□□ wt.□ in the alloy), with an increase in the temperatures of the different phases and transformations, reducing the undercooling . □ery fine acicular structures are expected in the reinforced samples. A better grain refining effect is expected for commercial TiB_2 than S□S-TiB_2, but in both cases the SDAS should be smaller.

Al_2O□ reinforced alloys

In Fig. 4.14 and 4.1□ we can observe the solidification curves of Al_2O_3 reinforced alloys, with the temperature evolution and 1st and 2nd derivatives. We are going to study the variations in the solidification parameters to determinate the possible refining effect of Al_2O_3 particles, the eutectic modification, the aluminium grain size, the microstructure and the precipitation phases with their temperatures. The red circle numbers (From 1 to □) correlates with the explained reactions during solidification of page □4.

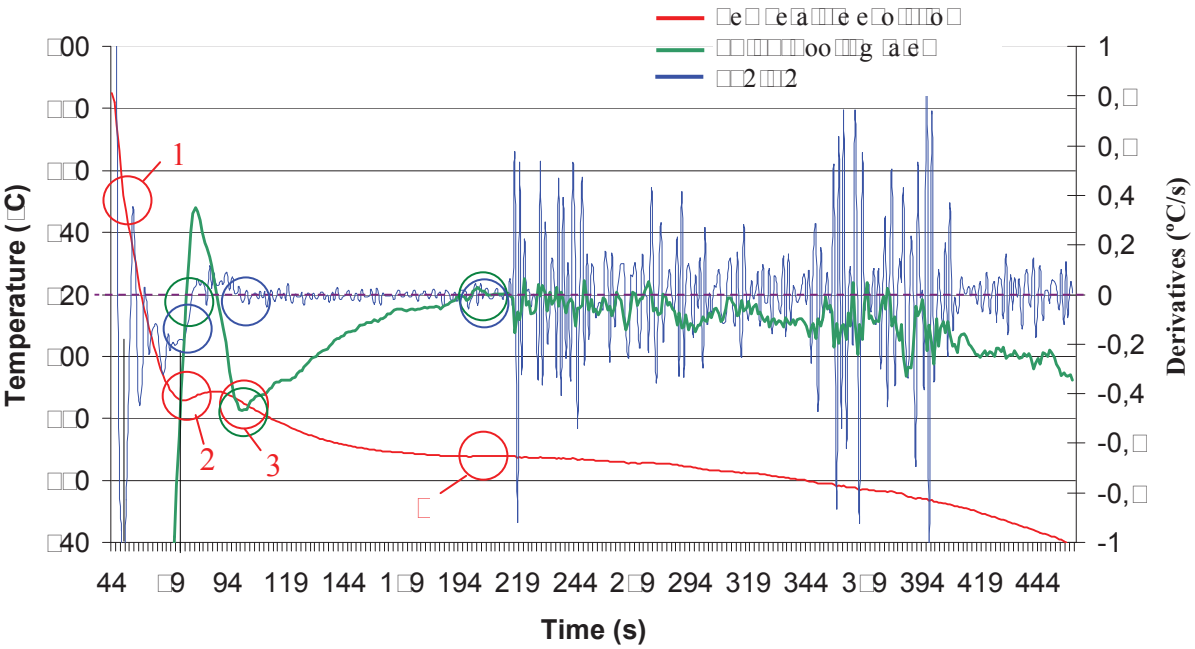

Figure 4.14.- DTA solidification of □.1□ of gamma Al_2O□ bri□uette

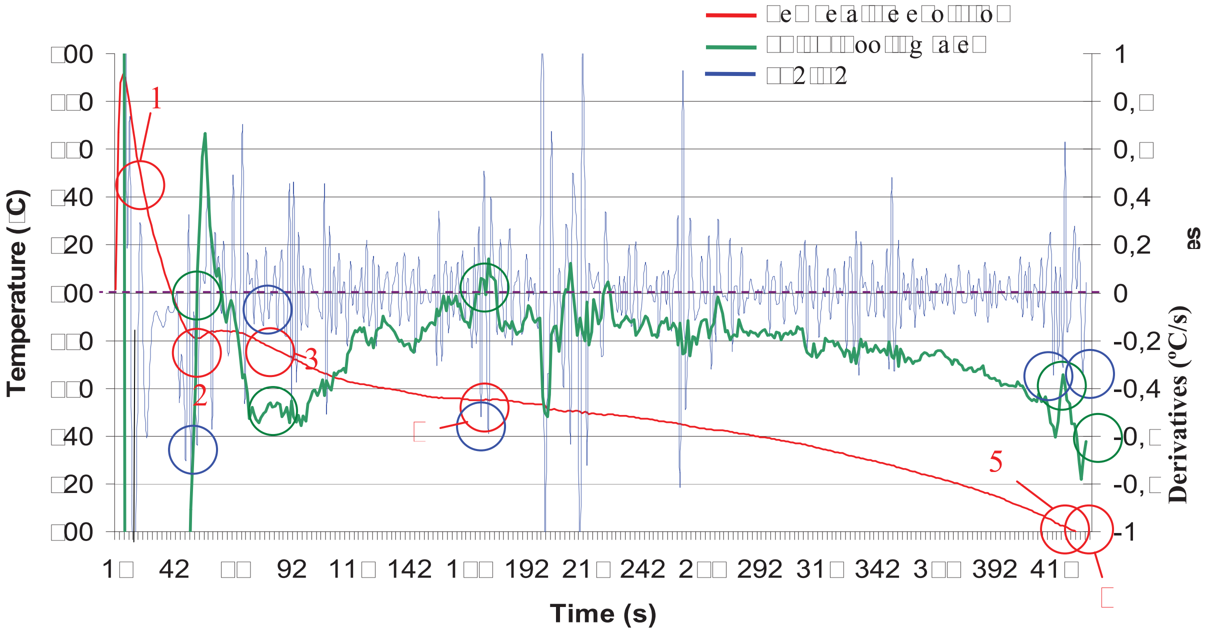

Figure 4.1□.- DTA solidification of □.1□□ of alpha Al_2O_3 briquette

The main solidification characteristics of the Al_2O_3 reinforced curves are in Table 4.□ with an accuracy in the temperature measure of 0.1 ºC. We can observe:

- An increase of temperature in the Al1□(Fe,Mn)3Si2 formation of about 10ºC. This increase is related with the incorporation of Al_2O_3 to the melt, as explained in the literature review section.
- An increase in the α □ aluminium dendrites development temperature, due to the refining effect of Al_2O_3, that tends to increase the nucleation temperature and to decrease the undercooling temperature. The difference is about □ ºC.
- The temperature of precipitation of Al Mn Fe based intermetallics is also higher in the reinforced alloys, because the effect of introducing ceramic particles as reinforcements. The difference variates from 2 to 10 ºC.
- The eutectic reaction is higher in γ-Al_2O_3, promoting a more acicular structure than in the Al Si9 Cu3 sample. However, in the gamma alumina reinforced alloy this value is smaller than the non reinforced sample and the structure should be a modified structure. In the 0.2 wt.% γ-Al_2O_3 sample the solidification curve has practically not a plateau zone with many intermediate reactions, so the determination of the eutectic point is quite confusing.

Solidification crystal structures	**Al Si□Cu□ (□C)**	**□.1□ □t.□ α $Al_2O_□$ (□C)**	**□.1 □t.□ γ Al_2O_3 (ºC)**
Preliquidus area with $Al_{15}(Fe,Mn)_3Si_2$ formation. Point 1 in the graphics.	641.9	652.0	651.7
Development of the α-aluminium dendrites. Point 2 in the graphics.	582.8	589.3	588.7
Precipitation of rich Al Mn Fe based intermetallics (point 3 in the graphics): Liquid ⟶ $Al + Al_{15}(Fe,Mn)_3Si_2$ + Liquid	574.9	584.8	577.2
Main eutectic reaction with rich Si and Mn-Fe phases (point 4 in the graphics). Liquid ⟶ $Al + Si + Al_5FeSi$	562.2	567.7	555.0

Table 4.6.: Main solidification crystal structures of the Al Si9 Cu3 based materials obtained from the experimental castings.

Other main parameters obtained from the curves have been summarized in the Table 4.7. with an accuracy in the temperature measure of 0.1 ºC. We can observe that:

- The nucleation (Tn), maximum undercooling (Tu) and maximum recalescence temperature (Tr) are increased with the Al_2O_3 addition. The explanation is that introducing Al_2O_3 as ceramic reinforcement, more nuclei are activated, acting as a nucleation points.

- The undercooling ΔT_{R-U} is higher after the Al_2O_3 addition. In the case of acicular grains, grains are large in one direction, and could modify the undercooling ΔTR-U parameter. Comparing the two alloys containing Al_2O_3 , gamma Al_2O_3 has a lower undercooling, but difference between the two alloys is small.

- The liquidus undercooling time is smaller or equal in Al_2O_3 reinforced alloys than in sample alloy. That should suppose a smaller grain size. As in the rest of parameters the nucleation is better unless the undercooling, we can expect also fine acicular dendrites in the microstructure of the reinforced alloys.

□eference	$T_{□}$ (ºC)	T_U (ºC)	T_R ºC)	ΔT_{R-U} (ºC)	$\Delta T_{□-U}$ (ºC)	$\Delta T_{□-R}$ (ºC)	t_1 (s)	t_2 (s)	t_3 (s)
Al Si9 Cu3 Sample	649.9	582.8	580.1	2.78	67.1	69.8	13	24	37
0.1□ of gamma Al_2O_3	658.6	588.7	585.9	2.88	69.9	72.8	13	27	40
0.17□ of alpha Al_2O_3	663.8	584.1	580.9	3.28	79.7	82.9	10	27	37

Table 4.□.: Main parameters obtained

We can see in Table 4.8. what are the controlled parameters in the zone eutectic as explained in Fig.4.9 with an accuracy in the temperature measure of 0.1 ºC. The eutectic temperature is increased except the 0.17 wt.□ of alpha Al_2O_3, how the coalescence time is increased and the plateau time is decreased.

Modification	T_{Re} (ºC)	Te, max (ºC)	Te, min (ºC)	ΔT_e (ºC)	ΔT_d (ºC)	$t_{coalesc.}$ (ºC)	$t_{e.plat}$ (ºC)
Al Si9 Cu3 Sample	566.4	562.4	562.2	0.23	4.0	100	90
0.1□ of gamma Al_2O_3	566.4	567.8	567.7	0.15	-1.4	150	21
0.17□ of alpha Al_2O_3	566.4	555.6	555.0	0.62	10.8	145	29

Table 4.8.: Eutectic temperatures and times

As a conclusion, Al_2O_3 ceramic particles act as **grain refiners**, with an increase in the temperatures of the different phases and transformations, but without reducing the undercooling. □**ery fine acicular structures** are expected also in the Al_2O_3 reinforced samples. We can explain why is so difficult to **automate the □TA□s** analysis for aluminium, as big changes are detected in the solidification curves with very few percentages of in situ or □*ex-situ*□produced reinforcing ceramic particles.

4.2.□.□□etermination of solidification parameters in function of the composition of the alloys

It□s very interesting to determinate the main solidification parameters without employing DTA analysis. If we can employ only a mass spectrometer to determinate the alloy composition, and use the alloy composition to determinate the nucleation time, the Silicon eutectic temperature and the eutectic Al Si Cu eutectic temperature it would give us a non expensive method to compare how variations in composition modify the solidification parameters.

The **li□uidus temperature** is important to study in order to determinate physical and metallurgical parameters of the solidifying alloy, as the solid fraction, the microstructure and chemical composition of the alloy at the solid□liquid interface, the solute super saturation point, the degree of undercooling... In order to determinate the liquidus temperature of hypoeutectic alloys they are 3 different formulas □D□u 04□. As the composition is near the limits of **□rossel formula** (only the □n is over the □0.63□ limit), we employ its formula:

$$T_{LIQ} = \square\square 1 - 4\square 7\, Si - \square 15\, \square Si\,\square^{\square} - \square 13\, Cu - 17\square 4\, Mg + \square 7\square Zn + 5\square 8\, CuMg\ \square\square C\square$$

If we employ the **□i□ayaragha□an formula** based on the aluminium-silicon-copper ternary phase, we must evaluate that the formula has not into account of the potential influence of other elements, so its accuracy is not so good:

$$T_{LIQ} = \square\square 4 - \square\square\square Si - \square 5\, Cu\ \ \square\square C\square$$

If we employ the second degree polynomial equations, we can obtain the Liquidus temperature in function of the **silicon e□ui□alent**:

$$T_{LIQ}^{Al-Si\sum X_i} = \square\square\square 45\square - \square 11\square\sum Si_{EQ}^{Xi} - \square\square 57\sum Si_{EQ}^{Xi\,\square}\left(\square C\right)$$

Where:

$$Si_{EQ} = Si + \sum Si_{EQ}^{Xi}\ \square wt\square\square\ \square$$

And we obtain the values registered in Table 4.9. in ºC with an accuracy in the temperature measure of 0.1 ºC:

Sample	□rossel □i□uidus temperature (ºC)	□i□ayaragha□an □i□uidus temperature (ºC)	Si□□ Calculated □i□uidus temperature (ºC)	□xperimental □i□uidus temperature (ºC)
Al Si9 Cu3 Sample	598.7	600.3	593.1	591.8
0.2 wt.□ S□S-Ti□$_2$	598.3	600.1	592.9	592.2
0.2 wt.□ Commercial Ti□$_2$	599.8	601.3	593.9	604.3
0.1 wt.□ of γ Al_2O_3	599.6	601.1	593.8	595.9
0.17 wt.□ of α Al_2O_3	599.9	601.3	593.9	592.8

Table 4.9.: Liquidus temperature from the Silicon equivalent formula

We can observe that there are differences between the calculated liquidus temperatures and the experimental liquidus temperatures, but the most exact formula is the silicon equivalent, with values very similar to values estimated in this study. So we can employ this formula for the calculation of Liquidus temperature of non-reinforced alloys, but when we add $Ti\square_2$ ceramic particles the formulations are not capable of predicting the changes produced by ceramic particles. We can adjust the Si_{EQ} formula to determinate the Liquidus temperature in order to introduce a coefficient to evaluate the effect of 0.02 wt.% of $Ti\square_2$ particle additions with the values obtained in table 4.9.:

$$T_{LIQ}^{Al-Si\sum X_i}{}_{TiB\square} = \square\square\square 45\square - \square\square 11\square\sum Si_{EQ}^{Xi} - \square\square 57\sum Si_{EQ}^{Xi\square} \quad \underline{\square 4.\square\square\ (ºC)}$$

The calculated **maximum eutectic temperature** for an unmodified alloy (T_R) is calculated by the equation suggested by Mondolfo (Mon 79):

$$T_{Re} \square 577 - \frac{1\square 5}{W_{Si}} \square 4\square 43 \cdot w_{Mg} + 1\square 43 \cdot W_{Fe} + 1\square\square 3 \cdot W_{Cu} + 1\square 7 \cdot W_{Zn} + 3\square\square \cdot W_{Mn} + 4\square\square \cdot W_{Ni} \square (\square C)$$

Another way to make the calculation is with the formula proposed by Gruzleski et al (Gru 95):

$$T_{AlSi,\square} \square 660.452 \square (6.11\ Si + 0.057\ Si^2)\ (12.6\ Si) \square (3.4\ Cu + 1.34\ Fe + 6.3\ Mg + 1218.9\ Sr \square 32965\ Sr^2 \square 4.293\ Sb + 186.3\ Sb^2 \square 495.5\ Sb^2)\ (ºC)$$

If we employ the second degree polynomial equations, we can obtain the eutectic nucleation temperature function of the silicon equivalent proposed by Djurdjevic (Dju 11):

$$T_{\square AlSi\square UC} \square 660.452 - \square(6.11\ Si_{\square\square} + 0.057\ Si_{\square\square}{}^2) \square (\ Si_{AL\text{-}Si\ \square U} \square Si_{ACTUAL}) \square (ºC)$$

The obtained results are show in Table 4.10 with an accuracy in the temperature measure of 0.1 ºC.

Sample	Mondolfo Eutectic nucleating temperature (ºC)	Gruzleski Eutectic nucleating temperature (ºC)	Si_{EQ} Calculated Eutectic nucleating temperature (ºC)	Experimental Eutectic nucleating temperature (ºC)
Al Si9 Cu3 Sample	566.4	569.8	561.5	562.8
0.2 wt.% SS-$Ti\square_2$	566.4	569.7	561.5	563.0
0.2 wt.% Commercial $Ti\square_2$	566.4	570.0	561.4	567.6
0.1 wt.% of γ Al_2O_3	566.4	570.0	561.4	567.9
0.17 wt.% of α Al_2O_3	566.2	569.9	561.4	563.8

Table 4.10.: Maximum eutectic temperature calculation

We notice that the most accurate calculation is made with the Si□□ method for the unreinforced alloy. So we can employ this formula for the calculation of Liquidus temperature of non-reinforced alloys, but when we add ceramic particles the formulations are not capable of predicting the changes produced by ceramic particles. □owever in this case the temperature variation is smaller than in the nucleation temperature (Maximum 5ºC).

We can ad□ust the Si□□ formule to determinate the eutectic nucleation temperature in order to introduce a coefficient to evaluate the effect of 0.02 wt.□ of Ti□$_2$ or Al_2O_3 particle additions:

$$T_{\square AlSi\square UC} \square 660.452 - \square(6.11\ Si_{\square\square} + 0.057\ Si_{\square\square}^{2}) \square(Si_{AL\text{-}Si\ \square U}\square Si_{ACTUAL})\square + \mathbf{4.\square\square\ (ºC)}$$

The higher the coalescence time, the longer the primary dendrites, with a smaller grain size in the longitudinal direction of base alloy. The diminution of plateau time denotes that the interdendritic liquid is less than in the sample, with smaller secondary arm dendritic spacing (SDAS). In the case of 0.17 wt.□ alpha Al_2O_3 alloy, the eutectic temperature is much lower than in the sample, and a better modification is expected in this sample, and worse in 0.1□ of gamma Al_2O_3 briquette and 0,2□ commercial Ti□$_2$ briquette with 90□ Al and 10□ Ti□$_2$.

4.2.2 □iscussion and conclusions of the solidification study

Solidification curves of both the reinforced and unreinforced materials have been obtained by casting the materials into normalized sand cups containing thermocouples lin□ed to a data acquisition system. The T-t curves and their corresponding dT□dt curves provide valuable information on the solidification and precipitation of intermetallic phases. We can observe the comparison of the curves in Fig. 4.16.

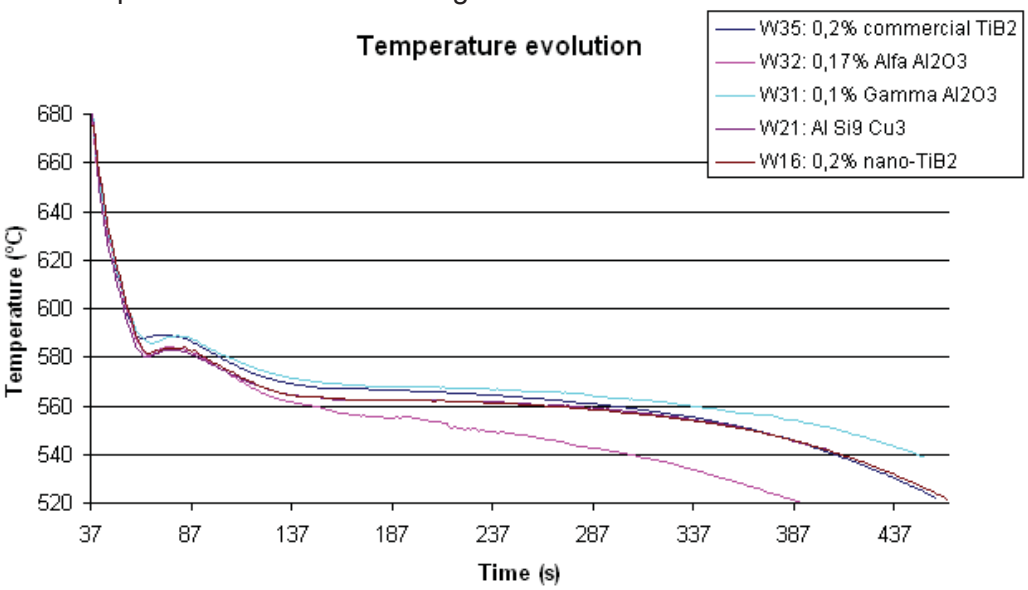

□igure 4.□6.□Temperature e□olution graphic

The **addition of ceramic particles made a modification of the solidification cur□e**, leading to:

- An increase of the recalescence temperature and a decrease in the temperature variation in the recalescence area. Only with the 0.17 wt.□ of α-alumina, the results are very similar to the results obtained with the alloy sample. An increase of the temperature of α-aluminium dendrites is also detected.

- An increase of temperature of intermetallics precipitation (Al Mn Fe, Mg_2 Si, Al_2 Cu, Al_5 Mg_8 Si_6 Cu_2).

- Liquidus temperature calculation by drossel □ □i□ayaraghavan and Silicon equivalent, give an approximate value of liquidus temperature, with a narrowest result for silicon equivalent technique. □owever, this formula is not prepared to determinate the variation in the liquidus temperature induced by the Ti□$_2$ and Al_2O_3 reinforcements. There is an increase between 2 and 8 ºC approximately.

With this results, in the **first area (□ucleation)**, we can deduce, due to the increase of the temperature and the decrease of the recalescence area and recalescence time, 1) that there is a better nucleation, and 2) the effect of the nanoparticles gets a better nucleated DTA profile for the TiB_2 particles, and something intermediate for Al_2O_3 particles. These results can be observed in Fig. 4.17., where the Al-Si9Cu3 has the smaller recalescence temperature and the biggest undercooling.

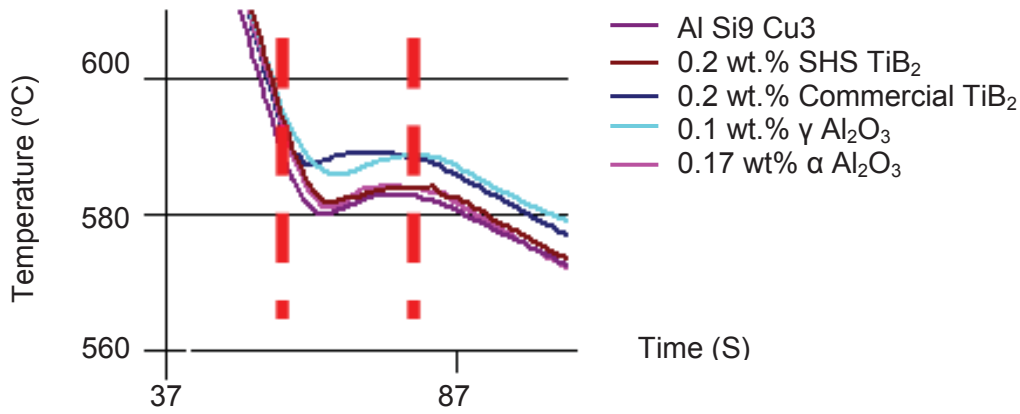

Figure 4.17.- Recalescence comparison between samples

□n the **secon□ area □□o□i□ication□□** we can observe in Fig 4.18. that the 0.1 wt.% γ-alumina and 0.2 wt.% commercial TiB_2 have a more acicular characteristic curve because the□are the ones with higher temperatures, the Al Si9 Cu3 sample and the 0.2 wt.% SHS TiB_2 are ver□similar with a fibrous structure and the 0.17 wt.% of α-alumina has a more laminate characteristic curve, because it has the smallest temperature in the eutectic area.

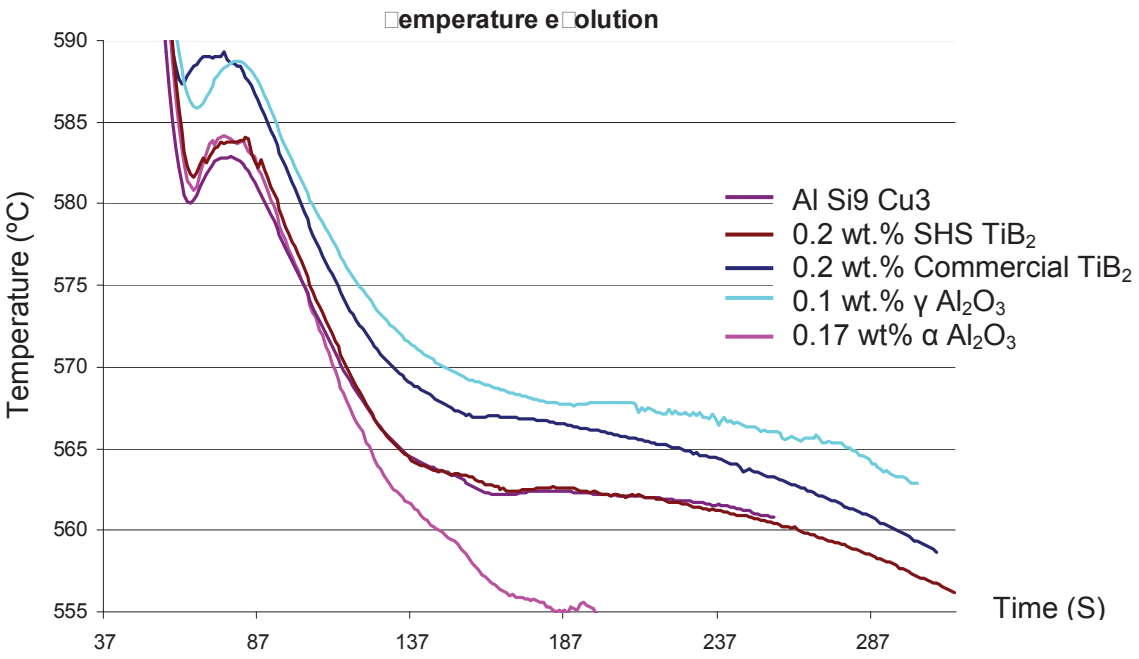

Figure 4.1□.- □o□i□ication comparison between samples

□onclusions o□t□e stu□□o□t□e comparison between samples

- An increase of eutectic main reaction temperature with Si and □n-Fe phases, e□cept the 0.17 wt.% of α-alumina, but in the rest of the different concentration essa□s studied in the pro□ect (10 samples of γ and α Al_20_3 nano-reinforced allo□s with concentrations between wt. 0.01% to 1%), the eutectic temperature is higher (The media is about 5 ºC higher). This difference in 0.1 wt.% γ-alumina can be e□plained b□variations during the DTA essa□.

- The coalescence time is bigger in all the reinforced allo□s. That corresponds with larger dendrites. A higher value can be also related with the directional dendrites, because the□have more time to grow.

- The plateau time is smaller in all the reinforced allo□s, corresponding with smaller secondar□dendrites arm spacing.
- The comparison between the TiB_2 and Al_2O_3 particles shows that TiB_2 particles have a lower coalescence time than Al_2O_3 particles, but the□have a bigger plateau time. That difference should give a larger and with a bigger SDAS in the case of TiB_2 particles.
- Calculation of eutectic temperature b□□ondolfo□s, □ru□les□i and D□urd□evic gives a ver□good estimation, especiall□with D□urd□evic formula (□ithin 1ºC). However, is not capable of determinate the variation promoted b□the reinforcement particles, with differences of about 5-10ºC.
- □er□small concentrations of in situ or e□situ produced ceramic particles modif□the DTA□s curves, ma□ing difficult to automate the control process.

4.□ □nfluence o□ □i□□ an□ nano-□l□□ particles on t□e microstructure

The microstructure of the TiB_2 and Al_2O_3 reinforced allo□s has been anal□sed with O□, S□□ and T□□. These studies have been completed with □DS anal□sis. Samples have been studied and their microstructures have been compared with the unreinforced allo□s cast in the same conditions.

The main ob□ective was to anal□se the chemical interactions between the particles and the aluminium allo□matri□components that helped understanding the measured change of thermal and mechanical properties of the reinforced material. □t is □nown that the TiB_2 particles have a grain si□e decreasing effect, following mechanisms alread□researched and used b□the aluminium grain refining industr□. The role and mechanisms of the Al-Ti-B grain refiners, that contain such particles, have been thoroughl□studied but the main interest of the microstructural anal□sis was to chec□an□other possible interactions that ma□appear with higher TiB_2 contents and smaller particles. □n the case of the Al_2O_3, man□studies have been carried out to ma□e A□Cs reinforced with alumina, and the stud□of the shape, □uantit□and surface treatments in order to increase the wettabilit□between the matri□and the alumina. □e are going to stud□Al_2O_3 and TiB_2 particles because the□don□t react with molten aluminium, and the□can have a relative good wettabilit□. Small particle si□e and narrow si□e distribution, large surface area, spherical morpholog□are □ualities that have the elected particles, in order to obtain the best microstructures and properties with rounded nano-particles of 40 and 15 nm in the stable and metastable α and γ Al_2O_3, and TiB_2 particles with round faces b□the decrease from 5 microns to about 500 nm after milling.

4.□.1 □icrostructure o□t□e □l-□i base□ materials rein□orce□ wit□ nano-□i□□ an□ nano-□l□□□

The Al-Si allo□s have been one of the most studied allo□s for sand, die casting and □□DC, but no so much the Al Si9 Cu3 Fe1 that it□s emplo□ed in aluminium H□DC. Due to the e□cellent combination of properties it shows, Al Si9 Cu3 is emplo□ed with good castabilit□ and mechanical properties. The number of wor□s related to the stud□ of the microstructure of the allo□ reinforced with nano-TiB_2 is ver□ low and not an□ reference has been found where the Al-Si9Cu3 □ nano-TiB_2 allo□s have been fabricated b□ H□DC. The anal□sis of those previous wor□s suggests that the presence of TiB_2 particles has an influence on the grain si□e and morpholog□ of α phase of the composite materials □□is 04□. □n some studies □Sch 07□□□um 09□, TiB_2 particles are observed at the grain boundaries, suggesting that the□ are pushed out during solidification, but a small proportion are also retained within the α-Al grains due to engulfment.

The number of wor□s related to the stud□ of the microstructure of the Al S□9 Cu3 allo□ reinforced with nano-Al_2O_3 is ver□ low, though some references has been found where the Al-Si □ Al_2 O_3. The anal□sis of those previous wor□s suggests that the increase of surface roughness of Al_2O_3 particles increase the wetting contact angle, reducing wetting □Agu 10□ .The presence of Al_2O_3 particles has an influence on the grain si□e and morpholog□ of the α phase of the composite materials because Al_2O_3 particles are pushed b□ the aluminium dendrites into the last free□ing eutectic li□uid. Thus, Al_2O_3 particles are surrounded b□ the eutectic silicon, with a good interfacial bonding, and some of the particles within the grains □□l- 10□. Aluminium dendrites became smaller and a more fine eutectic area is obtained □H□s06□. □n the case of Al-Si h□pereutectic allo□s reinforced with γ -Al_2O_3 and TiO_2, the□ have a refinement of microstructure, of the dendritic arm length, the SDAS, the interlamellar spacing in the eutectic silicon phase and the primar□ silicon particles □□l- 11□.

4.□.1.1 □ptical an□ □□□ microscop□ anal□sis

The comparison of the microstructure between the Al Si9 Cu3 and reinforced allo□s provides clear indications of the effect of the TiB_2 and Al_2O_3 particles. TiB_2 particles cannot be discerned at low magnifications due to their small si□e (0.5-2.5 microns) but their influence can be indirectl□ appreciated. The reinforcing particles modif□ the microstructure of the samples, giving two different areas, one granular in the peripher□ and another acicular in the center. □n this acicular area, the grains are orientated, and the subgrains are much smaller, with a best distributed eutectic. □f the percentage of solute is increased, the□ are more heterogeneous nuclei, promoting an e□uia□ial dendrite structure. Also if we increase the cooling rate, the structure tends to an e□uia□ial dendrite structure. □f the cooling is ver□ slow and the solute concentration is low, cellular dendrites are formed.

The reinforced allo□s were also anal□sed with the S□□ techni□ue. The main ob□ective was to identif□ the different phases and to observe the possible interaction and influence of the TiB_2 and Al_2O_3 particles.

a□□l □i □ □u□ □ample□

□ e are going to stud□ first the Al Si9 Cu3 base allo□, in order to establish a point to ma□e a comparison with the reinforced allo□s. As we can see in the micrograph of Fig. 4.19., there is homogeneous grain dispersion in all the areas, with e□uia□ial dendrites in the peripher□ and in the center.

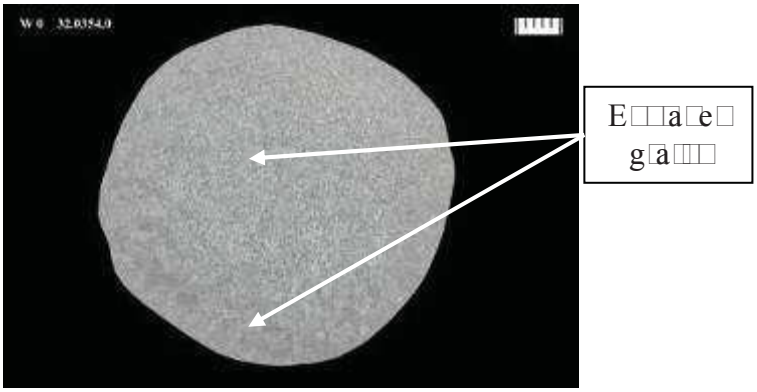

Figure 4.1□.- □l □i □ □u□ allo□ □□1 essa□ □□ macrograp□ anal□sis

□ e can observe in Fig. 4.20 that the□are some little microshrin□ages. The grains are e□uia□ial and the structure is □uite modified with rounded dendrites. Solute percentage is higher in the center than in the peripher□.

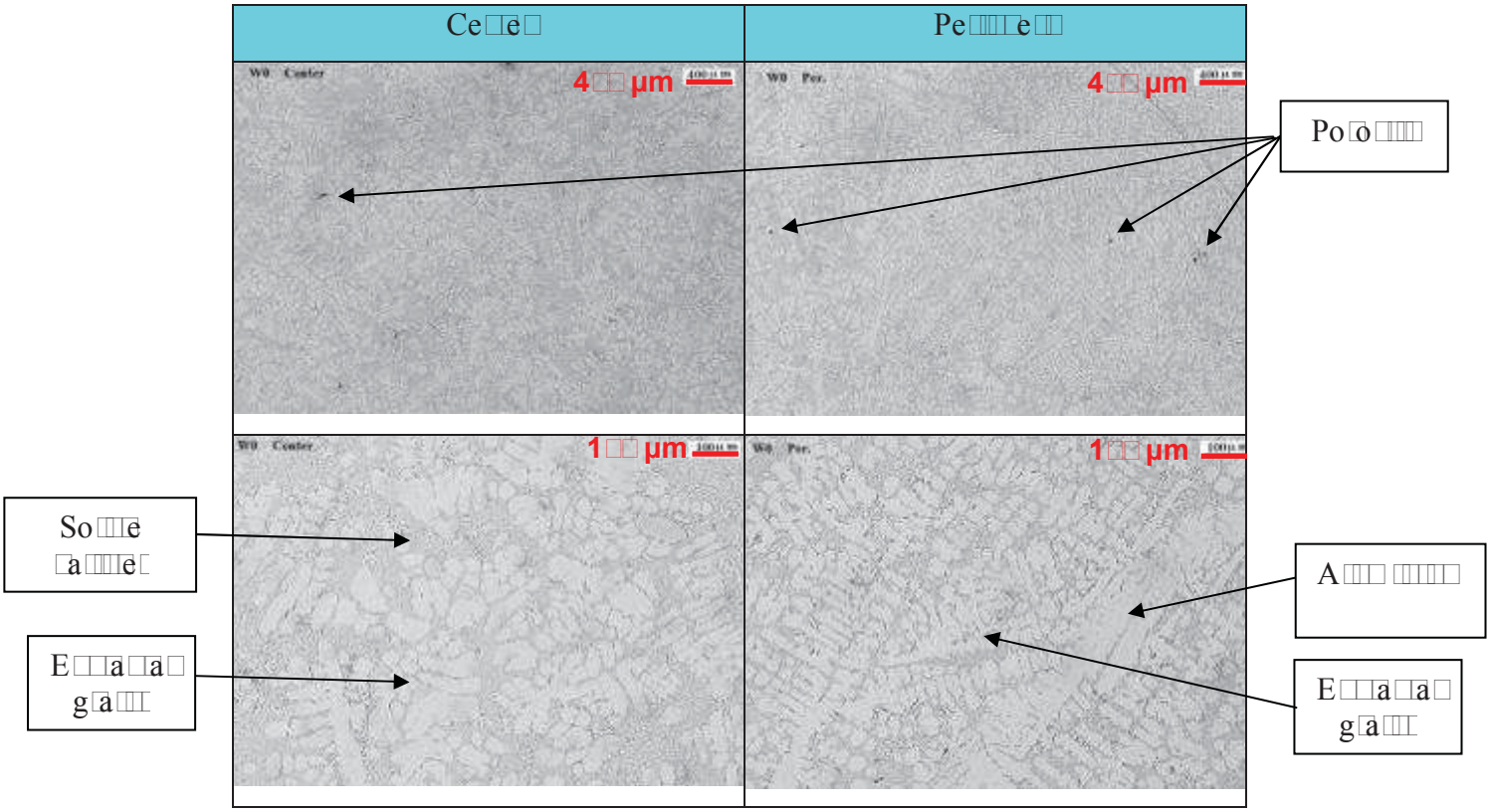

Fig. 4.□□.□□l □i □□u□ □□ micrograp□s

As we can see in Fig. 4.21., the aluminium dendrites (dar□ structures) are surrounded b□ eutectic aluminium silicon (gre□) and intermetallics (white rounded particles). The grains have an e□uia□ial form. As we can see, the aluminium dendrites are surrounded b□eutectic silicon and intermetallics. The grains have and e□uia□ial form. □ e can conclude that it□s a t□pical structure of an Al Si9 Cu3 allo□.

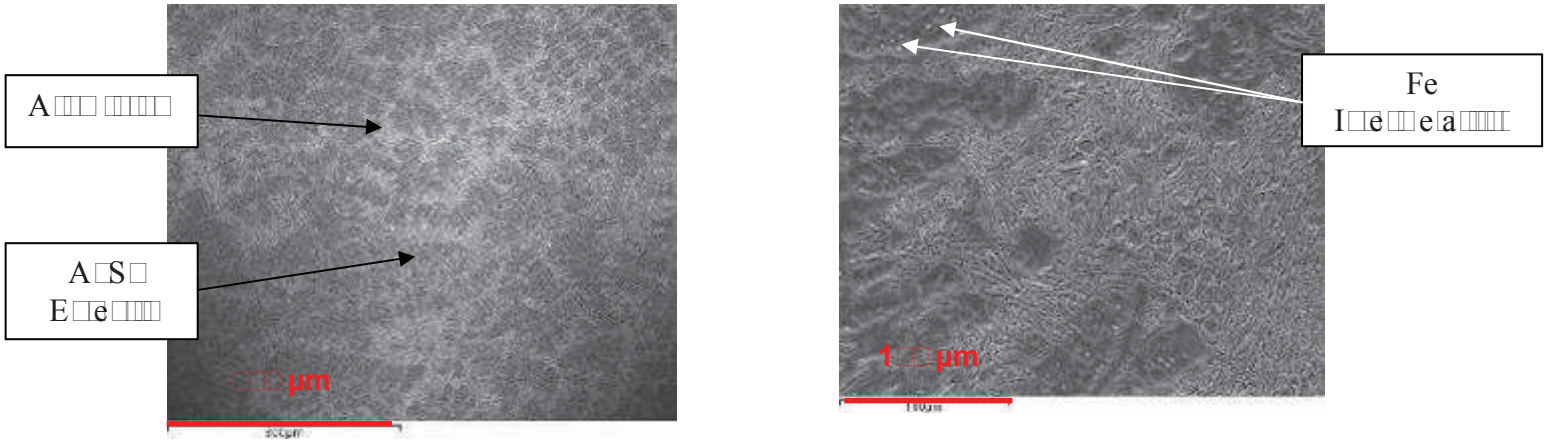

Figure 4.□1.- □l □i□ □u□t□pical □□□ micrograp□s

b□□.□wt.□ □□□-□i□ an□ □.□ □ommercial □i□

The stud□of the microstructure of SHS and comercial TiB_2 reinforced allo□s can give us an idea of how the nano-particles modif□the structure and properties of reinforced allo□s, due to the ver□difficult particle detection when we emplo□onl□a 0.2% of TiB_2 reinforcement. After the anal□sis of the different samples, we have conclude that micrograph structures are near the same in both TiB_2 reinforced allo□s. Because of that, we are going to show the results of the stud□of one of the allo□s, in this case the SHS-TiB_2 reinforced allo□. □e can observe in Fig. 4.22. that there is a non-homogeneous grain, with e□uia□ial dendrites in the peripher□and columnar dendrites in the center. □er□little microshrin□ages are observed.

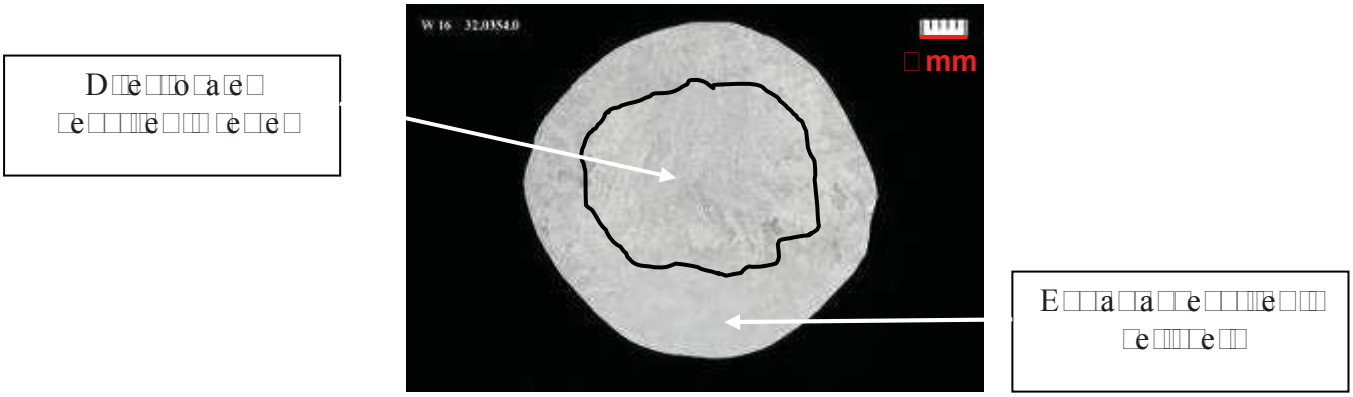

Figure 4.□□.- □□□-□i□ rein□orce□ allo□ □□1 essa□ □□ macrograp□ anal□sis

□t□s ver□important to □now how good the recover□of TiB_2 particles is after the dissolution in the molten aluminium. Ti recover□percentage is estimated (b□the base allo□composition, the percenta□e of added reinforcement and the obtained allo□composition) of 78.3% in the SHS TiB_2 reinforced allo□and 76.2% in the commercial TiB_2 reinforced allo□. □t□s not a ver□good recover□rate, because if we compare with Al Ti5 B1 standard row, the percentage is about the 98%.

As we can see in the micrographs in table 4.23, there is a non-homogeneous grain, with e□uia□ial dendrites in the peripher□ and columnar dendrites in the center. □er□ little microshrin□ages are observed.

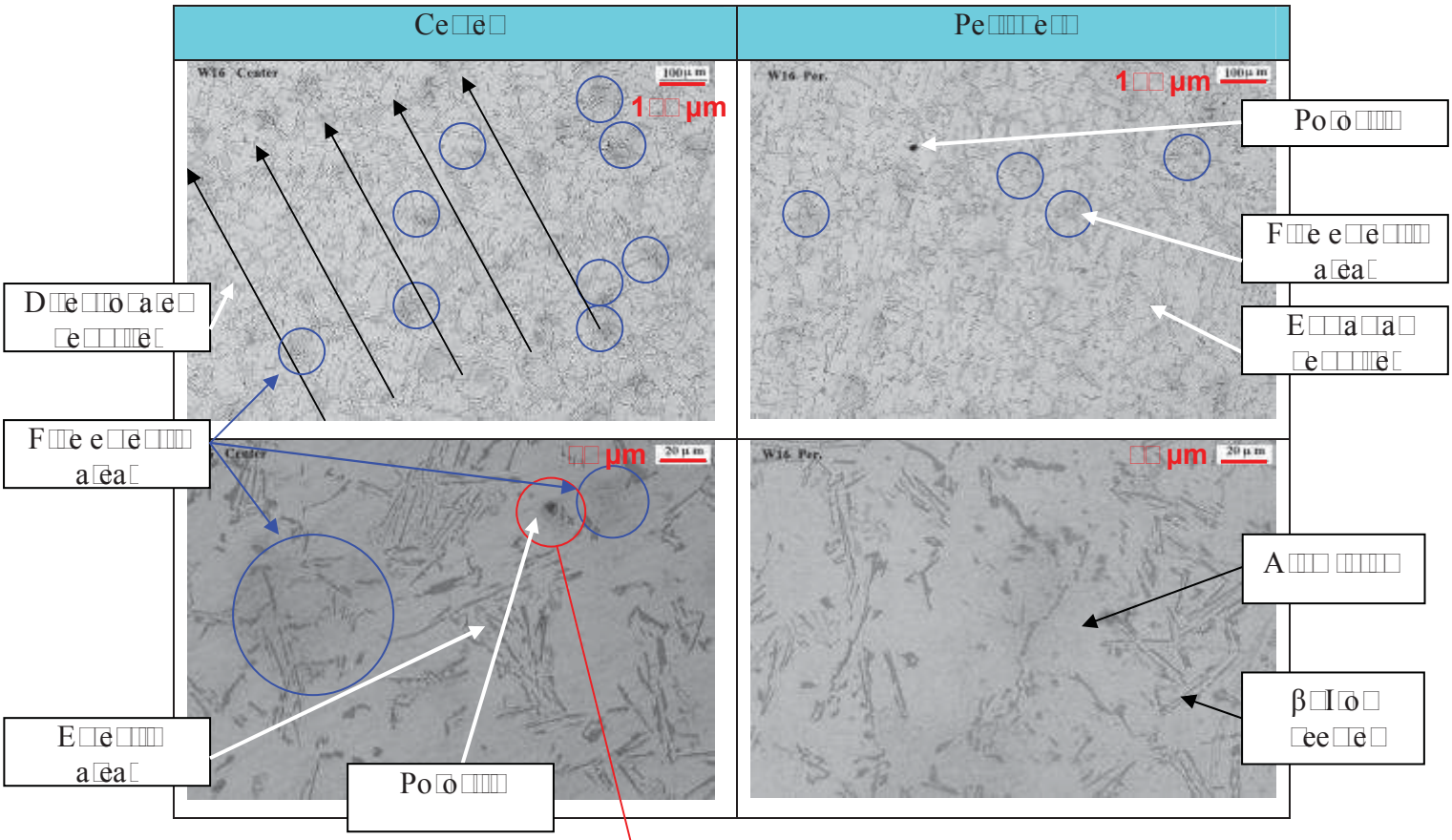

Fig. 4.□□□□ □ □tu□□o□grain an□ precipitates in t□e central an□ perip□eral areas

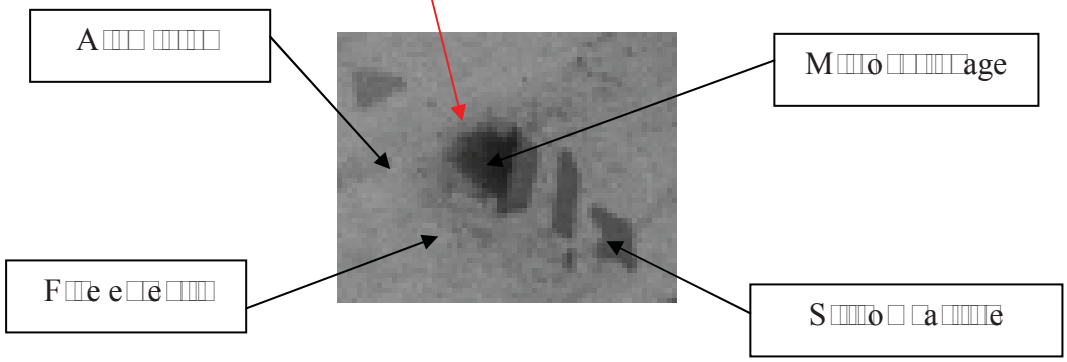

The porosit□decreases in the center, being stabili□ed b□eutectic silicon particles.

□ ith the combination of □DS and S□□ we determinate the different elements that constitute the allo□, as we can observe in Fig. 4.24 and Fig. 4.25. □ e can□t see in the pictures the composition and the presence of TiB_2 particles in the center or in the border of grain. There is a different structure in the peripher□ and the center of the sample, as we have seen in the optical microscop□. TiB_2 particles modif□ the microstructure of the samples, giving two different areas, one granular in the peripher□ and another acicular in the center. □n this acicular area, the grains are orientated, and the sub grains are much smaller, with a best distributed eutectic. □ e can see that the aluminium dendrites are surrounded b□ ver□ fine eutectic silicon and intermetallics, with a higher concentration of solute in the center, and the onl□ difference between the two TiB_2 reinforced allo□s is that in the case of commercial TiB_2 reinforced allo□ are less fine eutectic areas than in the case of reinforcing with SHS-TiB_2. The □DS and S□□ observed Fe intermetallics are formed as s□eleton structures in the center, but small β-iron rich needles are detected in the peripher□. □ot β-iron needles are detected. There is a higher solute concentration in the center, with narrowest dendrites. Same porosit□ is detected associated to the eutectic precipitations. There has been not possible to detect an□ TiB_2 particle in the sample. □ e suppose that the TiB_2 is well dissolved in the aluminium matri□ or in the grain boundar□, and in this case, the titanium concentration is so low that it□s ver□ difficult to detect b□ □DS.

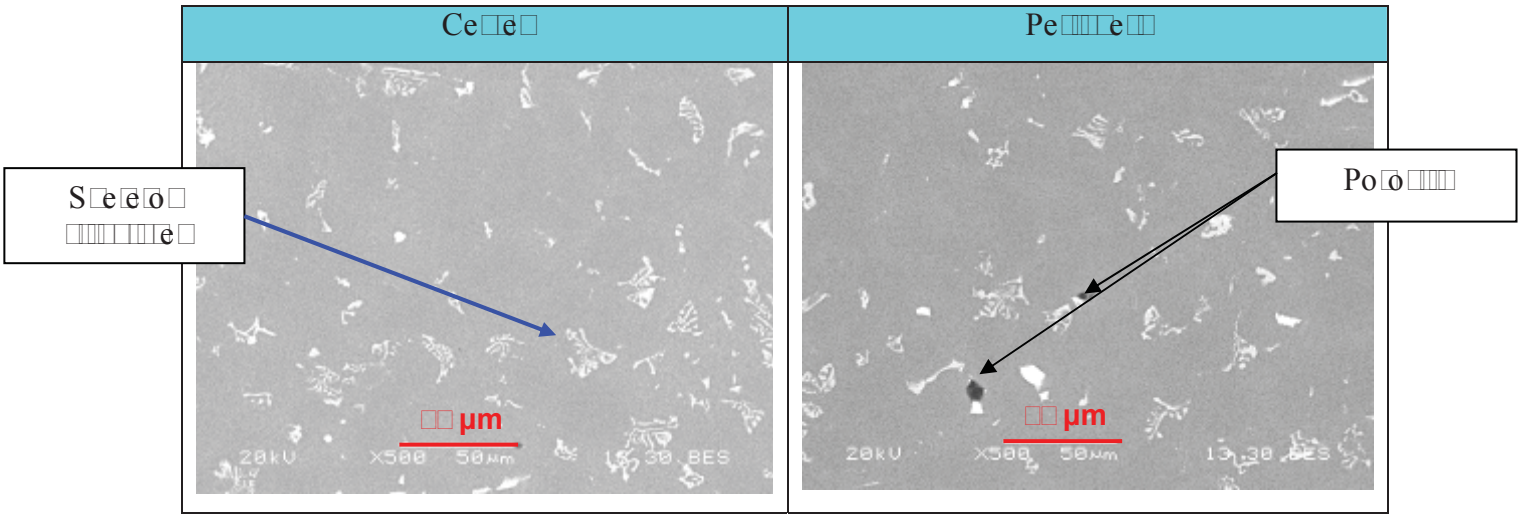

Fig. 4.□4.□□□□ stu□□o□□□□-□i□ rein□orce□ allo□

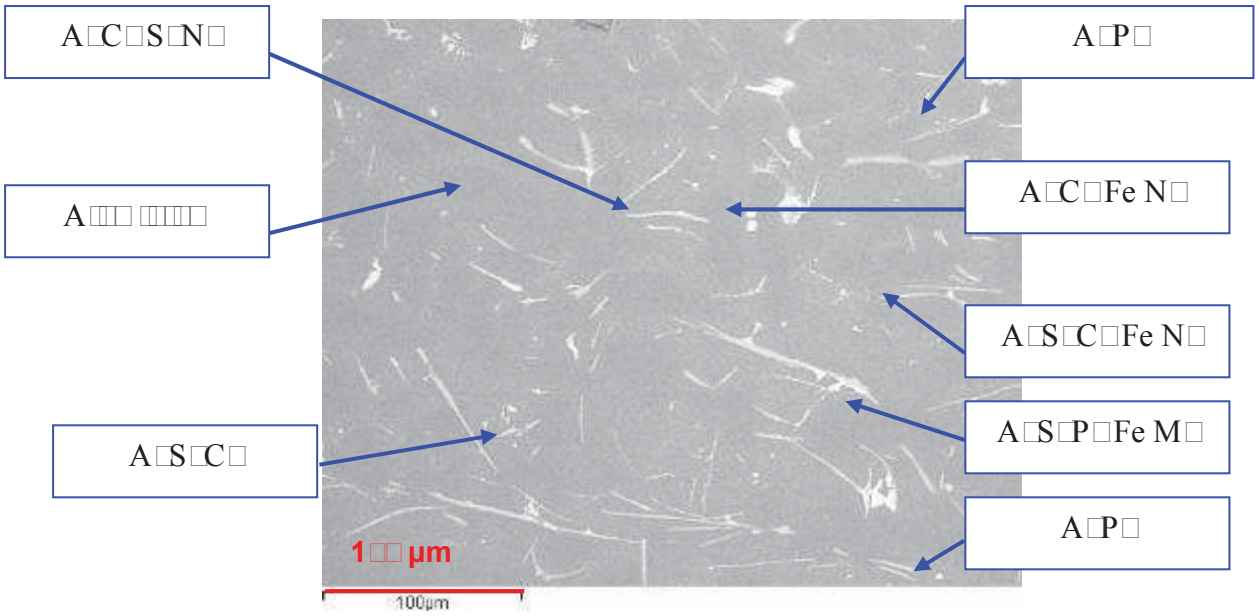

Figure 4.□□.- □□ase □etermination in □□□-□i□□ rein□orce□ allo□ b□ □□□ an□ □□□

□ e can obtain the ne□t conclusions after the anal□sis of the differences between the center and the peripher□□

- □□uia□ial dendrites in the peripher□, and □□uia□ial - Columnar in the center.
- Higher solute concentration in the center.
- □arrowest and directional □oriented dendrites in the center.
- □ore areas with the ver□fine eutectic structure in the central area (Blue circles in Fig. 4.23).
- The porosit□decreases in the center, being stabili□ed b□eutectic silicon particles (Fig. 4.23). □ess porosit□than the Al-Si9Cu3 base allo□.
- Free β-iron phases have been not detected. However lots of beneficial s□eleton structures are dispersed homogeneousl□.

□□□.1 wt.□ o□gamma □l□□□ an□ □.17wt. □ o□al□a □l□□□□

The stud□ of the microstructure of Al_2O_3 reinforced allo□ is important to determinate the structure and properties of the reinforced allo□s, and also can give us the distribution, si□e and function of Al_2O_3 particles in the grains and grain boundaries. After the anal□sis of the different samples, we have concluded that micrograph structures are near the same in both Al_2O_3 reinforced allo□s. Because of that, we are going to show the results of the stud□ of one of the allo□s, in this case the 0.1 wt.% γ-Al_2O_3 reinforced allo□. □e can observe in Fig.4.26. that there are e□uia□ial dendrites in the peripher□ and columnar dendrites in the center. □o microshrin□ages are observed.

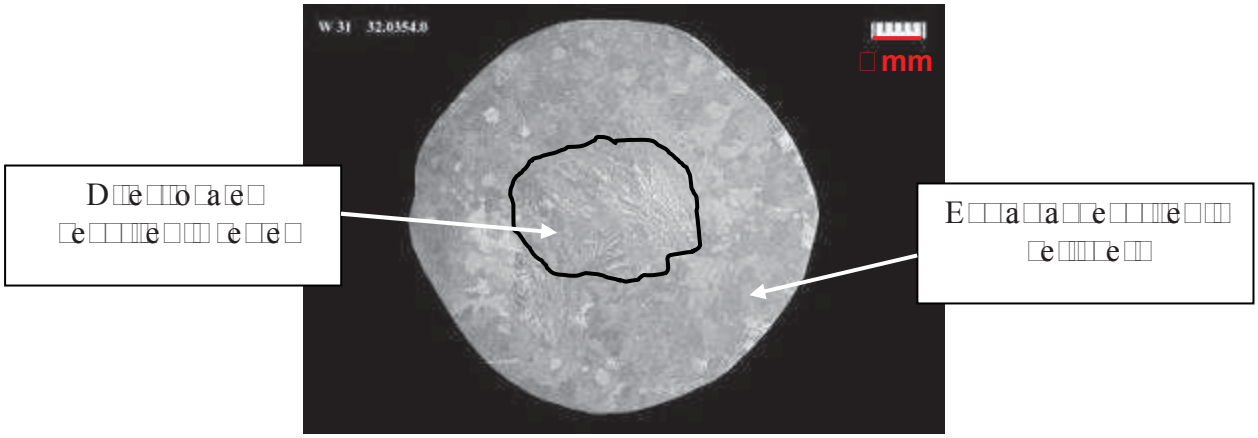

Figure 4.□□.- □.1 wt.□ γ-□l□□□ rein□orce□ allo□ □□1 essa□ □□ macrograp□ anal□sis

The alumina recover□ percentage is estimated (b□ the base allo□ composition, the percenta□e of added reinforcement and the obtained allo□ composition) in a 78.3%. □t□s not higher due to the low melting temperature and because we don□t use magnesium to increase the dissolution of Al_2O_3.

As we can see in the micrographs in Fig. 4.27., there is a non-homogeneous grain, with e□uia□ial dendrites in the peripher□and columnar dendrites in the center. □er□little microshrin□ages are observed.

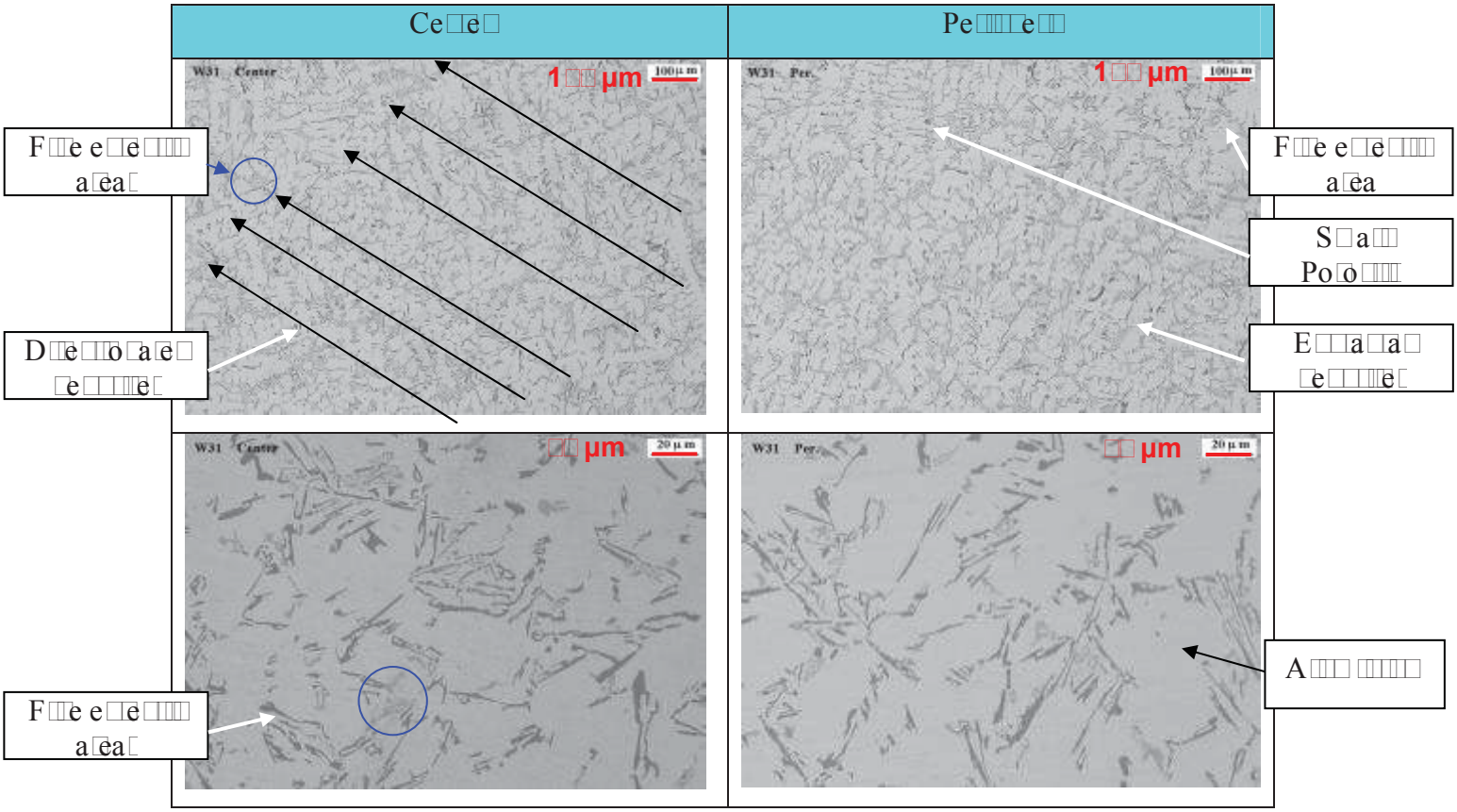

Figures 4.□7.□□□ □tu□□o□grain an□ precipitates in t□e central an□ perip□eral areas

□ ith the □DS and S□□ we determinate the elements that constitutes the allo□. □ e can observe the composition of the phases in the Fig. 4.28.

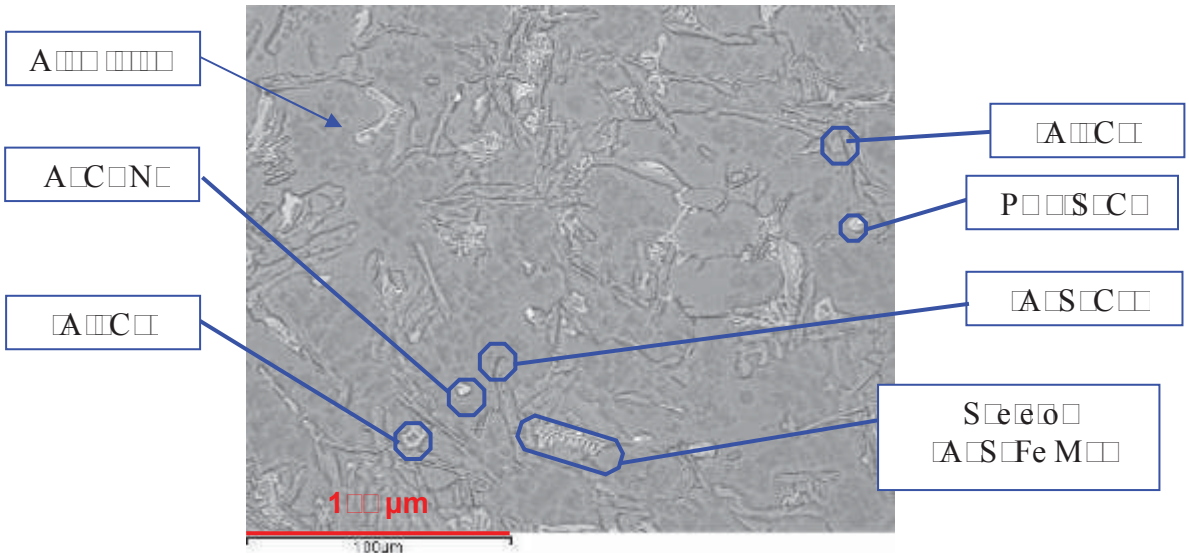

Figure 4.□□.- □□ase □etermination in γ-□l□□□ rein□orce□ allo□ b□□□□ an□ □□□

□ e can observe the presence of Al_2O_3 in the allo□in the center of the aluminium grains and in the grain boundar□ in the Fig. 4.29. A,B,C,D and □. The grains inside the aluminium grains affect the nucleation effect. The grains that are near the grain boundaries are pushed b□ the solidification front, but observed Al_2O_3 particles in spite of being near the grain boundaries, the□seem to be also nucleating sides.

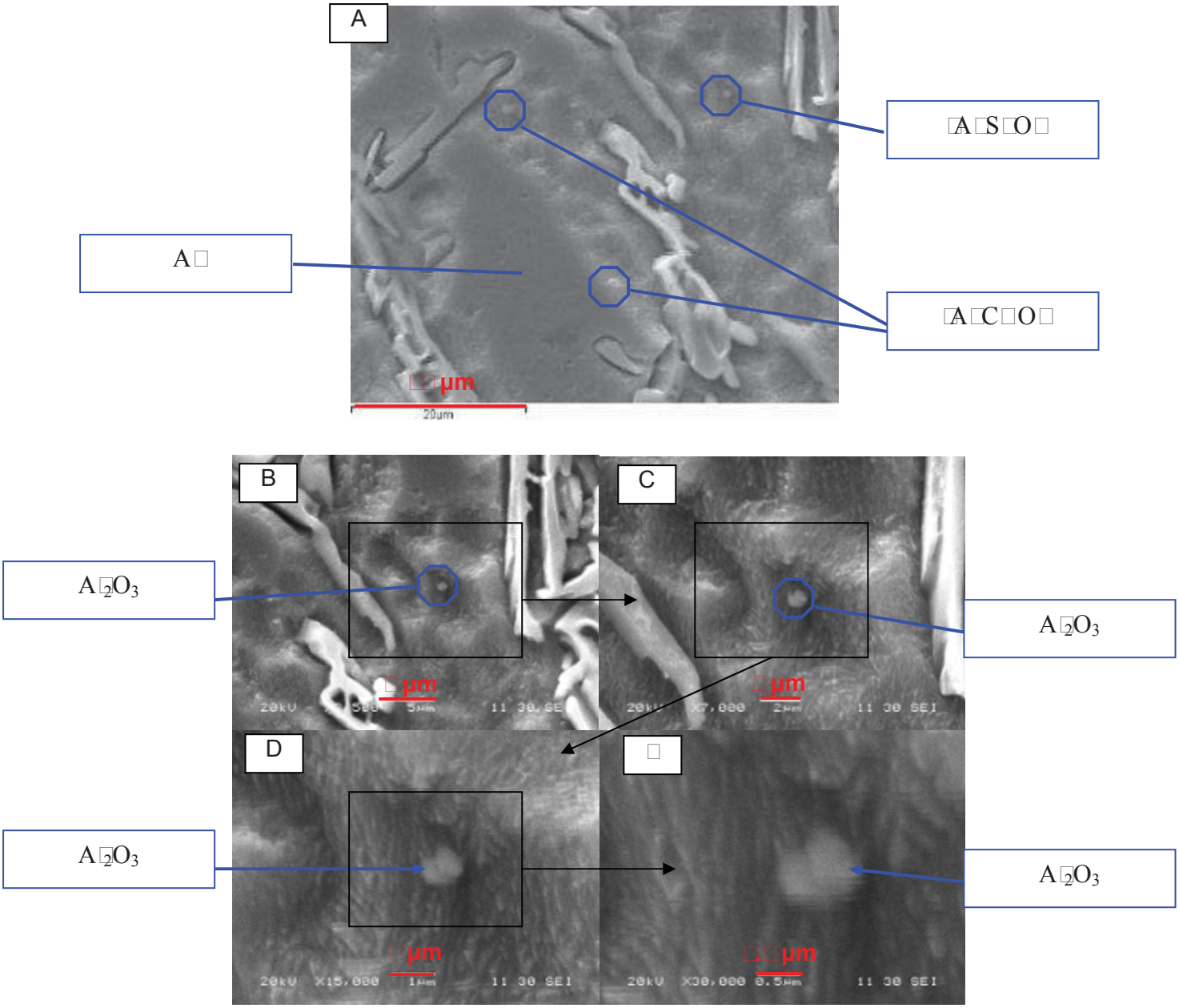

Figures 4.□□. □□□□□□□ an□ □.- □l□□□ particles □etection b□ □□□□ an□ □□□

Al_2O_3 particles are presented in the center of the grains. The□act as grain refiners, with an agglomerated structure of about 0.5 to 1 □icrons, which corresponds to the si□e more ade□uate to act as grain refiner for TiB_2 nucleating particles □□ue 04-02□.

□ e can obtain the ne□t conclusions after the anal□sis of the differences between the center and the peripher□, and from the microstructure□

- □□uia□ial dendrites in the peripher□ and □□uia□ial - Columnar in the center.
- □ear no porosit□ is observed and the detected porosit□ is ver□small. The porosit□ is mainl□in the interdendritic area.
- Higher solute concentration in the center.
- □ore areas with the ver□fine eutectic structure in the center area (Blue circles in Fig. 4.27), but less than the nano-reinforced TiB_2 samples.
- Detected Al_2O_3 particles are in the center of the grains, acting as solidification nuclei. The□show a rounded agglomerated structure of about 0.5 to 1 microns.
- □arrowest and directional □oriented dendrites in the center.

□ e can also observe the presence of Al_2O_3 in the allo□in the Fig. 4.30. A,B and C. The detected Al_2O_3 particles are again in the center of the grains, acting as nucleating sides.

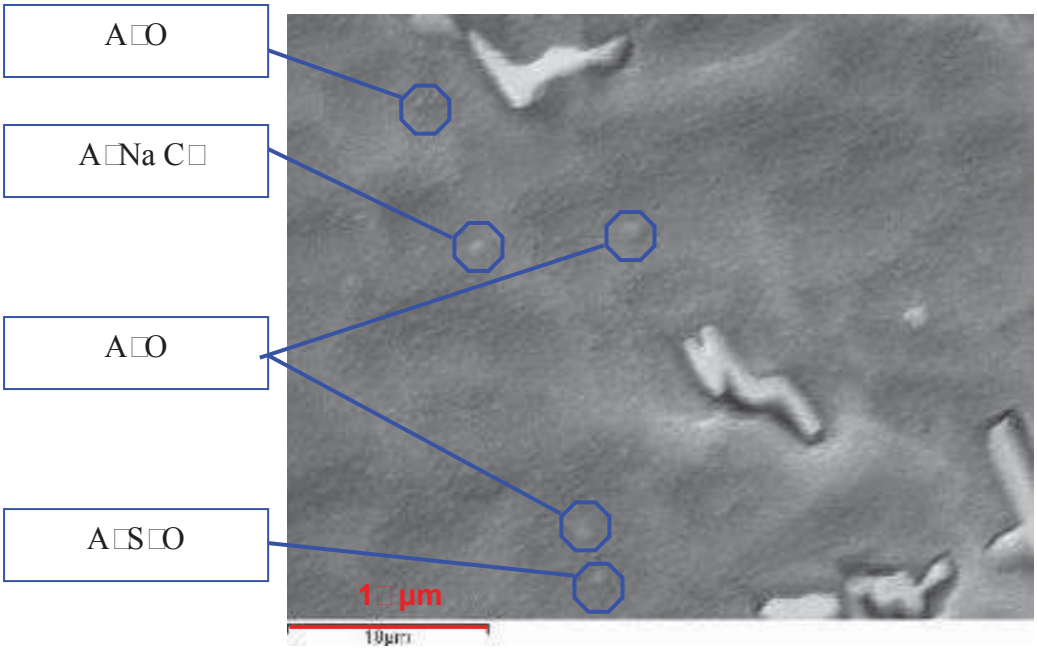

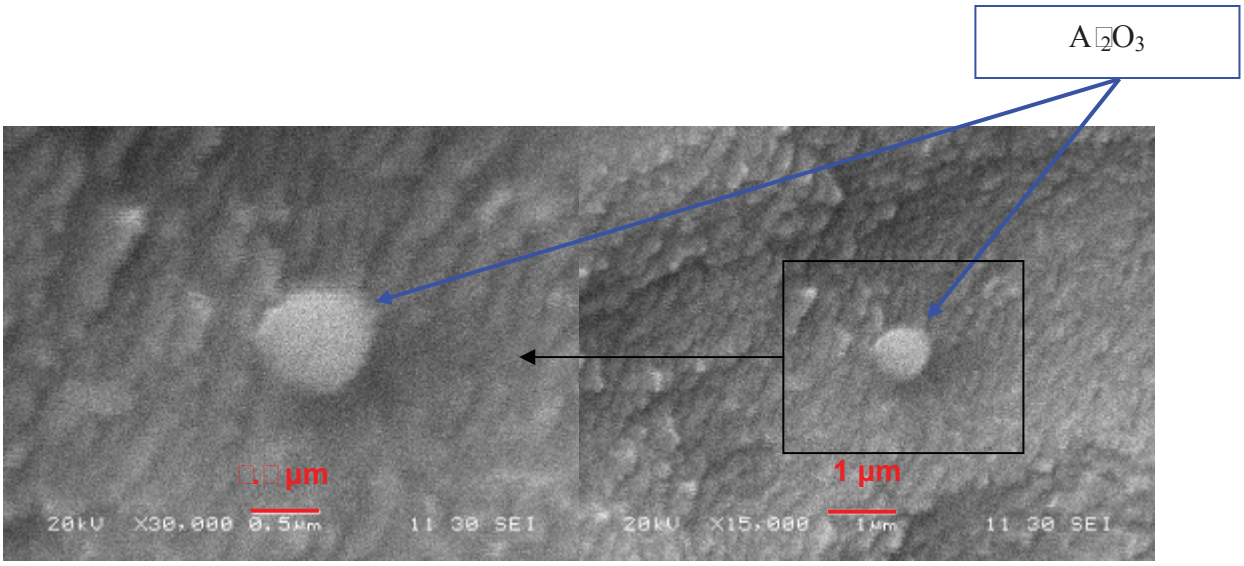

Figures 4.□□. □□□ an□ □.- □l□□□ particles □etection b□ □□□ an□ □□□

□ e can obtain the ne□t conclusions after the anal□sis of the differences between the center and the peripher□and from the microstructure□

- □□uia□ial dendrites in the peripher□and □□uia□ial - Columnar in the center.
- Higher solute concentration in the center.
- □er□small porosit□is detected. There is not big porosit□, and the presented porosit□ is in the interdendritic area.
- □arrowest and directional □oriented dendrites in the center.
- □ore areas with the ver□fine eutectic structure in the center area (Blue circles), but less in comparison with TiB_2 reinforced allo□s.
- Detected Al_2O_3 particles are in the center of the grains, acting as solidification nuclei. The□show a rounded agglomerated structure of about 0.5 to 1 microns.

4.□.1.□□ □□ anal□sis

□n order to determinate the differences between the peripheral and central area, □ DS anal□sis has been made. □an□ different precipitates have been determined, but we focus on defining if the central area has a higher solute concentration. □ ith this purpose a dendritic area has been anal□sed, to compare their compositions. □ e can see in Fig. 4.31 an e□ample of □ DS in the pheripheric area. □ e observe how the aluminium wt.% is appro□imatel□a 97.5 wt.%. The rest of elements remains □uite stable in their values, with a Cu and Si concentration of about 0.9 wt.%.

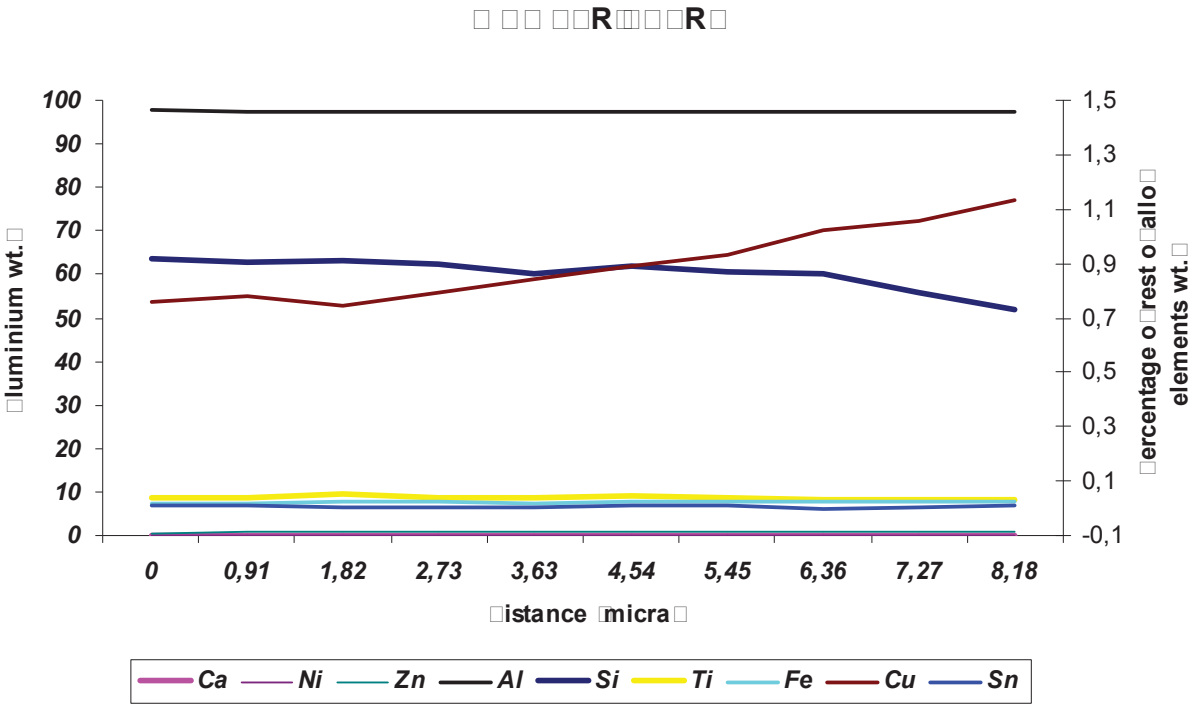

Figures 4.□1.- □etermination o□perip□eral □l □en□rite composition b□ □ □□

□f we observe the Fig. 4.32. of an e□ample of □ DS in the central area, the estimated aluminium wt.% is about 95.5 wt.%. The rest of elements have a bigger concentration, with a 0.7 wt.% Si, a 1.5 wt.% of □n and a 2 wt.% of Cu.

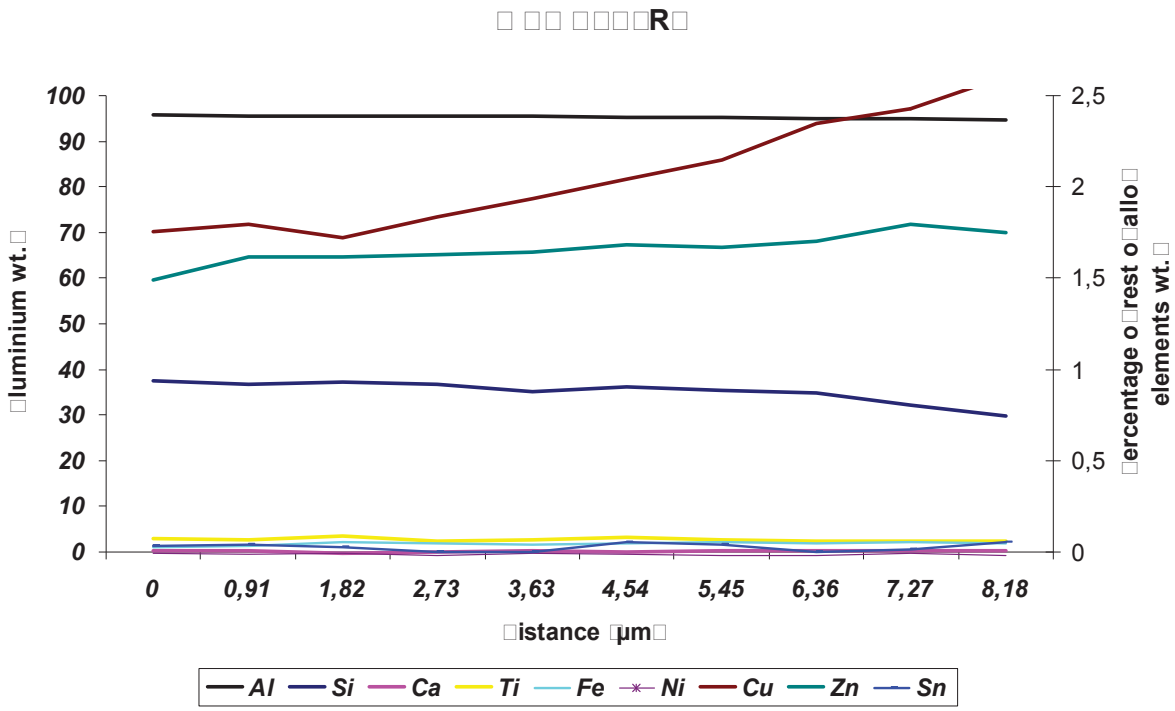

Figures 4.□□.- □etermination o□central □l □en□rite composition b□ □ □□

□n despite of been a ver□punctual detection s□stem, we see a tendenc□to increase the solute and to decrease the aluminium percentage between the samples in the wa□from the peripheral to central areas. The aluminium percentage changes from appro□imatel□the 97.5% to 95.5% in weight in from the e□ternal to the center area.

4.□.1.□ □□□ an□ □□□ anal□sis o□t□e rein□orce□ material

The reinforced samples were anal□□ed through T□□ in order to stud□the effect of the Al_2O_3 and TiB_2 particles in the generation of dislocations as well as possible reaction la□ers between the particles and the matri□ and to determinate the role of ceramics in the precipitation of intermetallic phases.

The T□□ anal□sis of the TiB_2 and nano- reinforced Al_2O_3 Al Si9 Cu3 allo□s shows some common features concerning the Al-Si based allo□. T□□ has been emplo□ed due to the difficulties with S□□ to detect the TiB_2 nano-particles in the matri□ and to determinate the particles that can□t be detected b□ S□□. The□ are not big differences between the reinforced Al_2O_3 and TiB_2 materials, and that□s the reason wh□we have focused the stud□ in determinate the differences between the central and peripheral area.

Two different samples have been emplo□ed. The first is has a 0.1% of gamma Al_2O_3 and the second has a 0.01% of commercial TiB_2, because the different reinforcement have same microstructure with the same reinforcement element.

The aluminium allo□ed samples reinforced with TiB_2 and Al_2O_3 were anal□□ed through T□□ in order to stud□ the effect of the reinforcement particles with the microstructure and with the chemistr□ of the matri□□reinforcement interfacial □ones. As alread□ described, 2 areas related to the acicular grain □one (mainl□ in the center of the foundr□ samples) and to the small grain □one (mainl□ on the edge of the foundr□ sample) have been anal□□ed b□ T□□ for both reinforced composite materials.

Basicall□ we have observed difference in the microstructure for the samples anal□□ed in the center and samples anal□□ed in the edge but we do not have observed an□ difference on the microstructure of the matri□ between sample reinforced with TiB_2 and sample reinforced with Al_2O_3. Therefore the discussion of this T□□ part will onl□ be associated with the locali□ation of the T□□ samples (center or edge) but not with the reinforcement t□pe (TiB_2 and Al_2O_3).

Figures 4.33. A and B shows t□pical microstructure of the matri□ ta□en into the **center** of the sample where acicular grains are found in two areas.

Fig. 4.33. A

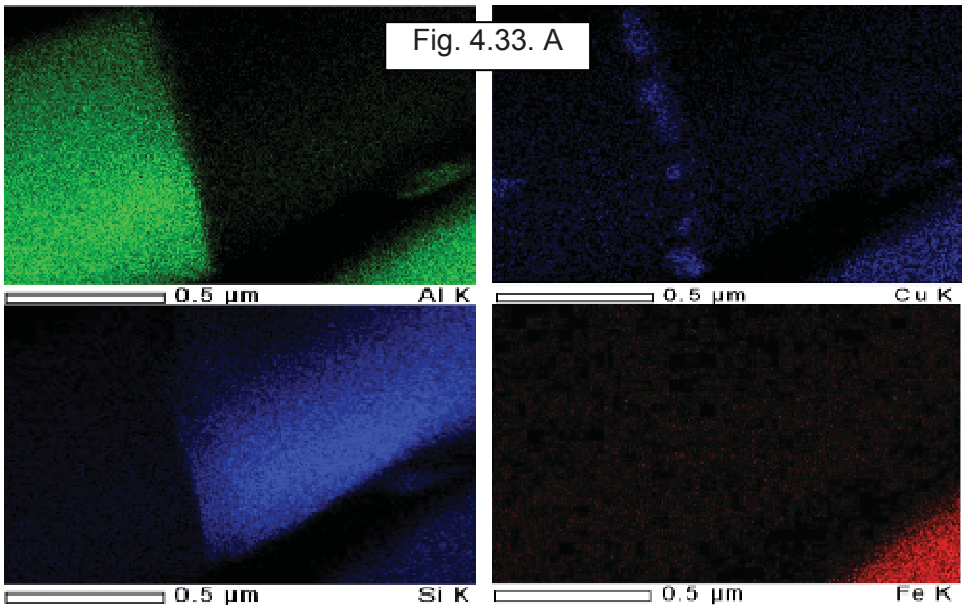

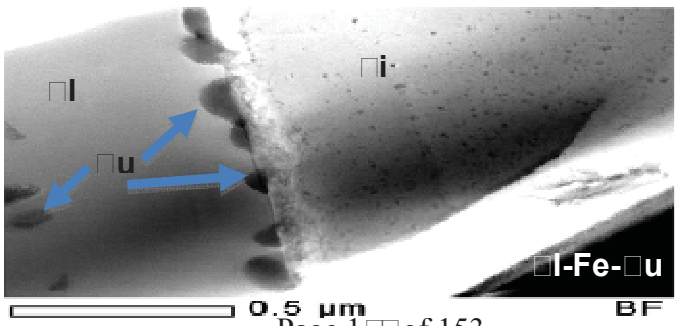

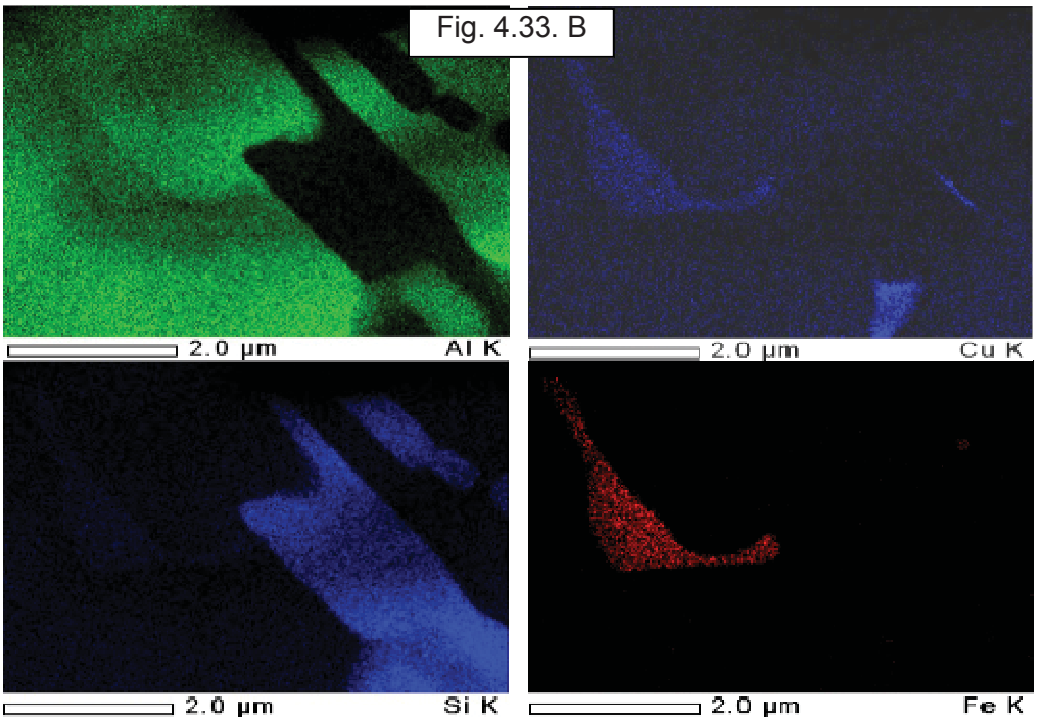

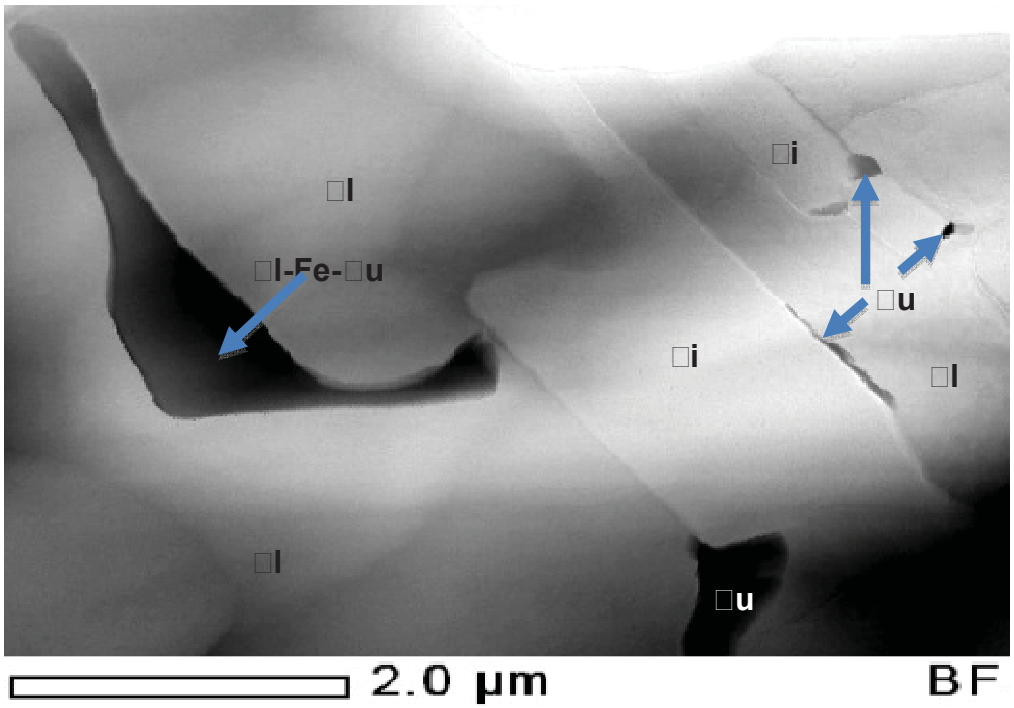

Figure 4.□□.- □ an□ □ □T□□ micrograph of t□pical microstructure of sample in the center of the foundr□sample namel□acicular grain □one. □ach T□□ micrograph (bright field image is associated with 4 □DS corresponding maps (Al, Cu, Si and Fe)).

Several features can be observed□

1. Densit□ of dislocation is negligible. □o dislocations are observed on T□□ pictures.
2. □arge single cr□stal grains of pure silicon are observed. Also ver□ small rounded silicon cr□stals are detected. There are normall□ Si cr□stals, but with few Cu inside, and same of the detected Cu could be attributed to the ion milling processing of samples.
3. At the boundar□ of the Si grain and inside the Al one, precipitation of pure Cu spot (grain si□e close to 150 nm) are observed.
4. Al-Fe-Cu grains are observed inside Al grains, normall□ relativel□ smalls (□5 microns) and with a no deleterious acicular shape.
5. Al grain si□e is in the order of few microns in diameter.

Figures 4.34. show t□pical microstructure of the matri□ ta□en into **t□e perip□eral area o□ sample**.

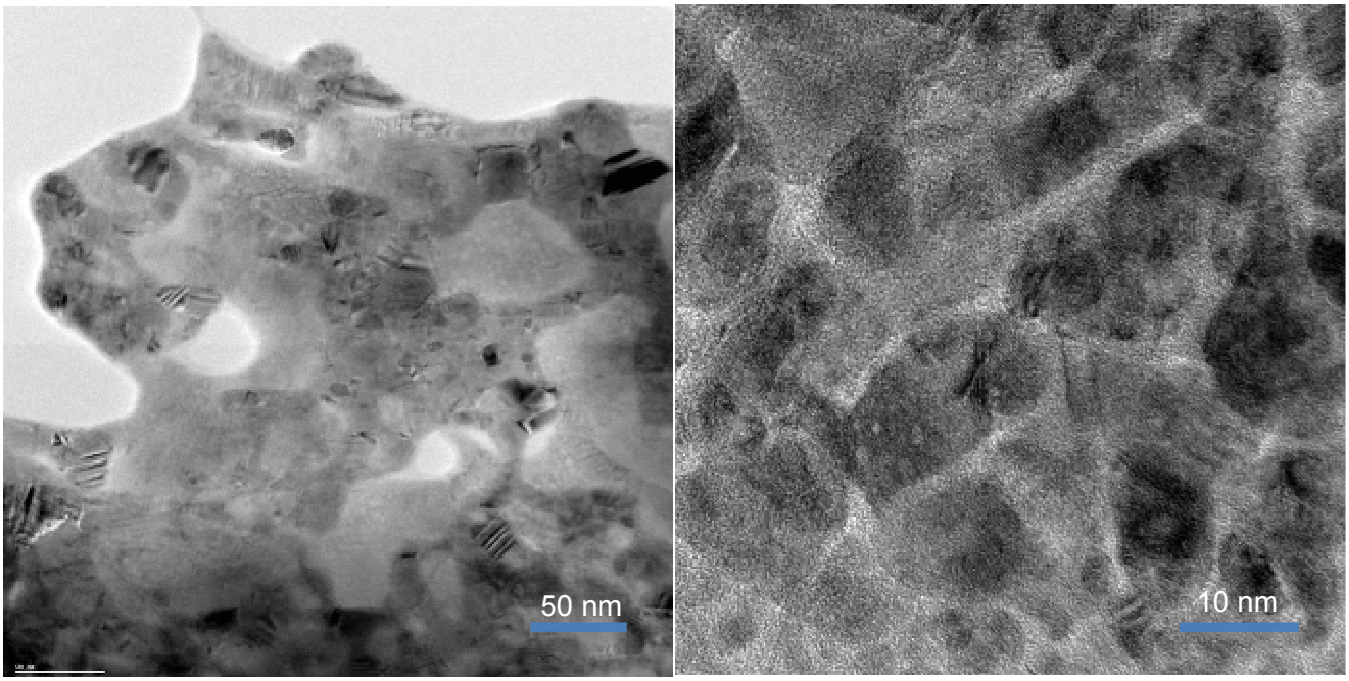

Figure 4.□4.- □□□ micrograp□ o□t□pical microstructure o□sample in t□e e□ge o□t□e □oun□r□ sample

Figures 4.35. A) and a B) show t□pical microstructure of the matri□ ta□en into **t□e perip□eral area o□sample**, where small grain □ones are found. □ach of the bright field micrograph is associated with □DS maps in order to anal□□e the distribution of the Al, Cu, Si and Fe elements within the T□□ anal□sis □one.

Fig. 4.35. A

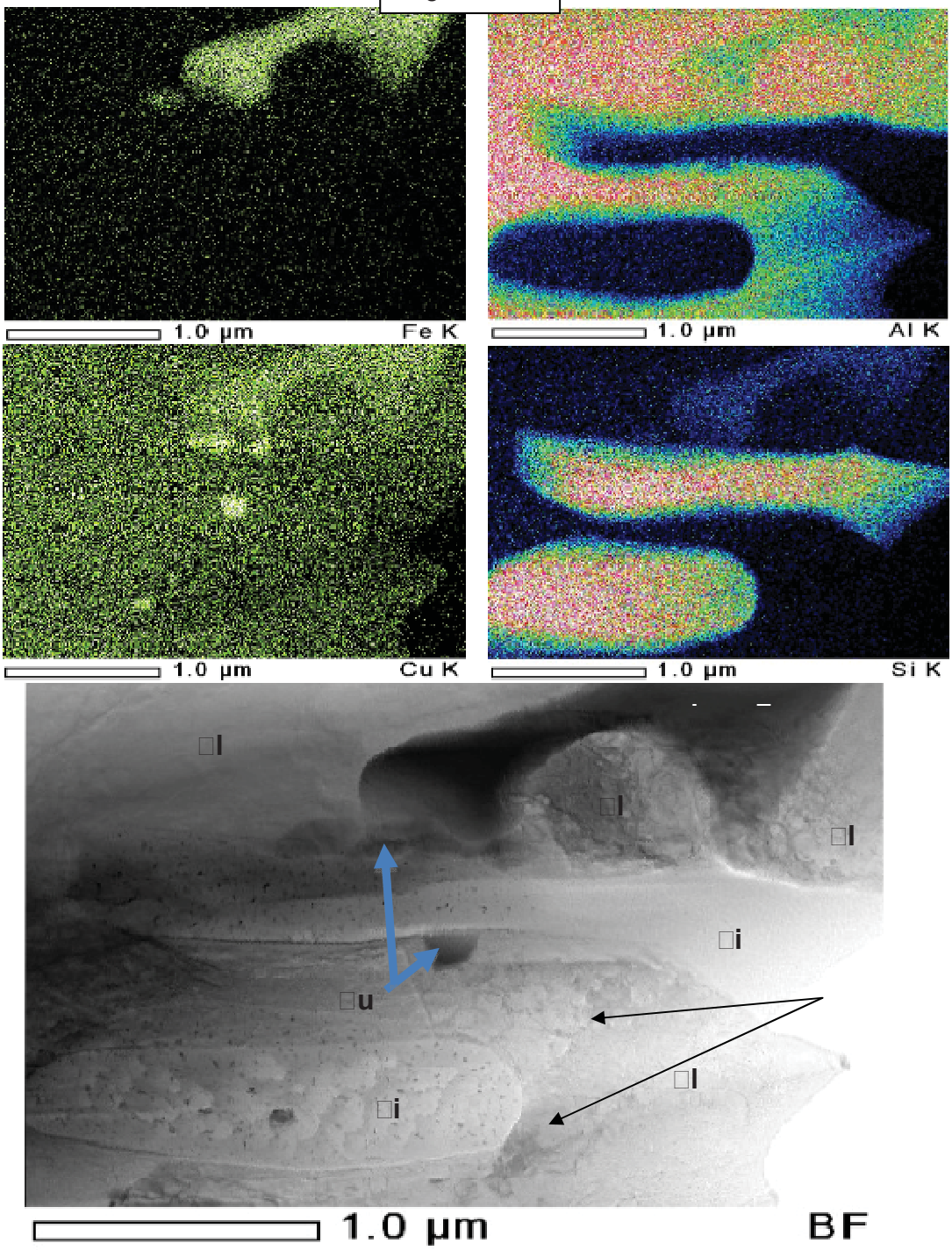

Fig. 4.35. B

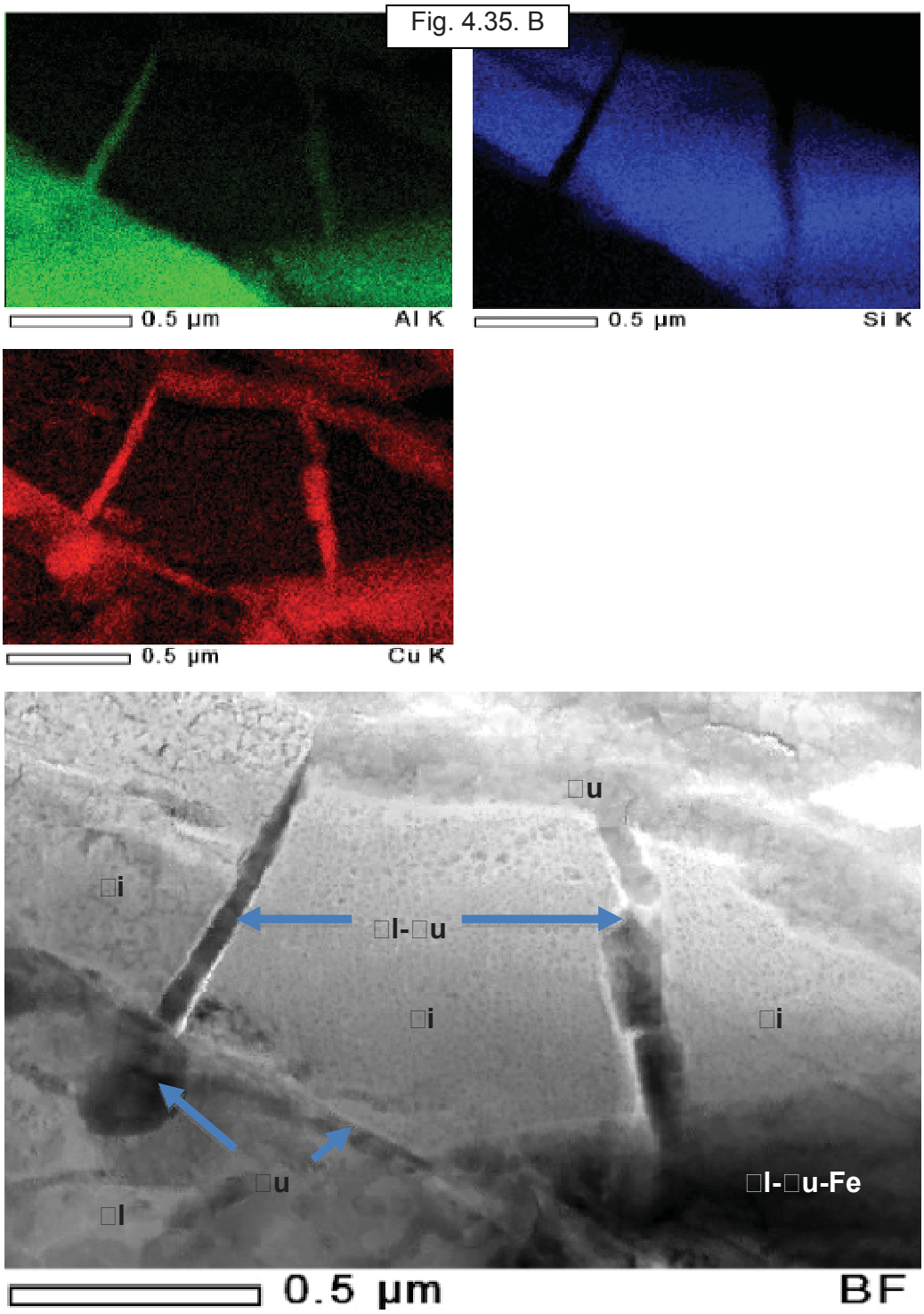

Figure 4.□□. □□an□ □□.- □□□ micrograp□ o□t□pical microstructure o□sample in t□e e□ge o□t□e □oun□r□ sample namel□ small grain □one. □ac□ □□□ micrograp□ □brig□t □iel□ image is associate□ wit□ 4 □□□ correspon□ing maps □□l□□u□□i an□ Fe□.

Several features can be observed□

1. Densit□ of dislocation is negligible. □o dislocations are observed on T□□ pictures.
2. □arge single cr□stal grains of pure silicon are observed.
3. At the boundar□ of the Si grain and inside the Al one, precipitation of pure Cu spot (grain si□e close to 150 nm) are observed. □n □ones of fracture of Si cr□stals, these copper grains are observed in the space between the Si cr□stals with length up to 1 µm.
4. Si is normall□ detected in combination with Al and Cu.
5. Al-Fe-Cu grains are observed inside Al grains.
6. Two Al grain si□e □one can be observed□□n first one, the Al grain si□e is in the order of few microns in diameter whereas in the second one (see Fig. 4.36.) Al grain si□e in the order of 10 nm in diameter can be observed.

Several differences can be observed between the central and peripheral area□

1. Densit□ of dislocation it negible in the center and in the peripheral area. □n the case of the peripheral area two different aluminium grain si□es are detected, with a si□e about few microns and the other are of about 10nm. □n the case of the central area, Al grain si□e is in the order of few microns.
2. The silicon is detected as single phase grains in the center, but Al Si Cu structures are more common in the e□ternal area. This can be e□plained b□ a solute enrichment in the center, in concordance with the □ DS anal□ses.

4.□.1.□ □luminium grain si□e

The T□1 samples anal□sis is a normali□ed method to determinate the aluminium grain si□e. But as we are going to observe this method is not ade□uated to determinate the grain si□e of reinforced allo□s. The determination of grain si□e is ver□ difficult, due to the acicular structure in the center of the samples. The first measures were determinate using the AST□ □ 112□1996 □2 standard, but with the criteria of considering the acicular set of subgrain as a uni□ue grain. The results obtained are summari□ed in Table 4.11., that don□t match the O□ observed grain si□es.

Re□erence	□rain □i□e □erip□. □□m□	□rain □i□e □enter □□m□
Al Si9 Cu3 Sample	888	888
0.2 wt.% SHS-TiB_2	944	3333
0.2 wt.% Commercial TiB_2	1059	3882
0.1 wt.% of γ Al_2O_3	1059	3705
0.17 wt.% of α Al_2O_3	1176	4588

□able 4.11.□□□□□ □ 11□□1□□□ □□grain si□e □etermination

This s□stem it□s not ade□uate to determinate the grain si□e, because the dendrites are ver□ long and ver□fines in the acicular □one with □ones where different dendrites can cross one to the other, as we can observe in Fig. 4.36.□

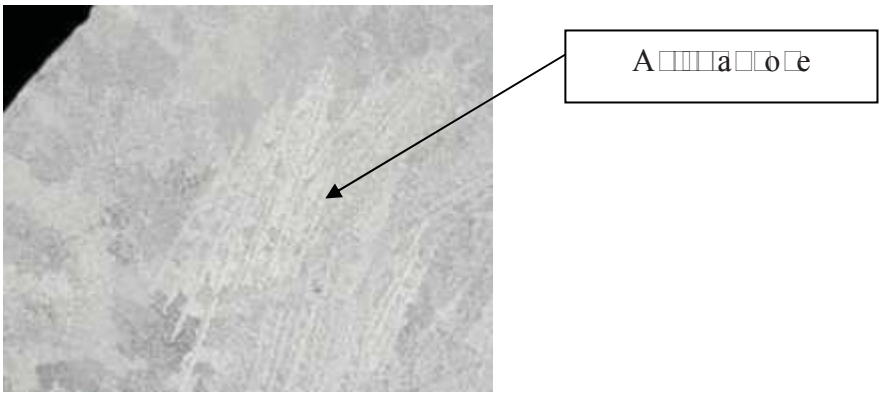

Figure 4.□□.- □cicular □en□rite □one □etail in t□e center o□a rein□orce□ allo□

As much as it□s ver□difficult to determinate the grain si□e of the central acicular □one we have chosen another method to determinate the real grain si□e. SDAS (Secondar□ dendrite arm spacing) determination has been done to determinate the nucleating effect of ceramic particles. □ hen there is a reduction in the SDAS, the nucleation is better and better mechanical properties are obtained □Cac 96□. The final SDAS variates with the solidification time and the solute profile of the solidif□ing allo□ □□as 10-1□. □ e observe in Fig. 4.37. what it□s the SDAS over a real dendrite.

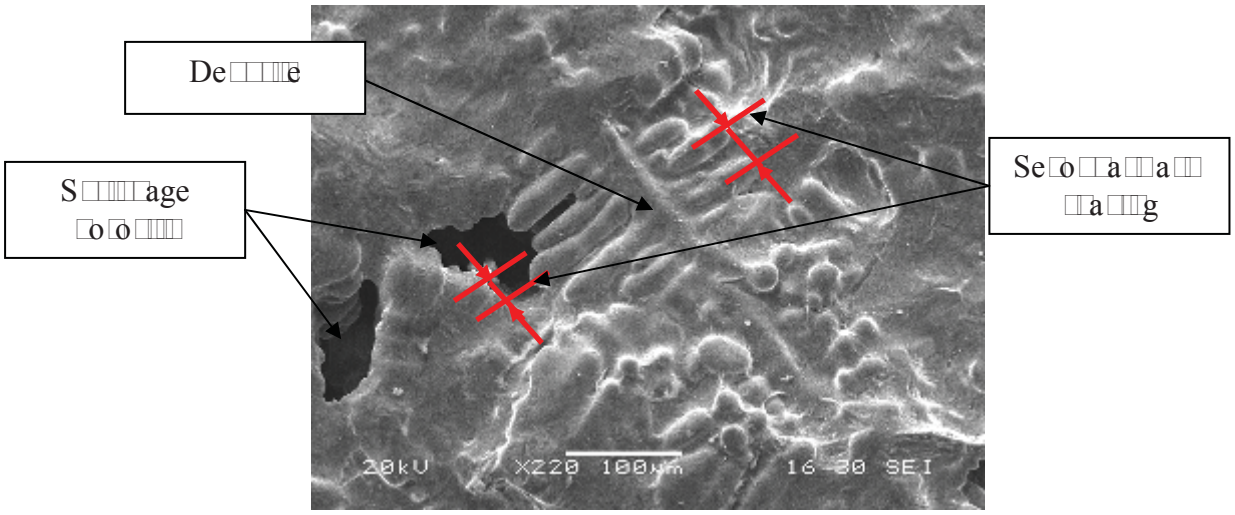

Figure 4.□7.- □econ□ar□ □en□rite arm spacing □etermination

□n order to determinate the SDAS, as the dendrite structure is not e□uia□ial all over the samples, □mage□ software has been emplo□ed, 20 different measure points have been determinate for ever□ allo□ to calculate the average SDAS value, as we can see in the red mar□s in Fig.4.38.□

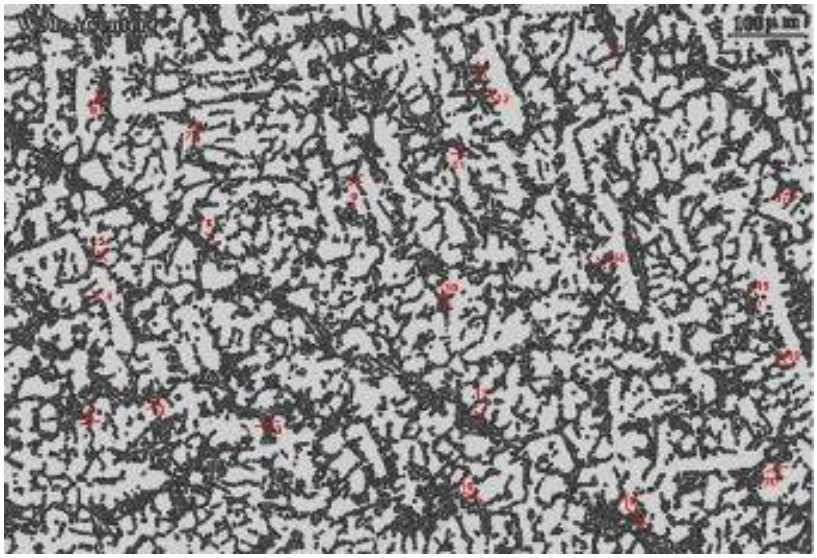

Figures 4.□□.- □econ□ar□ □en□rite arm spacing □etermination

□n H□DC castings, where there are ver□ high cooling rates the intermetallic particles are t□picall□ in the order of 10 to 50 μm □Ta□ 04□. □n our case, the T□1 essa□ has high cooling rates, but smaller than H□DC, because we have emplo□ed the obtained T□1 samples to determinate the grain si□es. □esults show that reinforced allo□s in DC samples have a SDAS that we can even compare with H□DC values. □ e see the results in the Table 4.12.□

Re□erence	□□□□ □erip□.□□m□	□□□□ □enter □□m□	□ariation □□m□
Al Si9 Cu3 Sample	26	34	□8
0.2 wt.% SHS-TiB_2	30	26	-4
0.2 wt.% Commercial TiB_2	22	18	-4
0.1 wt.% of γ Al_2O_3	28	26	-2
0.17 wt.% of α Al_2O_3	29	25	-4

□able 4.1□.□□□□□ perip□eral an□ central □etermination

□n the non reinforced Al Si9 Cu3 sample, the SDAS in the center is bigger than in the peripher□, due to the highest cooling rate in the peripher□. □n all of the reinforced materials, the SDAS is smaller in the center of the sample, promoting a better nucleation. This can be e□plained b□the increase of the solute and the presence of ceramic particles. There is an e□uation that relations the SDAS with the coalescence time (t_{coales}), that it□s the time were the dendrite arms grow b□coalescence between solidus and li□uidus □□as 10-2□.

$$SDAS = K \cdot t^{n}_{coalesc\square}$$

□ here □n□is between 0.33 and 0.5 and □ is a fitting factor dependent of allo□elemental concentration and constituents. The e□perimental obtained results are represented in Table 4.13., with the coalescence time calculated in Table 4.8., page 85.

□□□□	$t_{coalesc.}$ □□□	□□□□ perip□ □µm□	□□□□ center □µm□
Al Si9 Cu3 Sample	100	26	34
0.2 wt.% SHS-TiB_2	105	30	26
0.2 wt.% Commercial TiB_2	116	22	18
0.1 wt.% of γ Al_2O_3	150	28	26
0.17 wt.% of α Al_2O_3	145	29	25

□able 4.1□.□□□□□ perip□eral an□ central relation wit□ coalescence time

There is not a good relation between the e□uation and the obtained values, but it can be e□plained b□the dendrite form, that it□s not e□uia□ial. □f we emplo□the □time plateau□we observe that a reduction in the plateau time promotes a decrease of the SDAS in the center SDAS, resumed in Table 4.14. with the plateau time calculated in Table 4.8.

□□□□	$t_{□lateau.}$ □□□	□□□□ perip□ □µm□	□□□□ center □µm□
Al Si9 Cu3 Sample	90	26	34
0.2 wt.% SHS-TiB_2	67	30	26
0.2 wt.% Commercial TiB_2	86	22	18
0.1 wt.% of γ Al_2O_3	21	28	26
0.17 wt.% of α Al_2O_3	29	29	25

□able 4.14.□□□□□ perip□eral an□ central relation wit□ plateau time

□ e can detect the tendenc□ to decrease in the SDAS in the center with decreasing plateau time, but there is not also a good relation. Solute concentration in the center of the samples has an acicular directional structure, with a lower SDAS parameter and less porosit□. For the same composition, the higher the cooling rate, the smaller the SDAS and also the smaller the porosit□ □Sei 09□, what can e□plain the increase in the base Al Si9 Cu3 allo□ of SDAS in the center of the sample in comparison with the peripheral area.

4.□.1. □□lectrical con□ucti□it□ anal□sis

The electrical conductivit□ decreases when we add the element addition □□ac 98□and when the grain si□e decreases. □ e observe the different between the different allo□s and the variation in the properties in function of ma□ing the test in the peripher□ or in the center of the test bars, and also in the acicular and granular area, as we can see in Table 4.15 to 4.19.

Base sample

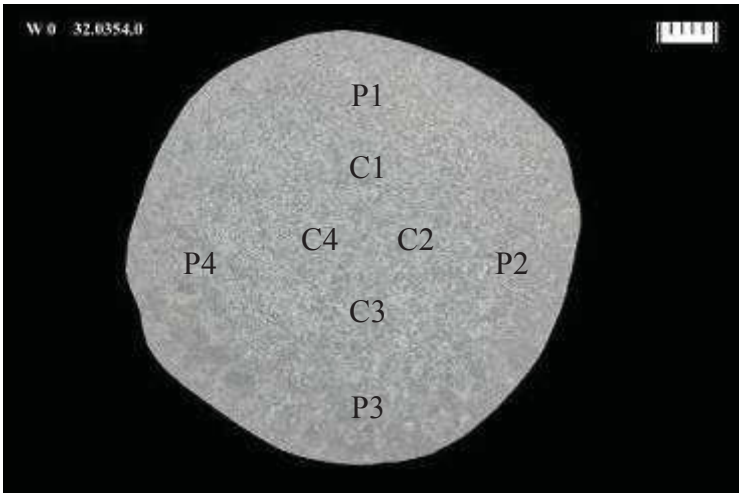

□oint	□alue (%□ACS)	Average (%□ACS)
□1	29.60	30,06
□2	30.15	
□3	30.55	
□4	29.95	
C1	30.00	30,31
C2	30.25	
C3	30.60	
C4	30.40	

□able 4.1□□□□□ □etermination

0.2% TiB_2 SHS

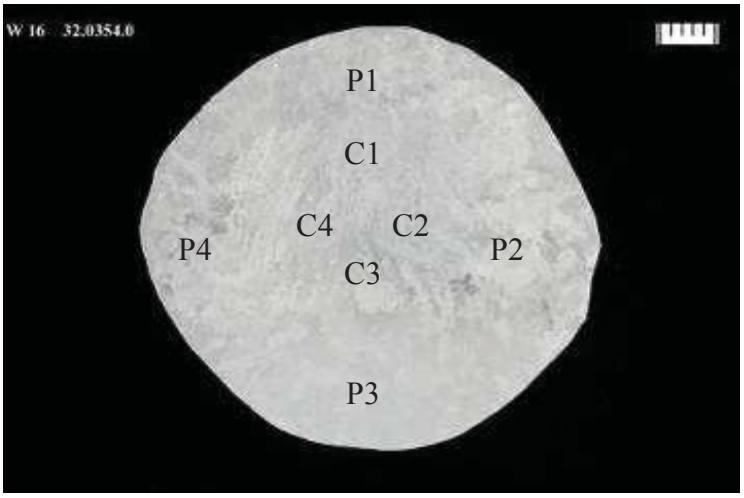

□oint	□alue (%□ACS)	Average (%□ACS)
□1	29.55	29,57
□2	29.60	
□3	29.60	
□4	29.55	
C1	29.55	29,56
C2	29.70	
C3	29.50	
C4	29.50	

□able 4.1□□□□□ □etermination

0.2% commercial TiB_2□

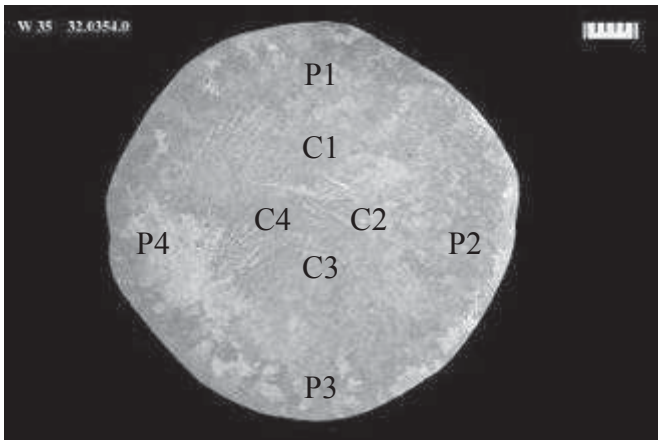

□oint	□alue (%□ACS)	Average (%□ACS)
□1	28.05	28.22
□2	28.75	
□3	28.10	
□4	28.00	
C1	28.05	28.25
C2	28.50	
C3	28.35	
C4	28.10	

□able 4.17□□□□□ □etermination

0.1% Al_2O_3 gamma alumina bri□uette□

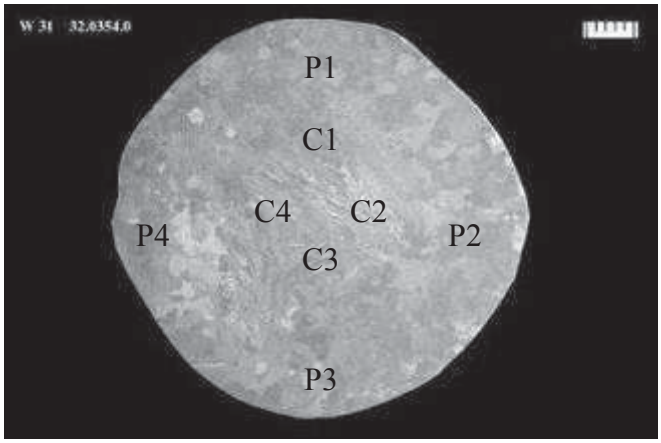

□oint	□alue (%□ACS)	Average (%□ACS)
□1	29.05	29,07
□2	29.05	
□3	29.05	
□4	29.15	
C1	29.00	29,06
C2	29.10	
C3	29.10	
C4	29.05	

□able 4.1□□□□□ □etermination

0.17% Al_2O_3 alpha alumina bri□uette□

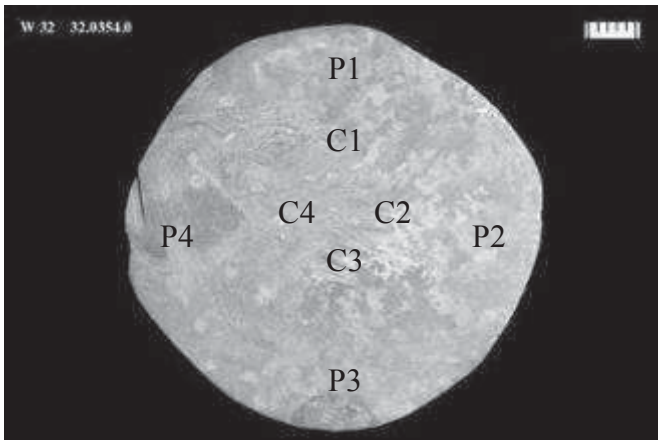

□oint	□alue (□ACS)	Average (□ACS)
□1	28.60	28,65
□2	28.85	
□3	28.85	
□4	28.30	
C1	28.70	28,76
C2	28.80	
C3	28.85	
C4	28.70	

□able 4.1□□□□□ □etermination

□alues for modified samples in both areas are similar. □ e compare the obtained results with the e□pected values obtained from □ADCA formula □□ac 98□ for the different compositions in the Table 4.20.□

□ACS% □ 36.44-0.72Si-0.26Cu-0.32Fe-0.63□g-0.08□n□0.01□i□0.02Cr-0.36□n-0.27Ti□0.31Sr.

	Si	Fe	Cu	Mn	Mg	Cr	Ni	Zn	Ti	Pb	Sr	IACS% NADCA	IACS% Obtained
Al Si9 Cu3 Sample	8.580	0.860	1.780	0.181	0.033	0.049	0.073	0.940	0.045	0.053	0	29.15	30.18
0.2 wt.% SHS-TiB_2	8.610	0.850	1.780	0.186	0.046	0.051	0.073	0.930	0.046	0.053	0	29.12	29.56
0.2 wt.% Commercial TiB_2	8.460	0.950	1.740	0.189	0.029	0.054	0.072	0.930	0.045	0.051	0	29.21	28.23
0.1 wt.% of γ Al_2O_3	8.480	0.880	1.770	0.186	0.012	0.053	0.074	0.930	0.045	0.052	0	29.23	29.06
0.17 wt.% of α Al_2O_3	8.460	0.900	1.730	0.181	0.023	0.051	0.073	0.930	0.045	0.050	0	29.24	28.7

Table 4.20.: IACS determination by NADCA formula and experimental results

As we can see, the values are quite similar, and approximately they match the expected values. A conductivity decrease can be explained, because if we have more grain boundaries is more difficult to conduct the electrical energy. The difference between the center and the peripheral areas are more similar in values when adding ceramic particles, but also the SDAS values difference is smaller between the two areas. In the non inoculated sample, the conductivity in the center is higher than in the periphery, which could be correlated with a higher SDAS value is the center. We can adjust the NADCA IACS% formula to determinate IACS% value, modify to evaluate the effect of 0.02 wt.% of TiB_2 or Al_2O_3 particle additions:

IACS% = 36.44-0.72Si-0.26Cu-0.32Fe-0.63Mg-0.08Mn+0.01Ni+0.02Cr-0.36Zn-0.27Ti+0.31Sr **- 0.31**

The variation of conductivity between the center and the peripheral is also bigger in the non inoculated sample, with a correlation with a higher difference between SDAS values in both areas, as it's reflected in Table 4.21.:

Reference	SDAS Periph.(μm)	IACS% Periph.	SDAS Center (μm)	IACS% Center	SDAS Average (μm)	IACS% Average
Al Si9 Cu3 Sample	26	30.06	34	30.31	30	30.18
0.2 wt.% SHS-TiB_2	30	29.57	26	29.56	28	29.56
0.2 wt.% Commercial TiB_2	22	28.22	18	28.25	20	28.23
0.1 wt.% of γ Al_2O_3	28	29.07	26	29.06	27	29.06
0.17 wt.% of α Al_2O_3	29	28.65	25	28.76	27	28.70

Table 4.21.: IACS and SDAS relation in the peripheral and central area

A decrease in the electrical conductivity can be observed by adding few quantities of ceramic particles □Around a 4% of IACS electrical conductivity value by adding less than a 0.2% of nanoparticles□. The tendency reflects that if the SDAS average value is increased, the IACS% also increase its value, as we can observe in Fig. 4.39.:

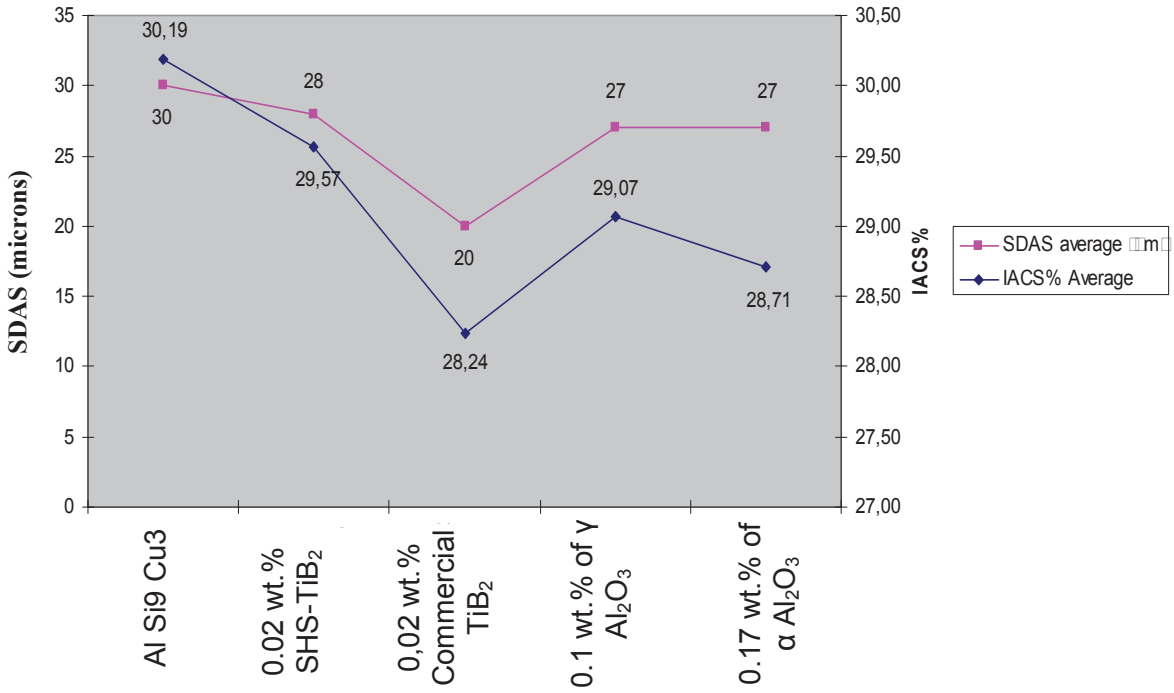

□igure 4.3□: Comparative diagram bet□een SDAS and IACS

4.3.2 Discussion of the results

The comparison of the reinforced alloys with the corresponding unreinforced alloy shows that there is homogeneous grain dispersion in all the areas, with equiaxial dendrites in the periphery and in the center in the case of the non reinforced alloy. Also micro shrin□ages are observed.

In the case of the reinforced alloys, there is a non-homogeneous grain, with equiaxial dendrites in the periphery and columnar dendrites in the center. □ery little micro shrin□ages are observed, and the central dendrites are oriented and are narrowest than the non reinforced alloy.

□ery small β-iron needles are detected, of about 20 microns si□e. The normal si□e of β-needles variates from 10-50 μm in HPDC standard Al Si9 Cu3 alloys □Tay 04□, but is always much smaller in comparison with DC samples employed for the metallurgical examination □Approximately 1□5 of β-needles in DC by comparison with HPDC samples□. This can be related with the si□e and morphology of dendrites and the secondary dendrites arms, than can promote the needles to brea□in smaller needles.

□ery fine eutectic structures are detected in the central area of the reinforced alloys. In the case of TiB$_2$ reinforced alloys there are more than in the case of Al$_2$O$_3$ reinforced alloys. The presence of small Si particles is attributed to Si enrichment of the remaining melt due to the formation of eutectic Al (Aluminium spi□es) at the eutectic temperature. Following the nucleation of eutectic Al on the primary α-Al dendrites, fine Si particles form at the solidification front upon which the eutectic Si fla□es and fibers could develop (Naf 08). This fine eutectic is very interesting to obtain good mechanical properties.

Observing the porosity, Al$_2$O$_3$ nano-particles promote the decrease in the si□e and number of porous. TiB$_2$ nano-particles also have a positive effect. This can be related with the capacity of ceramic particles to stabili□e porosity, and as the total surface of ceramic particles is bigger, the smaller the porosity diameter. In our case, the employed Al$_2$O$_3$ nano-particles si□e (15-40 nm) is much smaller than TiB$_2$ particles (690 nm aprox.), so also the total surface is higher. However as in Fig. 4.30. we can observe nano-particles agglomerations of about 0.5 μm, that reduced the total surface of ceramic particles in contact with the aluminium matrix, but they are placed at the center of the aluminium grains, and they act as grain nucleation sites. In the case of Al$_2$O$_3$ reinforced alloys near no porosity is observed in the microscopy examination. Also a smaller SDAS promotes and smaller porosity, and also SDAS is lower in reinforced alloys.

There is a higher solute concentration in the center of the samples than in the periphery. That promotes dendritic or equiaxial grains, in function of the cooling rate. Aluminium percentage variates approximately from a 97, 5 to 95, 5% Wt. in the center of the reinforced areas, determined by WDS

With the □DS and S□M we can't detect the presence of Ti B$_2$ particles in the center or in the border of grain, due to the small si□e of particles, but more because the very low reinforcing percentage. Al$_2$O$_3$ particles tend to get inside the grain and in the grain boundaries, with an agglomerated structure of about 0.5 - 1 micron. In the case of particles in the center of the grains, the Al$_2$O$_3$ particles act as grain refinement nucleus.

ASTM □ 112: 1996 □2 standards is more adequate to determinate grain si□e of equiaxial grains, and with the determination of grain si□e applying this standard is not possible to explain the behavior of reinforced alloys.

□sing the determination of SDAS, in all the reinforced alloys is smaller than in base alloy, with the smaller SDAS in the case of TiB$_2$. As much as SDAS is directly related with the □TS, its value should be increased as much as SDAS decreases. In the Al Si9 Cu3 sample, a SDAS bigger in the center than in the periphery, can be explained by the highest cooling rate in the periphery. In the rest of cases, SDAS smaller in the center of the sample, promotes a better nucleation, and can be explained by the increase of the solute and the presence of ceramic particles.

There is not a good relation between coalescence time (t_{coales}) and the obtained values, but it can be explained by the dendrite form, that it's not equiaxial. If we employ the time plateau we detect a tendency to decrease SDAS in the center with decreasing plateau time.

Values for electrical conductivity are quite similar, and approximately they match the expected values from NADCA. We can observe a conductivity decrease in comparison with the base alloy. We can explain the decrease in the conductivity because if we have more grain boundaries by a decrease in the SDAS value, is more difficult to conduct the electrical energy. In the non inoculated sample, the conductivity in the center is higher than in the periphery, in correlation with a higher SDAS value is the center.

A decrease in the electrical conductivity can be observed by adding few quantities of ceramic particles (Around a 4% of IACS electrical conductivity value by adding less than a 0.2% of nanoparticles). In our case, the higher SDAS in the non reinforced alloy is associated with an increase of the IACS%.

4.4 Conclusions

The solidification pattern of metallic materials is varied by adding nano and TiB$_2$ particles. The complete study has been determinate by the DTA, TP1 and injection test, simulating industrial parameters.

The microstructure has been determined from TP1 test and also from injected samples, employing different equipments as OM, SEM, TEM and WDS, determining the effect of Al$_2$O$_3$ and TiB$_2$ particles in the microstructure and properties of the alloys.

The analysis of the T-t curves and the corresponding derivatives curves up to the fifth derivative have confirmed the effect of particles in the solidification pattern. Main conclusions of thermal analysis of the reinforced alloys are:

1. Al$_2$O$_3$ and TiB$_2$ particles influence aluminium grains nucleation, eutectic reaction and intermetallic precipitations. The nucleation temperature is increased, as the recalescence temperature. This effect is related to the incorporation of ceramic particles as heterogeneous nuclei.

2. TiB$_2$ has more influence in the nucleation than Al$_2$O$_3$ particles. This is related to the employ of TiB$_2$ in commercial grain refiners as main refiner. Also TiB$_2$ particles are related in some studies as the most effectives for Aluminium grain refining.

3. The influence of the particles should have a positive influence on the mechanical properties of the reinforced alloys since it decrease the undercooling, promoting a better nucleation.

The analysis of the microstructure shows very interesting conclusions that determinate the effect of the Al_2O_3 and TiB_2 particles. It has been demonstrated that the presence of the ceramic nano-particles has a direct effect on the microstructure. These effects should have a corresponding effect on the electrical, mechanical and thermal properties of the reinforced materials. The most important conclusions are:

1□ The employ of ceramic nano-particles reduce the porosity si□e and quantity. It's more remar□able in the case of Al_2O_3 than in TiB_2 particles.

2□ Acicular oriented very fine dendrites are promoted by the nano-particle addition. The SDAS is smaller in the reinforced alloys and also the SDAS decrease in the center of the samples.

3□ Al_2O_3 and TiB_2 particles modify the structure, with smaller detrimental β-iron needles.

4□ □ery fine eutectic structures are detected in the center of the reinforced alloys, especially with TiB_2 reinforced alloys.

5□ The S□M analysis shows that Al_2O_3 particles acts as nucleating points, with agglomerate particles of about 0,5-1 micron.

6□ The T□M analysis shows a very small dislocation density. Alumnimium grains have two different si□es in the peripheral area, with also very fine aluminium grains about 10 nm. The center has a solute enrichment, also detected by WDS.

7□ □lectrical conductivity decreases by adding few quantities of ceramic particles and is quite similar in the center and periphery of reinforced alloys and a relation between SDAS and IACS has been observed.

8□ We can determinate what are the better particle for different industrial applications:

a. Parts with improved mechanical properties: As TiB_2 has an smaller SDAS than Al_2O_3 particles, the □S and □TS can be improved, so it□s more interesting to add TiB_2 particles than Al_2O_3. The shorter distances between particles and SDAS prevent crac□ growth and their interconnection, increasing the elongation. So for parts with plastic deformation it would be better to add TiB_2 particles.

b. Parts with internal pressure or fluids: As Al_2O_3 reinforced alloys has less porosity, they have a better behavior against lea□age.

CHAPTER 5: MECHANICAL PROPERTIES.

□.1 Introduction. Strengthening mechanisms

Introduction

Pure aluminium is a soft metal with insufficient strength for most engineering applications. In the automotive industry cast aluminium is increasing it percentage in the total weight of the car, displacing other materials with a higher density. In order to achieve the maximum decrease in weight to reduce energy consumption and emissions, the cast aluminium alloys should be employed in structural applications. New aluminium alloys have been developed to obtain better properties by a correct concentration of allowing elements.

In order to get interesting properties we can employ other strengthening process, as the employ of grain refiners and modifiers, increase of solidification rate, severe deformation, ultrasonic vibration, thermal treatments and reinforcements. In all the cases the mobility of dislocations is reduced, promoting the necessity of higher forces to move the dislocations through the aluminium alloy.

A dislocation is a defect or irregularity within a crystal structure. They have a strong influence on material properties □□TS, □S, elongation, hardness and fatigue□. They are classified in two main types: edge and screw, but normally we can observe a mixture of both types in real alloys.

□mploying different strengthening process we obtain the decrease of dislocation mobility, becoming the sum of the effect of the different strengthening mechanism and also of alloy composition □Mah 08□. The dislocation motion occurs by sequential bond brea□ing and bond reforming, so the resistance to deformation □strength□ can be improved by decreasing the possibility to move, putting obstacles in the way of displacement.

In general all the strengthening mechanisms increase the □TS and □S and decrease the elongation. In all the cases, the strength is got by impeding the motion of the dislocations. We define following the different strengthening mechanisms that are involved in the reinforcement of aluminium alloys:

1) □rain and subgrain strengthening: The Aluminium alloy is strengthened by the grain and subgrain reduction. The reason is that the slip in a grain is constrained by the presence or absence of slip in neighbouring grains or subgrains. Normally a discontinuity of slip planes or a change in the slip direction is needed to get slip across the grain or subgrain boundaries. In this case, grain and subgrain boundaries acts as barriers to dislocation movement.

There is a direct relation between the □S and the grain and subgrain si□e. This relation has the name of Hall-petch_□Hal 51□. We can see how they are related:

$$\sigma_y = \sigma_0 + \square d^{\square 1/2}$$

Where is the □S, σ_0 is the intrinsic □S, d is the grain diameter and □is a constant for a given material. So we can deduce that a decrease of grain si□e □d□promotes an increase of □S □σ_y□. A second phase is not required.

2) Solid solution strengthening (Solute hardening):

Impurities dissolved by addition to the melt promote the strengthening □Wi□ 11-02□. As much as there is a distort lattice mechanism, the distort can be produced by a substitution or interstitial mechanism. This implies an increase of energy of the crystal due to the lattice increase, and also the increase of dislocations near the distorted area. If the distortion increases, the dislocation mobility is reduced.

In the case of the aluminium alloys, some alloying elements have a great influence in the solid solution strengthening, li□e Cu or Mg. Any alloying element is not suitable to get this type of strengthening, because there must exist an atomic misfit with the aluminium matrix and also to have high solid solubility. The strengthening effect is increase if:

- The radius of the two particles is very different.
- If we increase the quantity of dissolved particles.

Of both effects, the most important is the ratio relation. The continuous solid solutions show a maximum strength at an intermediate composition. A second phase is not required.

3) Strain □ardening (□ or□ hardening □cold □or□):

The strain hardening is produced by low temperature plastic deformation □Wi□ 11-03□. The strengthening mechanism involves:

- Dislocation creation due to the plastic deformation.
- Multiplication of dislocation number and movement of dislocation induced by the repeated deformation than promotes that dislocations repel between them.

The main effect is an increase of □S, because the rearrangement of dislocations of the structure of crystals and the phases those are in the neighbourhood. Same areas of entangled dislocations don't allow the movement of surrounding dislocations. If we continue with consecutive strain hardening process, □S tends to be similar to □TS, but with a decrease in the □longation, promoting a brittle material. A second phase is not required. They are several processes to produce the strain hardening, involving forging, extrusion, rolling, drawing, bending and □CAP.

4) Dispersion strengthening (□ro□an strengthening):

The dispersion strengthening is promoted by the addition of elements as fibres, particulates, or others, with and strengthening effect due to the dispersion of a second phase in the aluminium alloy □□em 81□, □Cly 93□. The dislocation movement is reduced across grain boundaries with different phases, and the dislocations movement is only possible bypassing the addicted elements. It this movement dislocation loops are created, and they are called Orowan loops, and the strengthening mechanism is also □nown as Orowan strengthening. This motion promotes an increase of □S.

The effect is more important in case of:

- Hard second phase □□ess possibilities to have a plastic deformation□.
- Ductile matrix as aluminium matrix □More capacity of the matrix to have plastic deformation□.
- High percentage of second phase elements □More possibilities to reduce dislocation movement□.
- Spherical or rounded second phase □□ess stress concentration than sharp edges□.
- Small second phase □Higher specific surface area per volume unit□.

In order to promote a good dispersion strengthening, particle grain si□e range should be between 0.01 and 0.7 μm □Han 05□, □Cly 93□, but the most important points are the spacing between particles and their si□e.

□) Precipitation strengthening (Age hardening):

Is more common in aluminium alloys, and the strengthening effect is promoted by the precipitation of small particles, normally from a supersaturated solid solution □In this case is called □age hardening□□. A natural or artificial ageing treatment is necessary in order to convert second phase particles from solid solution to fine precipitate structure □□em 81□, □Cly 93□.

The strength is produced because dislocation movement is reduced across grain boundaries between different phases of fine dispersion of precipitates. If the process is at room temperature then is called natural aging, but if a heat treatment is needed, then is called artificial aging. The effect is similar to dispersion strengthening, because the nature of elements and strength distribution, but with an smaller precipitates size.

) Load transfer between matrix and reinforcement:

If the matrix contains a no plastically deforming reinforcement, when a load is applied to the aluminium, it can transmit that load to the reinforcement. Normally the reinforcement must have a high aspect-ratio, in order to promote the load transference by shear stress at the matrix-reinforcement interface. A ratio of 10:1 is usually recommended as the smallest ratio to transfer the load (Ai 97).

) CTE mismatch between the matrix and the reinforcements:

When the CTE between the matrix and the reinforcements are very different at microscopic level and can coexist, the strength is promoted by the strains produced in the cooling of the reinforced material, due to the different thermal contraction in the solidification process. Lot of new dislocations are created to absorb the CTE misfit. As much as there is an increment in the number of dislocations, the movement is reduced by the impediment to move, increasing US (Han 05, Arp 03).

In the case of an eutectic alloy (As 03), more than one strengthening mechanism can be produced at the same moment:

- Solid solution strengthening: Constituent B in α or A in β.
- Dispersion strengthening: For example alternative layers of α and β constituents, similar to a composite.
- Grain size strengthening: If a rapid cooling is promoted, narrower alternative layers are created.

The maximum strength of an alloy should be get in the eutectic composition (Han 02).

□.2 □xperimental results

□.2.1 □echanical properties at Room T

The tensile tests were carried out following the standard ASTM A-370 with cylindrical specimens produced by HPDC. The dimensions of the specimens were diameter = 6.25 □ 0.12 mm, $□_0$ = 25 □ 1, $□_c$ □ 32 mm, □ = □5 and □ =80 mm, and the elongation was measured with an extensometer at room temperature and at 200□C.

Table 5.1 shows the average results obtained in the 3 tensile tests of every alloy and of their corresponding unreinforced Al Si9 Cu3 alloy.

		□xperimental data				
T□NSI□□ PR□P□RTI□S AT 20□C	**State**	**Al Si□Cu3 Sample**	**0.2% S□S-$Ti□_2$**	**0.2% commercial $Ti□_2$**	**0.1% of gamma $Al_2□_3$**	**0.1□% of alpha $Al_2□_3$**
□TS □20□C□□MPa□	As Cast	277	291	304	297	296
□S □20□C□□MPa□	As Cast	132	128	130	128	123
□longation % □20□C□	As Cast	5,6	6,8	7,1	5,2	5,1
T□NSI□□ PR□P□RTI□S AT 200□C						
□TS □200□C□□MPa□	As Cast	166	169	173	167	161
□S □200□C□□Mpa□	As Cast	123	124	128	125	121
□longation % □20□C□	As Cast	4,0	4,0	5,5	6,0	4,0

Table □.1: Tensile properties of the unreinforced and reinforced alloys at room temperature and 200□C.

The first property to compare is the □TS at room temperature, which gives us the maximum value of stress that a part can support without the nec□ing effect on the test bar □See Fig. 5.1.□ It's very important for brittle materials, as a design value. In our case, we can observe an increase in the □TS of all the reinforced materials, which corresponds with the results of the literature review. This increase is high □About a 7%□ in comparison with the small quantity of reinforcement particles □0.2 wt.%□if we loo□ in the Fig. 5.1. the media it's quite similar for both reinforcement materials. In our case, it can be related with the dispersion of the nano-particles in the matrix, the small SDAS of dendrites and the decrease of the porosity.

We resume the variation in □TS properties as:

- A general increase in the □TS of about a 7% by a 0.2% of reinforcement with TiB_2 and Al_2O_3.
- For an equivalent volume fraction of reinforcement the commercial TiB_2 has a better behavior than SHS-TiB_2, with double percentage of increase in □TS □+4.9% for SHS-TiB_2 and +9.5% in commercial TiB_2□.
- For equivalent volume fraction of reinforcement of Al_2O_3, the values are very similar, and there is not a variation because of the type of Al_2O_3.

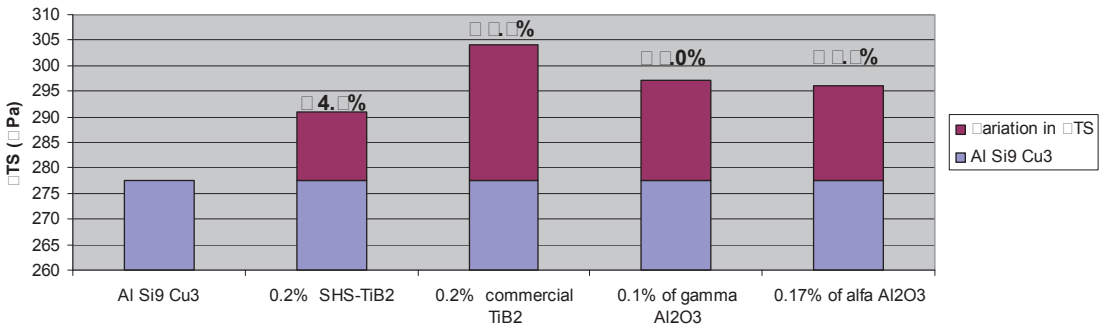

□ig. □.1: □TS at room temperature for reinforced and base Al Si□ Cu alloys.

The □S gives us the stress at which plastic deformation becomes noticeable. This value is employed in the design of parts were permanent plastic deformations are not allowed. □S tends to decrease as we increase the reinforcement, as we can see in Fig. 5.2. This is not a common behavior if we compare with the literature review, which shows as we have seen before that □S increases it value with the reinforcing elements. The explanation could be attributed to the agglomeration of reinforcement particles. We resume the variation in □S properties as:

- For equivalent volume fraction of reinforcement □0.2% TiB2 and 0.17% Al2O3□ decrease is much pronounced for the Al2O3 reinforcement type □Aprox. 2 times higher□.
- For an equivalent volume fraction of reinforcement the commercial TiB_2 has a better behavior than SHS-TiB_2, with one half the decrease in □S □-3.0% for SHS-TiB_2 and -1.5% in commercial TiB_2□.
- In the case of the Al_2O_3 reinforced alloys, the increase in the percentage of reinforcement of a 70% corresponds with a decrease in □S, that it's two times smaller in comparison □-3.4% in γ-Al_2O_3 and -7.2% in α-Al_2O_3□.

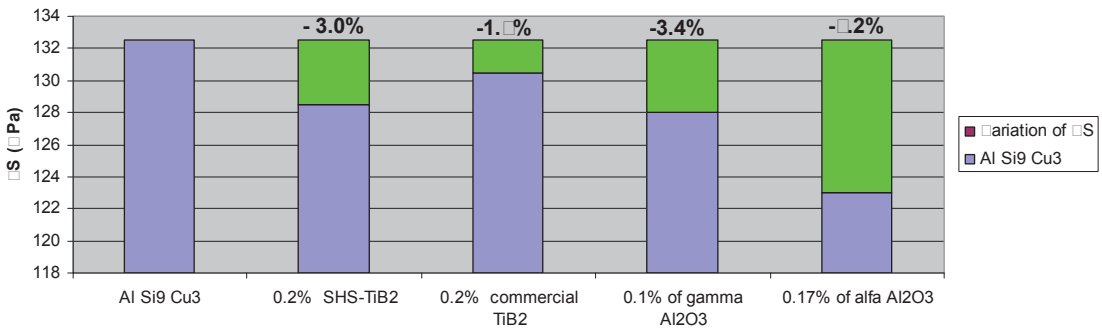

□ig. □.2: □S at room temperature for reinforced and base Al Si□ Cu alloys.

The □longation is the permanent deformation observed in the test bars after the essay. In this case the TiB_2 reinforced alloys shows an important increase in the elongation value, as we observe in Fig. 5.3. We □now that TiB_2 particles have a very important refining effect with a reduction in the SDAS grain si□e, which can permit the increase of the elongation value. The reduction of porosity in both cases has a positive effect. In the case of the Al_2O_3, the global elongation value decreases. The explanation could be an agglomeration of Al_2O_3 nano-particles in the aluminium grains, as seen on Fig. 4.21. We resume the variation in □longation properties as:

- TiB_2 reinforced alloys have an increase in the elongation □+20.4% with SHS and 25.7% with commercial TiB_2□. It may be related with the best solidification curves in the nucleation □one, especially with commercial TiB_2, and also with the smallest SDAS in the commercial TiB_2 sample.
- Al_2O_3 reinforced materials have a decrease in the elongation in comparison with the base alloy □-8% in gamma and -9.7% in alfa Al_2O_3□.
- In TiB_2 and Al_2O_3 reinforced materials, values are very similar for the two reinforcement types.
- □longation remains similar for the two different reinforcement volumes in the case of Al_2O_3.

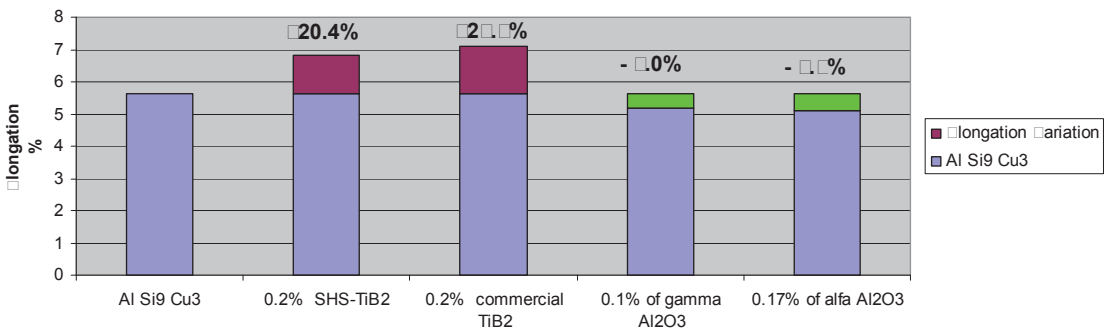

□ig. □.3 □longation at room temperature for reinforced and base Al Si□ Cu alloys.

All the samples were cast in the same conditions and the average of the valid values of four tensile tests were obtained for each of the data presented. The main conclusions are:

- □ltimate Tensile Strength □□TS□at 20□C is increased by the nano-reinforcement addition.
- □ield Strength □□S□ at 20□C decreases by the reinforcement addition. The decrease is more pronounced in the Al_2O_3 reinforced materials.
- □longation at 20□C is increased by TiB_2 nano-reinforcements and decrease with the Al_2O_3 reinforced materials.

□.2.2 □echanical properties at 200□C

The samples were also tested at 200□C. We can observe in Table 5.1 and 5.4. that the addition of nanoparticles increases the □TS. However, this effect is much less pronounced then for the same samples tested at room temperatures. Also 0.17 wt.% of alpha Al_2O_3 has a lower value than base material. TiB_2 reinforced materials have a higher value, but tendency show that increasing the temperature the □TS values tend to be more similar to the Al Si9 Cu3 base. As we increase the temperature, we may start the recovery process, with changes in the internal structure in order to decrease the energy of the system, promoting a decrease in the number of grain boundaries. However a decrease in dislocations number and also a coarsening of precipitates in the reinforced material may be also developed, with a therefore negative effect in □TS. In the case of 0.17% of Al_2O_3, we have observed a strange behaviour in the solidification curve, and may have more agglomerates and not as well dispersed Al_2O_3 particles. Also as we'll see in point 5.2.3. fracture analysis, an oxide is observed in the fracture area, which could reduce the □TS value of the essay. We resume the variation in □TS properties as:

- A general increase in the □TS of about a 3% by a 0.2% of reinforcement with TiB_2 and little or negative values in comparison with base alloy for the Al_2O_3 reinforced alloys.
- For an equivalent volume fraction of reinforcement the commercial TiB_2 has a better behavior than SHS-TiB_2, with double percentage of increase in □TS □+1.8% for SHS-TiB_2 and +4.2% in commercial TiB_2□.
- For the reinforcement with Al_2O_3, the values are better for a 0.1% of γ- Al_2O_3 than for α- Al_2O_3 □+0.6% for γ - Al_2O_3 and -3% for α- Al_2O_3□.

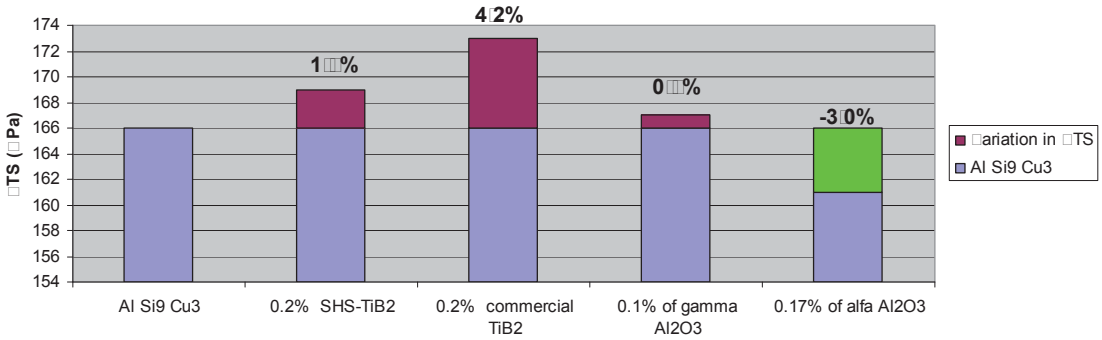

□ig. □.4: □TS at 200□C for reinforced and base Al Si□Cu alloys.

In the case of the □S at 200□C, we can observe in the Fig. 5.5 an increase of the value, which we can explain by changes in the internal structure in order to decrease the energy of the system, promoting a decrease in the number of grain boundaries. However the increase of temperature permits more movements and the appearance of plasticity, and □S is reduced by this action. In the case of 0.17% of Al_2O_3, we have observed a strange behaviour in the solidification curve, and may have more agglomerates and not as well dispersed Al_2O_3 particles. Also as we said before, we'll see in point 5.2.3 fracture analysis that an oxide is observed in the fracture area, which could reduce the □S value of the essay. The general behaviour is very similar to the tendency on □TS. We resume the variation in □S properties as:

- A general increase in the □S of about a 2.5% by a 0.2% of reinforcement with TiB_2 and little or negative values in comparison with base alloy for the Al_2O_3 reinforced alloys.
- For an equivalent volume fraction of reinforcement the commercial TiB_2 has a better behavior than SHS-TiB_2, with 3 times the percentage of increase in □S □+0.8% for SHS-TiB_2 and +4.1% in commercial TiB_2□.
- For the reinforcement with Al_2O_3, the values are better for a 0.1% of γ- Al_2O_3 than for α- Al_2O_3 □+1.6% for γ - Al_2O_3 and -1.6% for α- Al_2O_3□.

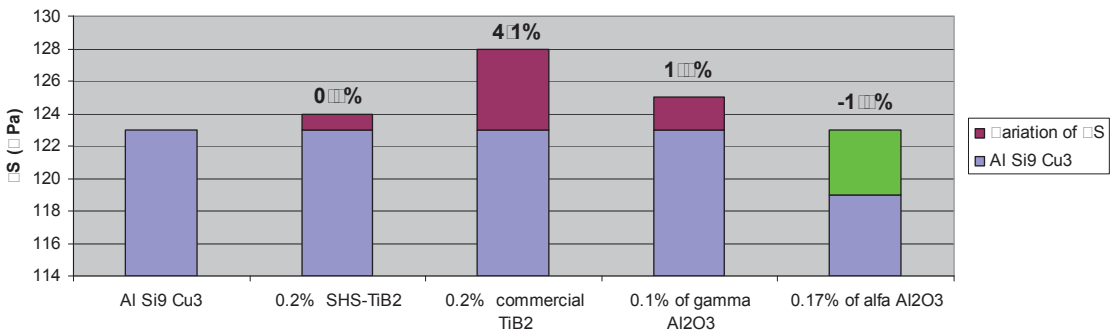

□ig. □.□: □S at 200□C for reinforced and base Al Si□Cu alloys.

In the case of the □longation at 200□C, we can observe in Table 5.6 how the values remains the same or better than the sample, but there is an increment in the Al_2O_3 alloys in comparison with the results at room temperature. In this case the change in the properties can be explained by the reduction of the total energy of the system, the grain boundaries total area reduction, the decrease in porosity. Also the presence of a ductile phase of Cu between the Si and Aluminium dendrites could improve the ductility. The difference between 0.2% SHS and 0.2% commercial TiB_2 reinforced alloys can be explained by the higher porosity in the first one, that we can also detect by the lower density and the presence of porosity in the tensile test bar.

- □longation values are smaller at 200□C than at room temperature, except for gamma Al_2O_3. The increase in the volume of the trapped porosity decreases the fracture area, and could decrease also the elongation.

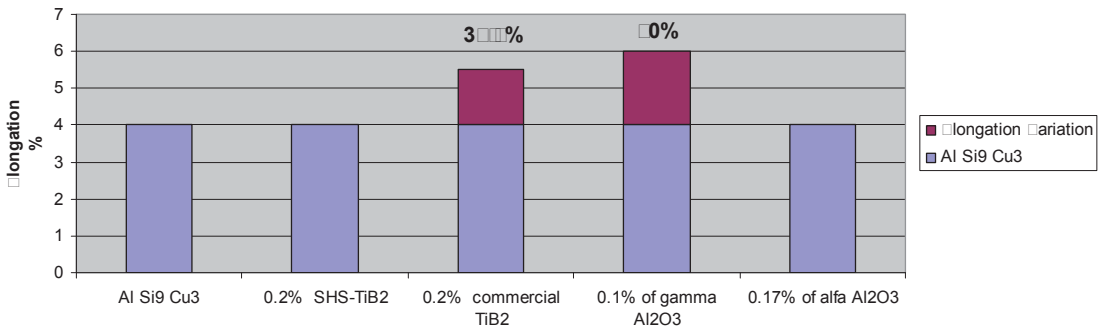

□ig. □.□ □longation at 200□C for reinforced and base Al Si□ Cu alloys.

The main conclusions are:

- □ltimate Tensile Strength □□TS□ at 200□C is increased by the TiB_2 nano-reinforcement addition.
- □ield Strength □□S□ at 200□C is increased by the TiB_2 nano-reinforcement addition.
- □longation at 200□C is increased in some concentrations and remains stable by TiB_2 and Al_2O_3 reinforced materials.

□.2.2. □easurement of physical properties

Physical properties of the materials have a direct influence in their eventual mechanical properties. Therefore the measurement of density and porosity was carried out in order to draw data to complete the analysis of the mechanical properties obtained. The obtained values are resumed in Table 5.2.:

Reference	S (Suspended mass into □ater gr.)	D (Dry mass gr.)	□ □D-S	□ □bul□ density (g□cc) □D□□	Theoretical density (g□cc)	Porosity (%)
Al Si9 Cu3 Sample	1.55	2.62	1.07	2.49	2.84	**12.3%**
0.2 wt.% SHS-TiB_2	1.73	2.87	1.14	2.53	2.86	**11.□%**
0.2 wt.% Commercial TiB_2	1.44	2.30	0.86	2.67	2.86	**□.□%**
0.1 wt.% of γ Al_2O_3	1.24	1.96	0.72	2.73	2.86	**4.□%**
0.17 wt.% of α Al_2O_3	2.29	3.62	1.33	2.71	2.86	**□.0%**

Table □.2: Density for reinforced and base Al Si□ Cu alloys.

Porosity decrease with the addition of ceramic nanoparticles. Al_2O_3 has a greater effect in porosity diminution than TiB_2 particles, but in both cases the total porosity is decreased by adding ceramic particles. The measures are in good relation with the observed less porosity in reinforced samples in the microscopy examination.

□.2.3 □racture analysis

Fracture analysis of specimens of samples in each of the conditions studied in the wor□ was determined with the optical microscopy. The main objective was the determination of the differences between the reinforced and non reinforced sample.

In metals brittle fractures are very dangerous and engineers try to avoid the use of brittle aluminium alloys, employing ductile alloys. Brittle fractures are characteri□ed by a bright and granular flat crac□ing area, with near no plastic deformation. In the case of ductile fractures, a plastic deformation is observed, with a fibrous aspect and it can content also flat or shear face areas. The color is not so bright, having a grey color.

□.2.3.1 □racture analysis of the Al Si□ Cu3 and Al Si□ Cu3 S□S-Ti□$_2$ tensile specimens

□ase alloy sample:

□arge porous are observed in Fig. 5.7. due to the increase of porosity volume □As see in page. 12□by the test temperature in the 200□C tensile sample, and in comparison with the reinforced alloys his much higher, as we detect in the density essay and in the microstructure observation. Some little oxides □Defects□also are detected. Fracture is ductile in all the samples.

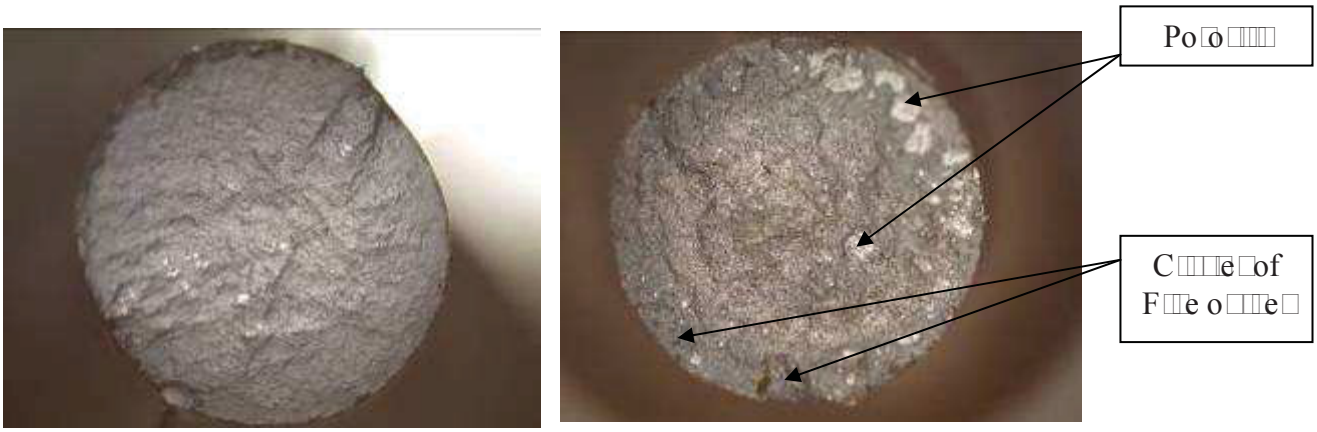

20□C Tensile essay sample 200□C Tensile essay sample

□igure □.□: □racture analysis of base alloy

<u>0.2% S□S Ti□$_2$</u>

The fracture analysis of the reinforced TiB$_2$ alloys has a very similar behaviour. Only little porosity in the 200 □C test bar is observed in Fig.5.8., due to the liberation of same of the gas porosity by the temperature. Some little oxides at 20 □C are also detected. Fracture is ductile in all the samples. No porosity or oxides are observed in the samples. Fracture is ductile in all the samples. This material has the better results in all the mechanical properties, and we can deduce that the internal soundness of the test bars has influence in the final mechanical properties, because it has the fewer defects in the fracture structure.

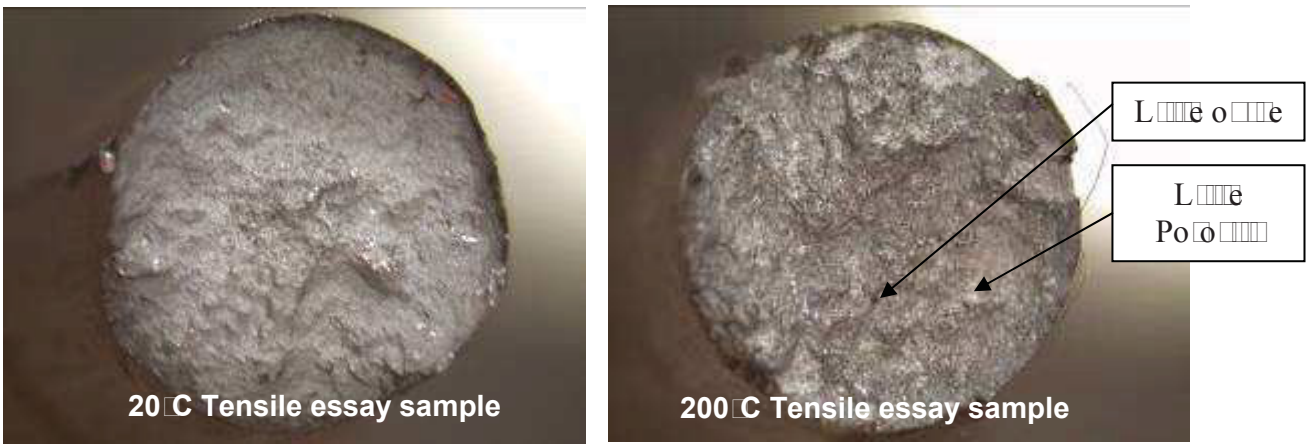

□igure □.□: □racture analysis of 0.02% S□S Ti□$_2$ reinforced alloy

<u>0.1% Al_2□$_3$ gamma alumina:</u>

The fracture analysis of the reinforced Al_2O_3 alloys has also a very similar behaviour. Only little porosity is observed in Fig 5.9. due to the liberation of same of the gas porosity by the temperature in the 200 □C test bar. A big cluster of oxides also is detected. The clusters of oxides are brittle and they act as a defect and as starting point for the fracture. This is the reason why we should try to have good nano-oxide dispersion, avoiding oxide clustering. Fracture is ductile in all the samples.

□igure □.□: □racture analysis of 0.1% Al_2□$_3$ gamma alumina reinforced alloy

□.2.4 Analysis of the experimental results

In order to determinate the tensile properties of the reinforced materials at room temperature and high temperature □200□C□ test were carry out, including internal porosity determination and fracture analysis, in order to complement the test developed and studied in the chapter 4.

It's remar□able that with a very little quantity of reinforcement, the mechanical properties have a great variation. At **room temperature** there is an increase of □TS of about a media of 7% by the reinforcement addition. That is directly related with the decrease in the SDAS decrease in the reinforced alloys. But in the other hand, as it occurs in MMCs, the □S is reduced. This reduction is much more important in the case of Al_2O_3, with an average reduction of a 5%.

In the case of □longation, the TiB_2 has a very beneficial impact of more than a 20%, related with the better nucleation solidification curve. In the case of Al_2O_3 reinforced alloys, □longation is reduced in a 9%.

At high temperatures □200□C□, in the case of 0.17 wt.% of α- Al_2O_3 we can observe a same oxide spots in the fracture area, that it can promote a slight decrease in the mechanical properties.

We observe an increase of □TS, especially for TiB_2 reinforced particles, of about a 3 %. The presence of the ceramic particles dispersed in the matrix and the nucleating effect can explain the increment of □TS.

We observe an increase of □S, especially for TiB_2 reinforced particles, of about a 2.5 %. The presence of a bigger porosity in the test sample is produced by the increase of temperature, which promotes an increment in porosity average diameter. As the no reinforced alloy has a bigger porosity, it's the more influenced, decreasing its □S.

□longation in all the reinforced alloys is equal or superior to base alloy. This could be explained by the presence of very small ceramic particles that reduce the recovery of the material at high temperatures and stabili□e porosity, and as porosity is higher in the base alloy, the elongation should decrease in comparison with the rest of alloys.

With density measures we can chec□ how the observations made in the metallurgical analy□e match well with the essays. It's very remar□able how very fine ceramic particles decrease porosity. Al_2O_3 particles has a lower porosity than TiB_2 particles, and in our case they are also the particles with the smallest si□e. In the case of γ-alumina, the porosity is lower, corresponding with a smaller particle diameter □15 nm□, in comparison with α-alumina of 40 nm.

In all the studied fracture test bars the fracture is ductile. In same cases porosity and oxides are detected. Big porosity is detected in the unreinforced alloy, which correspond to the alloy with the higher porosity. In same cases, the obtained values can be directly influenced by the internal sanity. Internal defects as oxides are difficult to relate directly with the alloy, but is more sense to relation them with the process parameters.

□.2.4 □odeling of the mechanical properties

In order to determinate the mechanical properties in function of the composition of the alloy, experimental formulas has been obtained by the equip of Ma□halouf, Apelian and Wang □Mac 98□, employing an experiment design employing an □16 and a modified □8 Taguchi orthogonal array in the limits of concentration of the allowing elements:

□ield Strength:

P1= □9.81 + 0.49 Si + 1.44 Cu + 1.48 Fe +13.07 Mg + 1.01 Mn + 1.45 Ni + 3.84 Cr + 0.34 Zn + 5.81 Ti + 12.72 Sr□x6.89512.

□ltimate Tensile Strength:

P2= □44.93 - 0.46 Si + 0.67 Cu - 0.18 Fe + 0.76 Mg - 0.13 Mn + 0.23 Ni + 0.16 Cr + 0.32 Zn + 0.20 Ti + 0.35 Sr□x6.89512.

□longation:

P3 = □10.62 - 0.61 Si - 0.50 Cu - 0.46 Fe - 0.57 Mg - 0.21 Mn -0.07 Ni + 0.06 Cr + 0.25 Zn +0.08 Ti + 0.07 Sr□x6.89512.

In Table 5.3 we can observe the variation of mechanical properties with the temperature and the compositions as cast:

	□xperimental data				
T□NSI□□ PR□P□RTI□S AT 20□C	**Al Si□Cu3**	**0.2% S□S-Ti□$_2$**	**0.2% commercial Ti□$_2$**	**0.1% of γ Al$_2$□$_3$**	**0.1□% of αAl$_2$□$_3$**
□TS □20□C□□MPa□	**2□□**	**2□1**	**304**	**2□□**	**2□□**
□TS □20□C□□MPa□NADCA formule	292	292	292	292	292
□S □20□C□□MPa□	**132**	**12□**	**130**	**12□**	**123**
□S □20□C□□MPa□NADCA formule	133	134	133	131	132
□longation % □20□C□	□□□□	□□□	□1	□2	□1
□longation % □20□C□NADCA formule	4,28	4,26	4,33	4,35	4,36

Table □.3: Comparison of properties obtained □ith NADCA formula and experimental essays □□ a□ □□□

We can observe that there is a little difference in the □TS and □S values, but there is much more variation with the elongation. However, the formula can not determinate the property variation due to the nano-reinforcement addition. We can modify the formulas, with adjusting coefficients in order to predict □from and industrial point of view in a very simplify way□the mechanical properties by the addition of the ceramic particles:

□ield Strength:

P1= □9.81 + 0.49 Si + 1.44 Cu + 1.48 Fe +13.07 Mg + 1.01 Mn + 1.45 Ni + 3.84 Cr + 0.34 Zn + 5.81 Ti + 12.72 Sr□x6.89512 □ □

□ltimate Tensile Strength:

P2= □44.93 - 0.46 Si + 0.67 Cu - 0.18 Fe + 0.76 Mg - 0.13 Mn + 0.23 Ni + 0.16 Cr + 0.32 Zn + 0.20 Ti + 0.35 Sr□x6.89512 □ □**.2**

□longation:

P3 = □10.62 - 0.61 Si - 0.50 Cu - 0.46 Fe - 0.57 Mg - 0.21 Mn -0.07 Ni + 0.06 Cr + 0.25 Zn +0.08 Ti + 0.07 Sr□x6.89512 **□2.□ (□or Ti□$_2$) or □0.□ (□or Al$_2$□$_3$)**

□.3 Conclusions

The mechanical properties of Al_2O_3 and TiB_2 particles reinforced aluminium alloys with have been determinate and compared with the unreinforced Al Si9 Cu3 alloy. The influence of ceramic particles has been also analy□ed□porosity levels and grain si□es and morphology have been determinate to explain the main strengthening mechanisms involved. The principal conclusions of mechanical properties analysis of reinforced aluminium are:

1□ The presence of very small percentages of Al_2O_3 and TiB_2 particles in the reinforced alloys can improve mechanical properties at room temperature. □TS is increased by the ceramic addition, but in the other hand the □S is decreased, but less in %.

2□ TiB_2 particles increase in a very important way the □longation, but Al_2O_3 particles has a negative effect on □longation at room temperature.

3□ At high temperatures the addition of ceramic nano-particles increase mechanical properties, but specially □longation. The increase in □TS is less important in percentage that at room temperature.

4□ Porosity quantity decrease and micro shrin□ages are smaller due to the presence of ceramic particles. This effect is stronger with particles than TiB_2 particles, but in both cases the tendency is to decrease the internal porosity.

5□ The increase in ductility with the Al_2O_3 and specially with TiB_2 particles is derived from the positive effect of SDAS reduction, very fine β-iron needles, very fine eutectic and fine precipitates, the smaller and less porosity, but also with a negative effect due to the non rounded shape of same of the milled particles, that can act as stress concentration points. However, the total effect is positive.

6□ The Al_2O_3 and TiB_2 reinforced alloys have a ductile fracture. In the case of TiB_2 particles it can be related to the effect of nucleation sites for the precipitation of silicon and Al_2Cu phases, and also the decrease of solute available for the precipitation of brittle precipitates. This is observed in the metallographic analysis with the fine precipitates and phases.

7□ The main strengthening mechanisms are in relation with the decrease of porosity and the grain refining effect of the Al_2O_3 and TiB_2 particles.

The **improvement of mechanical properties ta□es place in both room temperature and high temperatures**. □longation increase can have a very important interest in industry, in order to design new parts with higher requirements, and also high temperature applications.

CHAPTER 6: CONCLUSIONS.

□.1 Conclusions

□.1.1 Introduction

The present wor□ has been focused on studying the influence of nano- Al_2O_3 and TiB_2 particles on the solidification pattern, microstructure features, tensile and thermal properties of the Al-Si9 Cu3 alloys. Samples of reinforced materials have been cast by high pressure die casting in the same conditions than the unreinforced Al-Si9 Cu3 alloy. Following the main conclusions on the effect of Al_2O_3 and TiB_2 particles are summari□ed:

□.1.2 Influence of Al_2□$_3$ □Ti□$_2$ nano-particles on microstructure

1□ Al_2O_3 and TiB_2 particles influence aluminium grains nucleation, eutectic reaction and intermetallic precipitations. The nucleation temperature is increased, as the recalescence temperature. This effect is related to the incorporation of ceramic particles as heterogeneous nuclei.

2□ TiB_2 has more influence in the nucleation than Al_2O_3 particles. This is related to the employ of TiB_2 in commercial grain refiners as main refiner. Also TiB_2 particles are related as the most effectives for Aluminium grain refining.

3□ The influence of the particles should have a positive influence on the mechanical properties of the reinforced alloys since it decrease the undercooling, promoting a better nucleation.

4□ The employ of ceramic nano-particles reduce the porosity quantity and si□e. It's more remar□able in the case of Al_2O_3 than in TiB_2 particles.

5□ Acicular oriented very fine dendrites are promoted by the nano-particle addition. The SDAS is smaller in the reinforced alloys and also the SDAS decrease in the center of the samples.

6□ Al_2O_3 and TiB_2 particles modify the structure, with smaller detrimental β-iron needles.

7□ □ery fine eutectic structures are detected in the center of the reinforced alloys, especially with TiB_2 reinforced alloys.

8□ The S□M analysis shows that Al_2O_3 particles acts as nucleating points, with agglomerate particles of about 0,5-1 micron.

9□ □lectrical conductivity decreases by adding few quantities of ceramic particles and is quite similar in the center and periphery of reinforced alloys and a relation between SDAS and IACS has been observed.

□.1.3 Influence of Al_2□$_3$ □Ti□$_2$ nano-particles on the mechanical properties

The principal conclusions of mechanical properties analysis of reinforced aluminium are:

1□ The presence of very small percentages of Al_2O_3 and TiB_2 particles in the reinforced alloys can improve mechanical properties at room temperature. □TS is increase by the ceramic addition, but in the other hand the □S is decreased.

2□ TiB_2 particles increase in a very important way the □longation at room temperature, but Al_2O_3 particles has a negative effect on □longation at room temperature.

3□ At high temperatures □200 □C□the addition of ceramic nano-particles increase mechanical properties. The increase in □TS and □S are less important in percentage that at room temperature.

4□ Porosity and micro shrin□ages are smaller and lower due to the presence of ceramic particles. This effect is stronger with particles than TiB_2 particles, but in both cases the tendency is to decrease the internal porosity.

5□ The increase in ductility with the Al_2O_3 and specially with TiB_2 particles is derived from the positive effect of SDAS reduction, very fine β-iron needles, very fine eutectic and fine precipitates, the smaller and less porosity, but also with a negative effect due to the non rounded shape of same of the milled particles, that can act as stress concentration points. However, the total effect is positive.

6□ The Al_2O_3 and TiB_2 particles have a ductile fracture of the aluminium. In the case of TiB_2 particles it can be related to the effect of nucleation sites for the precipitation of silicon and Al_2Cu phases, and also the decrease of solute available for the precipitation of brittle precipitates. This is observed in the metallographic analysis with the fine precipitates and phases and in the T□M with the Cu in the interstices of silicon and aluminium dendrites.

7□ The main strengthening mechanisms are in relation with the decrease of porosity and the grain refining effect of the Al_2O_3 and TiB_2 particles.

It has been demonstrated that the **Al_2□$_3$ and Ti□$_2$ nano-particles have a direct influence on several important features of the alloys such as the microstructure□ precipitating of phases during solidification□mechanical properties□decrease of the amount of defects and change of electrical and thermal properties. Al_2□$_3$ and Ti□$_2$ particles can be used to improve properties of casting alloys**□and be very useful in the case of high mechanical and thermal requirements, also at high temperatures □200□C□.

They are also some processing conclusions that may have industrial interest:

1. A process to generate TiB_2 particles from commercial □gross□Ti and B has been developed employing the SHS process and by wet high energy ball milling. Also SHS reactions without reactor and the substitution of same of the raw material for cheaper salt based material can provide a cheap reinforcement material.

2. A process to introduce ceramic nano-particles in the liquid aluminium at relative low temperature and dissolution time.

3. □ery small quantities of *In-situ* or *Ex-situ* impurities modify the solidification curves. That could explain the difficulties to automate the DTA´s applications for Al Si9 Cu3 alloys. True DSC should be a better way to study the reinforced alloys.

4. There is a direct relation between the internal soundness of parts and the obtained mechanical properties. The effect of specially Al_2O_3 on reducing the internal porosity provides a good way to increase the mechanical properties.

6.2 Future directions

It has been shown that addition of Al_2O_3 and TiB_2 nano-particles to aluminium Al Si9 Cu3 alloy has a direct effect on some important properties such as microstructure, mechanical and thermal properties. The reinforcement percentages employed in the project are quite small, giving good results. Industrial processing of nano-particle and introduction in the alloy must be improved.

In order to advance in the use of nano-particles reinforced Al-Si9 Cu3 alloy for industrial applications same important aspects should be studied:

- **Industrialization of the and casting process.** The process must be robust and secure, without nano-particle emissions or explosion risk. Particle measure must be stable. Cheaper commercial materials must be investigated in order to decrease ceramic particle prices.

- **Optimization of particle composition, size and shape.** The particles must have the more adequate form and size in order to obtain the better results with the smallest material consume. Special care must be focus in particle degglomeration, in order to avoid losses of activity.

- **Study of the behavior of the nanoparticles in other alloys.** The present study has been developed with the Al-Si9 Cu alloy, but they are similar composition alloys that can have a very similar behavior. Also pure alloys can be tested, in order to change the grain refiners by nano-particles and to increase properties. In this case, the action of the thermal treatments should be studied over the nano-particles and properties.

- **Study of cheap nanoparticles compositions.** There many industrial sub products that they can be employed as nano-reinforcements for aluminium, as filter dusts, fly ashes and aluminium recycling wastes. Some of them have contaminants, but with a proper cleaning and preparation of raw materials it could be possible to decrease ACC´s prices.

- **Use of different consolidation and densification systems.** If the nano-particles are embedded in a good distribution in a very dense (no porous) matrix, nano-particles have a bigger recovery. In that way processes as CIC, SSS or other should be more investigated.

- **Understanding of the hardening mechanisms.** In order to improve the properties of ACC with nano-powders, in relation with the powder size and the distribution in the matrix, with the aim of optimize the process.

- **Detection of TiB_2 particles.** In order to detect TiB_2 particles, new preparing and observing methods can be employed.

□□**F**□□□□□□□

□Agu □□□Aguilar-Santillan □. □ etting of the □□□□□□α-Al_2O_3 sapphire surface by molten aluminium□□ffect of surface roughness. The minerals, metals □ materials society and AS□ international. 2□□□.

□Ai□9□□Ai□in □r. □.□.□The mechanical properties of in situ composites□ □O□. 49 □□□ □□99□□, pp. 3□-39.

□All □4□□nited States □atent □S 3.9□□.99□. □9□4. Alliot □., Beguin □.C., □outach □., □ercheron □.C. □other Alloy of Aluminium, Titanium and Boron and process for fabrication.

□Alu □□□http□□aluminium.matter.org.u□content□html□eng□

default.asp□catid□□□□pageid□2□□□2□2□□□

□Arp □3□Arp□n □., □olina □.□., Saravanan □.A., □arc□a Cordobilla C., □ouis □., □arciso j. □Thermal expansion behaviour of aluminium□SiC composites with bimodal particle distributions□ Acta □ateralia □□ □2□□3□pp. 3□4□-3□□□.

□As□ □3□The Science and □ngineering of □aterials, 4th ed. 2□□3. Broo□s and Cole. As□eland D. □. □□hul□ □. □.

□Bac □4□□nited State □atents □S 3□□□□□□. □9□4. Bac□erud S.□. □ethod for producing a master alloy for use in aluminium casting processes.

□Bac 9□□Solidification Characteristics of Aluminium Alloys, □ol. 2. □oundry Alloys. A□S and S□analuminium of □orway. □99□. A□S. Bac□erud □., Chai □., Tamminen □.

□Bac □□□□nited States □atents □S □.□□3.□□□. 2.□□□. B□c□erud □□□ohnsson □ □ Sigworth □. □ethod for optimi□ation of the grain refinement of aluminium alloys.

□Ban □□□□nited States □atent □S 4.□4□.□□□. □9□□. Banerji A., □eif □ . □roducing titanium carbide particles in metal matrix and method of using resulting product to grain refine.

□Boo □2□Boot D., Cooper □., St□ohn D.□., Dahle A.□. A Comparison of □rain □efiner □aster Alloys for the □oundry. T□S 2□□2.

□Bro 99□□oseco □on-□errous □oundry man□s □andboo□.□999. □lsevier □td.

Brown □. □.

□Buh □□□http□□www.buhlergroup.com

□Bru □□□□nited States patent □S 4.□□□.34□. □9□□. Brupbacher □.□., Christodoulou □., □agle D.C. □rocess for forming metal-ceramic composites.

□Cac 9□□C□ceres C.□., □ ang □. □. □Dendrite cell si□e and ductility of Al-Si-□g casting alloys□Spear and □ardner revisited□ International □ournal of Cast □etals □esearch. □99□. □ol.9, □□3. pp. □□□-□□2.

□Cti □□□Aleaciones de aluminio para el moldeo. □ersion □. CTI□. 2□□2. CTI□.

□Cly 93□Clyne T.□ ., □ ithers □.□. □An introduction to metal matrix composites□ Cambridge □niversity □ress. □993. ISB□ □-□2□-4□□□□-9.

□Con □□□Conrad □, □arayan □. On the grain si□e softening in nanocrystalline materials. Scripta □ater 2□□□42□□□. pp. □□2□□□3□.

□Dav □□□Davis B.□□yn □. Innovative forming and fabrication technologies□□ew opportunities. □inal report. Argonne □ational □aboratory. A□□-□□□3□. 2□□□.

□Dho □□□Dho□ey □. B., □ane □. □. □ ear Behavior and Its Correlation with□echanical □ropertiesof TiB2 □einforced Aluminium-Based Composites. Advances in Tribology. □ol. 2□□□, pp. □-□.

□Din □□□Aluminium and aluminium alloys □Castings □Chemical composition and mechanical properties. □nglish translation of DI□ □□ □□□□□2□□□-□□.

□Dju □4□Djurdjevic □.B., □rancis □., So□olows□i □.□. □maldi D., Sahoo □. Comparison of different analytical methods for the calculation of latent heat of solidification of 3□□ aluminium alloys. □aterial Science and engineering. 2□□4. A 3□□. pp. 2□□-2□3.

□Dju □□□Djurdjevic □.B. □Thermal Description of Al-Si Alloys □sing Their □nown Chemical Compositions□ □uropean Conference on Aluminium Alloys □□CAA 2□□□□. 2□□□.

□□as □□-□□□aston □., Davidson C., □ohn D.S. □ffect of alloy composition on the dendrite arm spacing of multi-component aluminium alloys. The minerals, □etals □ materials Society and AS□ international 2□□□.

□□as □□-2□□aston □., Davidson C., □ohn D.S. □ffect of alloy composition on the dendrite arm spacing of multi-component aluminium alloys. □etallurgical and materials transactions A. 2□□□. □□□□2□-□olume 4□A.

□□gi □□□□gi□abal □. Influence of Titanium Diboride □TiB_2□particles on the microstructure and properties of reinforced Al-Si□□g□.3 and Al-Cu□□gTi alloys for plaster casting applications. □niversit□ Bordeaux □. 2□□□.

□□l- □□□□l-□ahallawi I. S.□Shash □.□□igenfeld □.□□ahmoud, T. S.□□agaie □. □., Shash A. □., □l Saeed □. A. Influence of nano-dispersions on strength□ductility properties of semisolid cast A3□□Al alloy. □aterials Science and Technology. 2□□□. □ol. 2□, □□□□, pp. □22□-□23□.

□□l- □□□□l-□ahallawi I.S., Shash □., □agaie □.□., Abdela□i□□.□., □ayer □, Schwedt A. Influence of nano-dispersions on microstructure features of cast Al-Si □ypereutectic Alloys. □uropean conference on Aluminium Alloys. 2□□□. □oster A-□34.

□□u □□□□u □., □ agner T. Interaction of nano-structured metal over layers with oxide surfaces. Surface Science reports 2□□□. □□□2. pp. 43□-49□.

□□re □□□□reer A.□, Bunn A.□, Tronche A, □vans □.□, Bristow D.□. □odelling of inoculation of metallic melts□application to grain refinement of aluminium by Al□Ti□B. Acta □ateralia, 2□□□, □ol. 4□, Issue □□, pp. 2□23-2□3□.

□□ro □9□□rosselle □., Timelli □., Bonollo □., □olina □. Correlation between microstructure and mechanical properties of Al-Si diecast engine bloc□s. □etallurgical Science and Technology. □ol 2□.2. 2□□9.

□□ru 9□□□ru□les□i et.al. A□S Inc. Des □laines, Illinois. □99□.

□□u □2□□u □., □ian □., Chen □., □hou □. A mild solvothermal route to nanocrystalline titanium diboride. □ournal of Alloys and Compounds. □olume 3□2, Issues □-2. 2□□3. pp. 32□-32□.

□□u□ □□□□nited State patent. □S 4.□□2.□□3. □9□□. □u□ows□i □.□., Sentner D.A., Sigworth. Aluminium grain refiner containing duplex crystals.

□□al □□□□all □.D. □roc. □hys. Soc. Serie B □4. □9□□. pp. □4□-□□□.

□□an □2□□an □., □iu □., Bian □. □In situ TiB2 particulate reinforced near eutectic Al-Si alloy composites□ Composites A 33. 2□□2. pp. 439-444.

□□an □□□□an □. □□rocessing, microstructure evolution and properties of nano-scale aluminium alloys□. □hD. □niversity of Cincinnati. 2□□□. pp. 3□-44.

□□id 99□□ind A.□., Bhargava S.□., □rocott S. C. The surface chemistry of Bayer process solids□a review. Colloids and Surfaces A□□hysicochemical and □ngineering Aspects. □olume □4□, Issues □-3. □999. pp. 3□9-3□4.

□□um 9□□□umphreys □.□, Basu A., Dja□eb □.□. □The microstructure and strength of particulate metal-matrix composites□. □etal matrix composites. □rocessing, microstructure and properties. □2th □iso International Symposium on materials science. □99□. pp. □□-□□.

□□□s □□□□□seying S., □urna□C. □roperties of alumina particulate reinforced aluminium alloy produced by pressure die casting. □aterials and design. 2□□□. □□2□. pp. □□□-□□3.

□Iba 99□Ibarra D. □. Control of grain refinement of Al-Si alloys by thermal analysis. □c □ill □niversity. □999.

□Iva □4□Ivar □. □igh □ressure Die Casting of Aluminium and □agnesium Alloys - □rain Structure and Segregation Characteristics. □orwegian □niversity of Science and Technology □□T□□□. 2□□4.

□□ac □□□Alumina□sintering and optical properties. □9□□. Technische □ogeschool □indhoven. □acob □. □.

□□ia □□□□iang □., □u □.□. Si□e dependent interphase energy and its applications. Surface Science □eports. 2□□□. □□□3. pp. 42□□ 4□4.

□□au □□□□aufmann □., □ggowit□er □.□. □etallurgy and processing of high integrity light metal pressure castings. □achverlarg Schiele □ Sch□n □mbh Berlin. 2□□□. pp.□□.

□□as □□□□ashyap □. T., Chandrashe□ar T. □ffects and mechanisms of grain refinement in aluminium alloys. Bull. □ater. Sci., □ol. 24, □o. 4, 2□□□, pp. 34□□3□3.

□□um □9□□umar S., Subramaniya □., □urty B.S. □unctionally graded Al alloys matrix *in-situ* composites The minerals, metals □ materials society and AS□ international. 2□□9.

□□em □□□□rinciples of □echanical □etallurgy. □dward Arnold..□9□□. □lsevier. □e□ay. pp. □□□-2□□.

□□oe □□□□oeffler □. □ano-material roadmap 2□□□. Overview of promising nano-materials for industrial applications. Steinbeis-□uropa-□entrum. 2□□□.

□□i □3□□i □., □andalova □.□., □i□itin □.I., □uts A.□., □a□aren□o A.□., □hang □. □ffect of fluxes on structure formation of S□S Al□Ti□B grain refiner. □aterials □etters. 2□□3. □ol. □□. pp. 3□94□3□9□.

□□a □□□□a □.□., □i □.□., □uo □., □ing □.□., □u □.□., Bi □., □hang □.□. *In-situ* formed Al_2O_3 and TiB_2 particulates mixture-reinforced aluminium composite. Scripta □etallurgical et □aterialia, □994, □ol. 3□, Issue □, pp. □3□-□39

□□ac 9□□□ac□ay □. I. □uantification of Iron in Al-Si □oundry alloys via thermal analysis. □c □ill □niversity. □99□.

□□ah □□□□ahboob □., Sajjadi S. A., □ebarjad S. □. Synthesis of Al-Al2O3 □ano-Composite by mechanical alloying and evaluation of the effect of ball milling time on the microstructure and mechanical properties. The International Conference on □□□S and □anotechnology, IC□ □□□□.2□□□.

□□a□9□□□a□hlouf □., Apealian D., □ ang □. □icrostructures and properties of aluminium die casting alloys. □orth American Die Casting Assoc. □99□. □ADCA

□□ar □□□□artin □.I., □abanal □.□., □ome□□.S., Torralba □.□., □ilosevic O. □icrostructural and morphological analysis of nanostructured alumina particles synthesi□ed at low temperature via aerosol route. □ournal of the □uropean Ceramic Society 2□□□. □□2□, pp. 24□□-2494.

□□at □□□□atsunaga T., □atsuda □.□□atayama T., Shino□a□i □., □oshida □. □abrication of continuous carbon fiber reinforced aluminium-magnesium alloy composite wires using ultrasonic infiltration method. Composites. 2□□□. □art A 3□. pp □9□2-□9□□.

□□ax □□□□axwell I, □ellawell A. An analysis of the peritectic reaction with particular reference to Al-Ti alloys Acta □etallurgical, □9□□, □ol. 23, Issue □, pp. 9□□-9□9.

□□il 9□□□iller □ .S., □umphreys □.□ □Strengthening mechanisms in metal matrix composites□ □undamental relationships between microstructure □ mechanical properties of metal matrix composites. □aw □.□., □unger □.□. The □inerals, metals and materials society, □99□.

□□is □4□□isere□A., □uller □., □ossoll A. et al. 2□□4. □□article reinforced metals of high ceramic content□□at sci eng A-Struct 3□□-□9□pp. □22-□3□.

□□it 9□□□itra □., □ahajan □.□. Interfases in discontinuosly reinforced metal matrix composites□An overview. □ater. Sci. □99□, □ol. □□, □□4, pp. 4□□-434.

□□iy □3□□nited States □atent □S 3.□□□.□□□. □9□3. □iyasa□a □□□asuda □. Small grain promoting Aluminium-Titanium-Boron mother Alloy.

□□or □□□□ortensen A. □etal □atrix Composites in industry□An overview. □cole □olitechnique □□d□rale de □ausanne. 2□□□.

□□on □9□Aluminium Alloys, structures and properties. □ondon, Butherworths. □9□9. □ondolfo □.□.

□□un 9□□□unro □. □. □□valuated □aterial □roperties for a Sintered alpha-Al_2O_3,□ □ournal of the American Ceramic Society. □99□. □ol. □□, pp. □9□9-□92□.

□□ □C □□-2□http□□www.ceramics.nist.gov□srd□summary□scdaos.htm

□□un □□□□unro □. □. □□aterial □roperties of Titanium Diboride□, □ournal of □esearch of the □ational Institute of Standards and Technology. 2□□□.□ol. □□□, pp. □□9-□2□.

□□ □C □□-□□http□□www.ceramics.nist.gov□srd□summary□scdtib2.htm

□□an □□□http□□www.nanophase.com□products□details.aspx□□roductId□□

□□i□ □□□□i□itin □.I., □ anqi □I.□., □andalova □.□., □a□aren□o A.□., □ong □. □reparation of al-ti-b grain refiner by shs technology. Scripta mater. 2□□□. □ol. 42. pp. □□□□□□□.

□□i□ □□□□i□las A., Abaun□a □., □ernande□Calvo A.I., □aca□e □, Suare□ □. Thermal an□lisis as a microstructure prediction tool for A3□□ aluminium parts solidified under various cooling conditions. The □9th □ □C paper. 2□□□.

□□ue □4-□□□□uested T.□□□reer A.□□The effect of the si□e distribution of inoculant particles on as-cast grain si□e in aluminium alloys. Acta materalia. 2□□4, □ol. □2, Issue □3, pp. 3□□9-3□□□

□□ue □4-□2□□uested T. □., Solidification of Inoculated Aluminium Alloys. □niversity of Cambridge. 2□□4.

□□am □□□□amachandran T.□., Sharma □.□. , Balasubramanian □. □rain □efinement of □ight Alloys. □□th □ □C - □ orld □oundry Congress□th - 2□□□, pp. □□9-□93.

□Sat □□□Sato T. □anostructure Control for □igh-Strength and □igh-Ductility Aluminium Alloys. □anomaterials 2□□□. pp. 3□□-34□.

□Sch 9□□Schumacher □, □reer A. □ew studies of nucleation mechanism in aluminium alloys. Implication for grain refinement practice. □ater Sci Technol. □99□□□4□394.

□Sch □□□Schi□t□ □. Simulations of nanocrystalline metals at the atomic scale. what can we do□ what can we trust□. Science of □etastable and □anocrystalline Alloys□ A.□. Dinesen et al., 2□□□. A.□. Dinesen et al. pp. □2□-□39.

□Sch □4□Schi□t□ □. Strain-induced coarsening in nanocrystalline metals under cyclic deformation. □aterials Science and □ngineering. 2□□4. A 3□□□3□□, pp. 9□□□9□9.

□Sch □□□Schaffer □.□., □iller D. □., Dahles A. □. Crystallography of engulfed and pushed TiB_2 particles in aluminium. Scripta □ateralia. 2□□□. □□□□, pp.□□29-□□32

□Sei □9□Seifeddine S. The influence of □e and □n content and cooling rate on the microstructure and mechanical properties of A3□□-die casting alloys. Svensson. □etallurgical Science and Technology. □ol.2□-□. □d. 2□□9.

□She □□□Shen □., □ujii □., □atsumoto T., □ogi □. Critical □actors Affecting the □ ettability of α-Alumina by □olten Aluminum. □ournal of the American ceramic society. □ournal of the American Ceramic Society. 2□□4. □ol. □□, Issue □□, pp. 2□2□-2□□9.

□Sig □□□□nited States □atent □S 4.□□2.29□. □9□□. Sigworth □. Third element additions to Aluminium-Titanium □aster Alloys.

□Sig 9□□□nited States □atents, □S □.□□□.2□□. □99□. Sigworth □ □□u□ows□i □. □rain refiner for aluminium containing silicon.

□Spa □□□Spar□man D. Thermal Analysis □etrics by derivatives. □eltlab. 2□□□. www.meltlab.com□hottopics□feb2□□□htopic.pdf

□Tam □□□Tam □.□. □echanical and thermal characteristics of □I□ed A□-TiB2 □ □Cs. City university of □ong □ong. 2□□□.

□Tay □4□Taylor □A. The effect of iron in Al-Si9 casting alloys. 3□th Australian □oundry Institute □ational Conference. 2□□4.

□Tee □□□Tee □.□., □u □., □ai □.O. □In situ stir cast Al-TiB2 composite□processing and mechanical properties□ □aterial Science and Technology. 2□□□. □ol. □□. pp 2□□-2□□.

□Tjo □3□Tjong S.C., Tam □.□., □ u S.□. Thermal cycling characteristics of *in-situ* Al-based composites prepared by reactive hot pressing. Composites science and technology 2□□3, □3, pp. □9-9□.

□Tjo □□□Tjong S.C., □ ang □.S., □ai □.□ . □ow-cycle fatigue behaviour of Al-based composites containing in situ TiB2, Al2O3 and Al3Ti reinforcements . □aterials Science and □ngineering□A. 2□□3. □olume 3□□, Issues □-2, pp. 99-□□□

□Tjo □□□Tjong S.C., Tam □.□. □echanical and thermal expansion behaviour of hipped aluminium-TiB_2 composites □aterials. Chemistry and physics. 2□□□. 9□, pp. 9□-9□.

□□ i□ □□□http□□en.wi□ipedia.org□wi□i□Alumina

□□ i□ □□-□2□http□□en.wi□ipedia.org□wi□i□Solid□solution□strengthening

□□ i□ □□-□3□http□□en.wi□ipedia.org□wi□i□□ or□□hardening

□□ha □□□ □uo □., Saunders □., □iodowni□ □., Schill□ □.□. □rediction of room temperature mechanical properties in aluminium castings. International Congress of Aluminium Alloys ICAA□□. 2□□□.

□□ho □□□□hong □.□., □ ong □ .□.□., □upta □. □nhancing strength and ductility of magnesium by integrating it with aluminium nanoparticles. Acta materalia. 2□□□. □ol. □□ pp. □33□-□344.

□□ol □□□Casting aluminium alloys. □lsevier. 2□□□. □olotorevs□y □.S.□Belov □.A.□ □la□off □.□. pp. 3□9-3□2.